UNIVERSITY OF CALIFORNIA SAN DIEGO

Neural-Vascular Interactions in Retinal Development and Disease

A dissertation submitted in partial satisfaction of the
requirements for the degree Doctor of Philosophy

in

Neurosciences
with a Specialization in Computational Neurosciences

by

Geoffrey Aaron Weiner

Committee in charge:

Professor Richard Daneman, Chair
Professor Jeffrey L. Goldberg, Co-Chair
Professor David Kleinfeld
Professor Jonathan H. Lin
Professor Eric D. Nudleman

2018

The Dissertation of Geoffrey Aaron Weiner is approved, and it is acceptable in quality and form for publication on microfilm and electronically:

_____

_____

_____

_____
Co-Chair

_____
Chair

University of California San Diego

2018

DEDICATION

This work is dedicated to my parents, Barbara Weiner and Larry Weiner. Everything I have accomplished in life is due to your guidance, support, and love.

EPIGRAPH

The marble index of a mind for ever
Voyaging through strange seas of Thought, alone.
William Wordsworth

TABLE OF CONTENTS

LIST OF ABBREVIATIONS

ACh	Acetylcholine
AMD	Age-related macular degneration
AMP	Adenosine monophosphate
APB	2-amino-4-phosphonobutyric acid
BBB	Blood-brain barrier
BRB	Blood-retinal barrier
CNO	Clozapine-n-oxide
CNS	Central nervous system
EAE	Experimental autoimmune encephalomyelitis
EPI	epibatidine
ERG	Electroretinogram
FEVR	Familial exudative vitreoretinopathy
GCL	Ganglion cell layer
GPCR	G-coupled protein receptor
HIV	Human immunodeficiency virus
INL	Inner nuclear layer
IOP	Intraocular pressure
IPL	Inner plexiform layer
JAM	Junctional adhesion molecule
MRI	Magnetic resonance imaging
MS	Multiple sclerosis
NFL	Nerve fiber layer
OCR	Oxygen consumption rate
OIR	Oxygen-induced retinopathy
ONC	Optic nerve crush
ONH	Optic nerve head
ONL	Outer nuclear layer
RGC	Retinal ganglion cell
ROP	Retinopathy of prematurity

SAC	Starburst amacrine cell
TTX	Tetrodotoxin
VEGF	Vascular Endothelial Growth Factor

LIST OF FIGURES

LIST OF TABLES

ACKNOWLEDGEMENTS

I would like to thank EJ Chichilnisky, Lauren Jepsen, Alexander Heitman, Martin Greschner, Daniel Ahn, Peter Li, and Clare Hulse for being outstanding mentors and lab mates as I was first transitioning in to retinal research.

I would like to thank members of the Goldberg lab not otherwise acknowledged. Evan Cameron, Joana Galvao, Xiong Zhang, Kevin Tenerelli, Noelia Kunzevitzky, Karl Kador, and Minjin Ju for contributing to a great overall lab environment and thoughtfully helping me out with my projects. Yan Wang for patiently teaching me how to do surgery on mice, and almost everything else in the lab. Most especially, and most exuberantly, I need to thank Kristina Russano, probably the one single person without whom I could not have completed graduate school.

I would like to thank members of the Daneman lab for taking me in and making every accommodation so that I could finish my PhD with them. Especially Rich himself, who adapted to having me around despite not asking for it. Catie Profaci, Marie Blanchette, Roeben Munji, Stephanie Liaw, Cayce Dorrier, and Rob Pulido all made my second lab transition as smooth and welcoming as possible for someone crashing the party.

I would like to thank Alfredo Dubra and other members of his lab for teaching me about adaptive optics and retinal imaging generally. And for keeping plenty of food in the fridge every time I visited Milwaukee.

I would like to thank my committee members for your invaluable insight and support throughout this process. You have provided encouragement and advice for years and this project would not have been a success without you.

I would like to thank the members of all the labs I've worked in - Chichilnisky, Goldberg, and Daneman - past and present, for all of your helpful comments and advice throughout my time in lab. It has been a pleasure to work with you.

Most importantly, I would like to thank my mentor, Jeff. You showed me that there is a truly encompassing, interesting, compelling way to be both a physician and a scientist. Your scientific rigor, broad interests, and success have inspired me to continue on this pathway. You always gave me the support and space I needed to pursue the questions I found captivating, and I will remember the wisdom you've shared with me throughout my career. Thank you.

Chapter 1 is an original document written by Geoffrey Weiner with oversight from Jeffrey Goldberg, Richard Daneman, and Eric Nudleman. Geoffrey Weiner was supported by a grant from the San Diego Foundation. Jeffrey Goldberg is Professor and Chair of Ophthalmology at the Byers Eye Institute at Stanford University and is supported by grants from the NIH and the GRF. Richard Daneman is an Assistant Professor in the Department of Pharmacology at UCSD and is supported by grants from the NIH. Eric Nudleman is Assistant Clinical Professor of Ophthalmology at UCSD,

Chapter 2 is an original document written by Geoffrey Weiner with oversight from Jeffrey Goldberg, Richard Daneman, and Eric Nudleman currently being prepared for submission to peer-reviewed journals. This project was led by Geoffrey Weiner, with additional contributions from Sahil Shah, who I thank and will be listed as authors on the manuscript. This work was supported by the NIH and the GRF.

Chapter 3 is an original document written by Geoffrey Weiner with oversight from Jeffrey Goldberg, Richard Daneman, and Eric Nudleman. This project was led by Geoffrey Weiner, with additional contributions from Sahil Shah, who I thank and will be acknowledged if a manuscript is written. This work was supported by the NIH and the GRF.

VITA

2003- 2008	Lake Forest College Bachelor of Arts, Mathematics (major), Biology (minor) *Summa Cum Laude* *Phi Beta Kappa Honor Society*
2008-2010	Rosalind Franklin University Lab of Dr. Dominik Duelli Research Assistant
2010-2012	University of California San Diego, School of Medicine Medical Scientist Training Program, Years 1-2 Medical Student
2012-2017	University of California San Diego, School of Medicine Medical Scientist Training Program, Years 3-7 Neurosciences Graduate Student
2013-2014	The Salk Institute Systems Neurobiology Laboratory Graduate Research
2014-2017	University of California San Diego, School of Medicine Department of Ophthalmology Graduate Research
2018	University of California San Diego Doctor of Philosophy, Neurosciences with a Specialization in Computational Neurosciences
2017-2019	University of California San Diego, School of Medicine Medical Scientist Training Program, Years 7-8 Medical Student

Peer-Reviewed Original Research

Leahy C, Radhakrishnan H, **Weiner G**, Goldberg JL, Srinivasan VJ. Mapping the 3D Connectivity of the Rat Inner Retinal Vascular Network Using OCT Angiography. Invest Ophthalmol Vis Sci. 2015 Sep;56(10):5785-93. doi: 10.1167/iovs.15-17210.

Jepson LH, Hottowy P, **Weiner GA**, Dabrowski W, Litke AM, Chichilnisky EJ. High-Fidelity Reproduction of Spatiotemporal Visual Signals for Retinal Prosthesis. Neuron. 2014:1-6. doi:10.1016/j.neuron.2014.04.044.

Palma J, Yaddanapudi S, Pigati L, Havens M, Jeong S, **Weiner GA**, Weimer K, Stern B, Hastings M, Duelli D. "MicroRNAs are exported from malignant cells in customized particles." Nucleic Acids Res. 2012 Oct 1;40(18):9125-9138.

ABSTRACT OF THE DISSERTATION

Neural-Vascular Interactions in Retinal Development and Disease

by

Geoffrey Aaron Weiner

Doctor of Philosophy in Neurosciences with a Specialization in Computational Neurosciences

University of California San Diego, 2018

Professor Richard Daneman, Chair
Professor Jeffrey L. Goldberg, Co-Chair

The network of blood vessels in the central nervous system is critically important for nutrient delivery and waste removal in higher organisms. A special set of properties distinguishes blood vessels in the central nervous system from those in other organs, because these vessels must provide an extra layer of protection and responsiveness to the real-time demands of neurons. Much is known about way the normal physiology of neurons induces

changes in local blood vessels to re-direct nutrient flow and relieve the buildup of waste products. However, there are many potential interactions between neurons and blood vessels about which we know very little. Whether vessels respond to different types of neuronal dysfunction, and if neural activity plays an important role in development of the vascular network are two such unexplored questions. This dissertation is comprised of several projects which all address the underlying mechanisms, consequences, and applications of, neural-vascular interactions in retinal development and disease.

The aim of the first study (Chapter 2) was to determine whether early spontaneous neural activity is the postnatal mouse retina is related to contemporaneous angiogenesis. We found that activity of the cholinergic retinal circuitry was necessary to establish proper layer-specific vascular development and to turn on blood-retinal barrier properties, and elucidated the signaling pathways involved in this process.

The aim of the second study (Chapter 3) was to determine whether specific injury to neurons in the retina would alter transcription in endothelial and microglial cells. We found a number of transcriptomic changes in these cells that may represent RNA originating from non-microvascular cells.

These studies describe new findings concerning the basis for intercellular communication between neurons and blood vessels in the retina, both during development and disease. A better understanding of neurovascular interactions may promote novel therapeutic strategies and biomarker discovery for blinding diseases of development and aging.

Chapter 1

The Retina as a System to Study Neurovascular Interactions

Abstract

This chapter serves as an introduction to neurovascular interactions. It begins with an introduction to the unique properties of blood vessels in the CNS and retina. It then discusses the connection between neurons and these properties, with a focus on the role of neural activity-driven metabolism in coordinating multiple aspects of neurovascular physiology. Open questions in the field are discussed, and the organization of this dissertation is outlined.

Dissertation Introduction

Blood-retina and blood-brain barrier properties

In the CNS, blood vessels tightly regulate the passage of soluble molecules and cells from the blood into the tissue parenchyma (*1*, *2*). This situation contrasts with peripheral vasculature, where small molecules move relatively freely across the vascular wall, up to specific size and charge limits that typically prevent highly charged molecules and proteins from entering the tissue. This set of properties is called the blood-brain barrier (BBB) in the brain and the blood-retinal barrier (BRB) in the retina, although the two terms may be used interchangeably as no specific differences in molecular function of the two barriers has yet been identified (*3*). Molecular and transciptomic profiling of isolated endothelial cells has revealed genes that are unique expressed at endothelial cells of the CNS. Multiple independently regulated systems contribute to the overall function of the BRB, and it is consistent with the available evidence to think of the BBB in the CNS as both a suppression of 'leaky' properties that may normally be present in peripheral peripheral vessels, combined with an activation of 'tight' properties that are not normally present in peripheral vessels. In addition, the CNS vasculature expresses its own special set of 'leaky' properties that enable the influx of CNS-specific necessary molecules. Many CNS pathologies lead to a breakdown of the BBB, which may constitute a primary insult of the disease process, or a secondary insult that adds damage on top of the primary pathology (*1*, *2*, *4*).

Junctional proteins between endothelial cells in the retina are responsible for preventing paracellular diffusion of small molecules, lipids, and proteins into the retina (*5–7*). At the level of electron microscopy, these junctions appear to fuse the membranes of two neighboring endothelial cells with tightly intertwining strands (*8*, *9*). Major families of junctional proteins that subserve this function in the BRB are adherens, tight junctions, and junctional adhesion molecules (JAMs) (*10–12*). Fenestrations are typical in non-CNS vasculature and in early CNS vessels, but disappear in the CNS in development (*13*). The structure of junctional proteins at the BRB involves tight junctions like Cldn5 and occludin anchored by ZO-1 to the actin cytoskeleton, and adherens junctions like VE-cadherin anchored to the actin cytoskeleton through alpha- and beta-catenin (*3*). The functions of occludin can be modulated by VEGF-induced phosphorylation, which results in increased endocytosis and degradation of junctional proteins and may explain VEGF's role in increasing vascular permeability(*14–17*).

CNS environment in BRB formation

Elegant transplant studies have demonstrated that the CNS microenvironment is responsible for induction of BRB and BBB properties in the CNS (*18*). The CNS is composed of numerous non-endothelial cell types, including neurons, pericytes, astrocytes, microglia, and oligodendrocytes (in the brain but not the retina). Which of these cell types contribute to the environmental cues that support BRB formation? As previously mentioned, Muller glia in the retina are the source of the Wnt ligand norrin that regulates both angiogenesis and barrier formation (*19*). Pericytes secrete Ang1, which acts on endothelial cells to induce tight junction expression (*20*). In co-culture models, pericytes reduce the permeability of primary endothelial cells in part by TGF-B secretion (*21*). Knockdown or expression of a hypomorphic form of platelet-derived growth factor (PDGFR) beta (PDGFR-B) prevents endothelial cell PDGF-

dependent recruitment of pericytes to vessels, is lethal, and leads to massive hemorrhage and edema (*22–24*). Astrocyte-conditioned media, cyclic AMP analogs, and corticosteroids can induce some barrier properties in vitro (*25–28*). In early transplant studies, astrocytes and Muller glia injected into the anterior chamber of rat eyes were vascularized with vessels that did not leak Evans blue or horseradish peroxidase, suggesting that these cells are able to induce barrier properties (*29*, *30*). Importantly though, no culture model fully recapitulates the barrier properties observed in vivo, and many of the proteins and molecules that can induce barrier properties in these models are of uncertain significance in the in vivo physiologic condition.

Molecular signaling in barrier formation and maintenance

Wnt

Very few regulators of BBB properties have been discovered, but Wnt signaling is the main driver of the expression of BBB-related proteins in the CNS (*31*). In canonical Wnt signaling, one of a family of Wnt ligands binds to the extracellular domain of a Frizzled receptor in concert with the Lrp5/6 co-receptor, sequestering Axin and APC at the inner membrane. Axin and APC would normally be targeting beta-catenin for degradation by the ubiquitin-proteasome pathway, but after being sequestered beta-catenin accumulates and travels to the nuclear to induce the transcription of Wnt-related genes (*32*). Wnt7a increases the expression of the transporters Glut-1, Cat1, and Ta1 (*33*), and just as Wnt-dependent angiogenesis across differing CNS regions is mediated by a heterogenous set of receptors and ligands, so is Wnt-dependent acquisition of BBB properties (*34*). Cldn5 may be regulated by Wnt signaling, since its expression is decreased in norrin knockout (*19*).

VEGF

In contrast to Wnt signaling, which is pro-angiogenic and induces BBB properties, VEGF is pro-angiogenic and leads to increased vascular permeability. Many pathological

conditions with elevated VEGF and corresponding retinal edema are effectively treated with anti-VEGF therapy, reducing both the abnormally high angiogenesis and the abnormally high leakiness of the vessels. As previously stated, VEGF may exert its anti-barrier effect by altering occludin regulation (*35*). Alternatively, injecting VEGF into the vitreous of monkey eyes lead to increased permeability and increased ultrastructural evidence of transcytosis, but no increase in endothelial cell fenestrations (*36*, *37*). It may be that VEGF affects vessel permeability at multiple levels of BBB function.

Other pathways

DR6 and TROY, in addition to being involved in angiogenesis, are also involved in barrier function. It is unclear whether this is an effect confounded with the hemorrhagic lesions frequently observed in models of compromised angiogenesis, or a direct effect on the function of BBB-specific properties in endothelial cells. In either case, knockdown of DR6 or TROY increases small molecule leakage into the mouse brain during development and adulthood (*38*). Gpr124 also regulates barrier formation, perhaps by crosstalk with the Wnt/beta-catenin pathway, by controlling Glut1 expression (*39*–*41*).

Neurons and CNS vasculature

Neural activity and metabolism

Most of the energetic demand in the retina originates from neural activity (*42*), specifically the activity of ATP-drive membrane-bound ion pumps (Na/K/ATPase) (*43*) to restore the electrochemical gradient across the membrane after membrane depolarizations. Other functions of the neurons contribute to energy demand, such as protein synthesis (*44*), neurotransmitter trafficking (*45*), and active transport of cellular organelles (*46*), but overall these make minor contributions to energy demand. It is important to note that it is membrane depolarization that drives ATP usage, not necessarily action potential generation. Cells which rarely fire but have extensive dendritic arbors and receive many subthreshold inputs may

consume far more energy that neurons with compact dendrites and strong synaptic connections (*42*). Cytochrome c, which reflects the oxidative capacity of cells (*42*), stains most strongly in cone inner segments and the dendritic layers (*47*). Tetrodotoxin (TTX) inhibition of action potentials in vivo leads to decreased cytochrome c and Na/K/ATPase staining in RGCs, the predominant spiking cells in the adult retina (*48*), demonstrating a linkage between neural activity and metabolism.

In the retina, the link between metabolism and neural activity has been suggested in a number of experiments. Retinal vessels do respond to light-induced activity by adjusting blood flow (*49*). Low oxygen, and thus impaired oxidative metabolism, leads to a decrease in the electroretinogram (ERG) amplitude (*50*) and visual field defects (*51*, *52*). Photoreceptors utilize 2-3 ATP to regenerate each molecule of retinal that isomerizes after absorbing a photon, but this accounts for possibly an order of magnitude less energy consumption than the dark current, which maintains a constant state of depolarization across the membrane (*53*). Perhaps counterintuitively, overall retinal energy consumption increases in the dark (*54–56*), presumably because of the large contribution of dark current to overall retinal energy consumption.

Dissertation Organization

Chapter 2 introduces work done on the role of starburst amacrine cells and cholinergic retinal waves in establishing the developing retinal vasculature in the mouse. Chapter 3 introduces work done on the response of retinal microvascular cells to whole-retinal injury.

Acknowledgements

This chapter is an original document written by Geoffrey Weiner with oversight from Jeffrey Goldberg and Richard Daneman. Geoffrey Weiner is supported by a fellowship from

the San Diego Foundation. Jeffrey Goldberg is Chair of Ophthalmology at Stanford University and is supported by the Foundation Fighting Blindness, the Glaucoma Research Foundation, and the NIH. Richard Daneman is Assistant Professor of Pharmacology at UCSD.

Chapter 2

Retinal Waves Regulate Angiogenesis, Blood-Retinal Barrier Formation, and Metabolism in the Developing Retina

Authors

Weiner GA, Shah SS, Daneman R, Goldberg JL.

Abstract

Blood vessels in the central nervous system (CNS) develop unique features not found elsewhere in the vascular system. These include the ability to adjust blood flow to match the metabolic demand of local neuronal activity and the maintenance of extracellular CNS homeostasis by expressing the set of properties known as the blood-brain- or blood-retinal-barrier (BRB). What role does neural activity play in establishing these properties? During postnatal development in the mouse, endothelial cells are rapidly proliferating and migrating through the retina and acquiring these properties. At the same time, waves of patterned electrical activity are sweeping across neurons in the retina, driven by distinct neural circuits that change over time. Although these two events are occurring contemporaneously, it is not known whether they are related. Here we report that inhibiting cholinergic activity during the period of cholinergic retinal waves selectively prevents growth of one of the vascular plexuses and leads to BRB breakdown. Pharmacologic blockade of cholinergic activity and starburst amacrine cell-specific depletion profoundly inhibits the ability of the superficial retinal vasculature to invade the deeper layers of the retina, and leads to increased vessel permeability. VEGF, a regulator of endothelial cell growth, and norrin, the Wnt ligand that induces BRB properties in the retina, are decreased after activity blockade. Restoring VEGF by injection of recombinant protein and Wnt signaling by expressing stabilized beta-catenin in endothelial cells rescues the effects of activity blockade on vessel growth and BRB function, respectively. Our findings suggest that retinal waves lie upstream of developmental VEGF and norrin production, and play a coordinating function between angiogenesis and BRB formation. Neural activity originating from distinct neural circuits may be a general mechanism for

driving angiogenesis and barrier formation across multiple CNS regions and developmental timescales.

Introduction – retinal waves

Spontaneous correlated activity during development

In adult mammals the retina is the primary organ for sensory transduction of visual signals. During development there is a period in some animals when retinal neurons, even though not yet capable of full phototransduction, have spontaneous propagating activity (*1*–*3*). This activity is mediated by a succession of distinct neural circuits (*4*, *5*), is usually observed at the level of RGCs, and occurs in many species including rabbit (*6*), turtle (*7*), chick (*8*), primate (*9*), mice (*10*), and ferret (*1*). In mice, from E16 to P0, non-synaptic mechanisms (gap-junction coupling between RGCs) predominate. Around P0 cholinergic cells take over the task of driving retinal waves, and this period lasts until P11. From P11 to P14 glutamatergic-driven activity takes over. Intriguingly, each stage of circuit maturation appears to be causally linked to the end of the previous stage (*11*, *12*). For example, preventing the onset of glutamatergic waves by deletion of VGlut1 extends the period of cholinergic activity from P11 to P14 (*13*). Similarly, deletion of nicotinic receptor subunits required to propagate cholinergic activity (alpha-3 and beta-2) leads to an extension of the period of non-synaptic activity (*4*, *14*, *15*).

Cholinergic circuitry

One of the earliest neural circuits to develop in the retina is the cholinergic circuit. Acetylcholine (ACh) was the first neurotransmitter discovered. Its functions both inside and outside of the nervous system are well-described and include classic neurotransmission at the neuromuscular junction, differentiation and cell cycle control, and regulation of immune function. ACh acts on one of two distinct subgroups of receptors - the nicotinic acetylcholine

receptors (nAChRs) or the muscarinic acetylcholine receptors (mAChRs). nAChRs are ligand-gated ion channels, but mAChRs are G-protein coupled receptors (GPCRs). Cholinergic neurons are responsible for the previously described retinal correlated activity from P0 to P11, and contribute to the establishment of neural circuits that utilize other (non-acetylcholine) neurotransmitters. Acetylcholine (Ach) in the retina is particularly interesting because of the seven neuronal types and dozens of subtypes (*16*) of each neural type in the retina, only one subtype of amacrine cells - the starburst amacrine cell (SAC) - expresses the enzymatic machinery necessary to produce Ach (*17*). SACs are extensively studied in both anatomical and physiological detail (*18–20*). SACs are distributed in two layers of the retina - the OFF subtype has its cell bodies in the INL and the ON subtype has its cell bodies in the GCL. In adult animals, SACs are an integral part of the direction-selective computation circuit (*21*) and Ach modulates the activity of ganglion cells (*22–24*). Importantly, during the phase of correlate cholinergic activity from P0 to P11 SACs and RGCs express functional nAChRs that respond to SAC-derived ACh (*25*), but in adults only non-SAC cells express a mix of mAChRs and nAChRs and SACs are no longer responsive to ACh or nicotinic agonists. During development, nAChR subunit transcripts have been detected widely distributed in the retina, and mitotic precursor cells have mAChR-dependent calcium responses (*26*, *27*).

SACs initiate cholinergic activity by having regular spontaneous depolarizations (*28*). A retinal wave then spreads through the cholinergic network at both the level of SACs and level of RGCs. Propagation of the wave is dependent on alpha-3 and beta-2 but not alpha-7 nAChRs (*29*). It is thought that volume transmission of acetylcholine plays an important role in the propagation of waves. This is the concept that ACh may be released at nonfunctional or functional synapses and may diffuse away from the site of the synapse and exert action at a receptor distant from the initial synapse. Waves are a potential example of volume transmission, because activity in cells distant from the canonical cholinergic synapses has

been observed to correlate with classical cholinergic activity. Examples include alignment of RGC dendritic arbors (*30*), slow electrophysiologic responses of connected SACs revealed during paired recordings (*25*), the lack of ultrastructural evidence for functional synapses during the early period of cholinergic waves (*31*), and calcium waves in the ventricular zone that synchronize with local wave activity (*32*). ACh spillover from cholinergic synapses can also initiate mAChR-dependent calcium elevations in glial cells (*33*). After the period of cholinergic waves, SACs become insensitive to nicotine (*22*) and retinal expression of acetylcholinesterase increases (*34*).

Functions of early cholinergic retinal activity

Cholinergic waves are occurring during a developmental window in the retina when many changes are happening, and thus have the potential to influence or be involved in these processes. Three major functions of early cholinergic retinal activity have been described. One is the refinement of retinal projections back to the LGN and SC. Early in development retinal projections to these brain relay regions from both eyes overlap. During maturation the projections from the two eyes retract from each other and come to occupy mostly non-overlapping anatomical territory. This is referred to as 'eye-specific segregation', and retinal waves play an important role in shaping the phenomenon by providing clues as to which projections may be arising from the same eye (due to their propensity to have action potentials in close temporal proximity during periods of correlated activity) (*35–37*). Another function is the refinement of intraretinal connections. The IPL is forming from P0 to P10 in mice, and the IPL contains all the dendrites and synapses between amacrine and bipolar cells and RGCs. Part of this formation is lamination. Although the IPL appears to be a mess of neuronal processes, the processes from different neuronal subtypes are placed at characteristic locations within the IPL. In particular, ON-pathway (cells which increase their activity in response to light increments) and OFF-pathway (cells which increase their activity in response to light

decrements) stratify in distinct bands with the IPL. The final stratification is the result of a stepwise process that includes an initial overgrowth of RGC dendrites followed by a pruning back to allow ON- and OFF-RGCs to remain only in the appropriate layer (reviewed in (*38*)). Circumstantial evidence suggests that SAC activity may direct IPL stratification. SACs do not overgrow their processes past the intended IPL sublayer (*39*) and RGCs specifically target the layers of pre-existing SAC processes (*40*). Pharmacological blockade of the nAChRs reduces RGC dendritic motility (*41*) and prevents dendritic outgrowth (*42*). Another function of cholinergic waves is the refinement of retinotopy in the LGN in rodents (*43*), but not in ferrets.

Retinal angiogenesis

Anatomical formation

Mouse retina is commonly used as a model system for both pathological and developmental angiogenesis (*44–46*) in the context of the central nervous system (CNS). Partly practical, because mice are born with an undeveloped retinal vasculature that rapidly develops to maturity in the first two postnatal weeks (*47*). Full maturation of the vascular circuit requires regression of the hyaloid vasculature, vessels that connect the inner retinal blood supply to the lens during development (*48*). Inner retinal vasculature matures along a well-stereotyped trajectory in C57/BL6 mice and other strains, but C57/BL6 are the most well-studied (*44*, *49*). Endothelial cells invade the retina from the optic nerve head (ONH) and spread out peripherally by a combination of proliferation and migration. From P0 until roughly P8, these endothelial cells are confined to the ganglion cell layer (GCL) and nerve fiber layer (NFL), forming what is also known as the superficial vascular plexus or superficial layer, which contains a dense capillary network alongside well-specified vein and artery branches. Beginning around P7 and ending around P13, endothelial cells begin diving deeper into the retina, turning away from the superficial plexus and sprouting until they reach the proximal border of the inner nuclear layer (INL), forming another capillary plexus known as

the deep layer. Sprouting of the deep layer also occurs radially from the ONH outward. The final capillary plexus to form is at the distal border of the INL - the intermediate or middle layer - from P12 to P15. In contrast to the superficial and deep plexuses, the middle layer appears to sprout off the penetrating vessels that connect the superficial and deep layers, as opposed to a new set of sprouts coming from either the superficial or the deep layer. Development of the middle layer does not proceed radially, but rather at all points in the retina all at once. Further refinement of the vascular network occurs until around P21, when the network is considered to be in its fully mature form (*50*).

Molecular signaling in angiogenesis – Wnt

Wnt signaling has been demonstrated to be involved at multiple steps in retinal angiogenesis, including Wnt7b and its receptor Fzd5 being required for regression of the hyaloid vessels (*51*, *52*). Wnt-dependent angiogenesis uniquely differentiates CNS angiogenesis from angiogenesis in other organ systems (*53*, *54*). Other Wnt signaling components - Fzd4, Lrp5/6, Tspan12, and Norrin, have been shown to be required for normal intraretinal vascular development (*55–57*). Norrin is secreted by Muller glia and activates canonical Wnt signaling cell autonomously by binding to Fzd4 on endothelial cells (*57*). Human retinal vascular abnormalities observed in Norrie disease (ND) and familial exudative vitreoretinopathy (FEVR) mimic the defects seen in mouse model Wnt-pathway knockouts (*56*, *58–64*). Wnt ligands and receptors are comprised of a large family of proteins, and they show different expression patterns and specificities for different regions of the CNS, also varying by developmental stage (*53*, *65*). Norrin is not only important for retinal angiogenesis, but also inner ear angiogenesis and placental angiogenesis (*66*, *67*).

Molecular signaling in angiogenesis – VEGF

Vascular endothelial growth factor (VEGF) is one of the most important and well-characterized signaling molecules in angiogenesis, both physiological and pathological. VEGF

expression is normally localized to NFL astrocytes just past the leading edge of vessel development during superficial layer formation, and to presumptive Muller glia cell bodies in the INL closely preceding deep layer formation(*68*). The gradient of VEGF created by this expression pattern has been shown to be a vascular guidance cue for filopodia extending from endothelial tip cells (*69*). No reports have described the expression pattern of VEGF that correlates with middle layer development. By regulating the oxygen content of the housing environment of animals, VEGF expression has been shown to be regulated by hypoxia. It is presumed that physiologic relative hypoxia during development is driven by neural activity, but this has never been demonstrated experimentally. Multiple VEGF isoforms have been shown to have different effects on vascular development, including a role in normal arteriovenous patterning (*70*).

Molecular signaling in angiogenesis – Notch and other pathways

Notch signaling, a pathway involved broadly in patterning and growth, regulates the sprouting behavior of endothelial tip cells through competitive antagonism between the Notch ligands Jagged1 and Dll4 (*71*, *72*). Notch and VEGF signaling may interact by VEGF-mediated inhibition of Dll4 (*73*). Gpr124, an orphan G-protein coupled receptor (GPCR) was shown to be required for normal CNS angiogenesis, and may interact with the transforming growth factor beta (TGF-B) pathway (*74–76*). DR6 and TROY, receptors that were found to be enriched in CNS vasculature, play a role in linking VEGF and Wnt signaling by both regulating VEGF-induced Jnk activation and themselves being activated by Wnt signaling (*77*). This may suggest that VEGF-induced angiogenesis is gated by Wnt signaling to ensure that barrier properties are turned on as soon as vasculature is present.

Neurons and glia in angiogenesis

Neurons have been shown to play a direct role in angiogenesis in various regions of the CNS and peripheral nervous system (PNS). There is a hypothesized link between neural

activity, relative hypoxia, VEGF production, and angiogenesis. In the PNS, it has been shown that VEGF-A and Cxcl12 produced by neurons regulate arterial differentiation and alignment of vessels to neurons in developing limb skin, respectively (*78*). Vascular morphology is dependent on the gradients of VEGF-A present in the extracellular environment (*69*, *79*), and it has been shown in the retina that retinal ganglion cells expressing VEGF receptors are responsible for maintaining the appropriate amount and distribution of VEGF (*80*).

Retinal metabolism

Retinal energy demands

The CNS consumes a disproportionate amount of energy in the body - 20% of total energy consumption but comprises only 2% of the body weight (*81*). The retina is thought to consume energy at an even higher amount of energy per unit weight than the brain (*82*, *83*) and has an enormously high production of lactate (*84*, *85*). Such a high energy consumption demands that energy substrates such as glucose and oxygen be constantly and efficiently delivered to the tissue, and waste products removed. Visual function is exquisitely sensitive to lack of oxygen. Retinal ischemia results in loss of vision in 4 to 9 seconds, far shorter than any other CNS function known to be sensitive to oxygen (*83, 86*). Neuroglobin, a CNS-specific oxygen-binding protein with higher affinity than hemoglobin or myoglobin, is 100 times more concentrated in the retina than the brain (*87*). The retinal vascular network, properties of which have already been described, is the main pathway by which these goals are accomplished. One reason for the high metabolic demand of the retina is the constant maintenance of ion gradients across the cells in preparation for phototransduction and neural transmission, which has been demonstrated by studies involving in vitro preparations of retina in the light and dark, both before and after mature visual circuits have formed (*84, 88, 89*). Retinal anatomy dictates that there are two different compartments of metabolic activity, which exist independently of activity in the other. Photoreceptors and Muller glial processes -

the so-called outer retina - receive oxygen from the choroidal circulation, while all other cells of the retina receive oxygen from the intraretinal vessel (*90*). Measurements of energy substrates and breakdown products into and out of the two different retinal circulations give some clue about the relative contributions of oxidative and glycolytic metabolism in the two compartments (*91*). The outer retina consumes more glucose and produces more lactate than the inner retina, although their overall oxygen consumption is similar (*92*), which suggests an anaerobic metabolic component not present in the inner retina. Meeting the energy demands of neurons is important, because neurons are known to be far more sensitive to hypoxia than glial cells (*93*).

Crosstalk between metabolism, angiogenesis, and BRB formation

How do the pathways that govern metabolism, angiogenesis, and barrier properties interact? One clue comes from recent studies on metabolic substrate utilization. Retinal neurons are obligate users of glucose (*94*), though they may also use Muller glia-derived lactate in vivo, and recently it was discovered that photoreceptors can use beta-oxidation of free fatty acids (FFAs) for energy (*95*). As previously described, the BRB tightly regulates the flux of molecules into the retina, including glucose. Therefore it is necessary to have glucose transporters (GLUTs) and lipoprotein receptors expressed at the BRB to supply enough substrate to the tissues. Glucose shuttling is accomplished by in the retina primarily by GLUT1 (*96*, *97*), which is also expressed on the membrane of photoreceptors (*98*), Muller glia (*96*), and RGCs. GLUT3 has been found expressed in the dendritic retinal layers (*99*). Experimentally manipulating neural activity can alter the expression of GLUT1 at the BBB (Robert Pulido, unpublished observations), suggesting a connection between the metabolic requirements of neural activity and BBB function.

Disruption of normal retinal metabolism can have downstream effects on angiogenesis and BRB function, demonstrating a linkage between these basic aspects of physiology.

Knockout of the Vldlr receptor prevents circulating FFAs from being used for energy by photoreceptors, but Ffar1 responds to the increased levels of circulating FFAs by suppressing GLUT1 expression, leading to an Hif1-alpha (Hif1a) stabilization, over-production of VEGF, and consequent pathological angiogenesis and BRB dysfunction (*95*). In this scenario, it is not hypoxia that drives VEGF but rather the lack of the metabolic substrate alpha-ketoglutarate (aKG), generated during the TCA cycle, that prevents Hif1a from being degraded (*100*). A deficit of either oxygen or aKG, which are both metabolic substrates, can lead to VEGF production. Hypoxia and hyperoxia models, which directly alter the ability of the retina to do oxidative metabolism, have well-described effects on angiogenesis and the BRB. Oxygen-induced retinopathy (OIR) is a mouse model of the human disease retinopathy of prematurity (ROP). In OIR, P7 mice - where the superficial vascular layer is developed, but the deeper layers are not - are placed in a hyperoxic environment that leads to obliteration of the newly developed vessels and angiogenic arrest, presumably due to increased retinal PO2 and reduced physiologic hypoxic drive. On return to standard 20% oxygen room air a neovascular phenotype develops with preretinal buds vascular buds that leak and hemorrhage and, in ROP, retinal detachment and loss of vision can ensue. What is the contribution of metabolic supply flux to these phenotypes? This question is largely unaddressed, and it is commonly assumed that high oxygen PO2 alters the normal relative hypoxic drive that leads to Hif1a stabilization and VEGF production, and this explains the vaso-obliterative phase of the model. However, the only study of in vivo oxygen measurements in the OIR model failed to find a difference in PO2 in rats at the height of neovascularization (*101*). Whatever the underlying pathophysiology, it is clear that altering metabolic inputs into the retina can have dramatic consequences on angiogenesis and BRB function.

Role of the present study

We recognized that the stages of layer-specific vascular formation are occurring contemporaneously with the progression of neural circuit maturation (Figure 2.1A). To further understand the relationship between this early neural activity and vascular function we examined the role of starburst amacrine cell activity in developmental angiogenesis during the period of cholinergic waves. We used multiple approaches to modulate SAC activity and measured the impact on vascular growth, BRB function, metabolism, and the molecular pathways associated with these phenotypes.

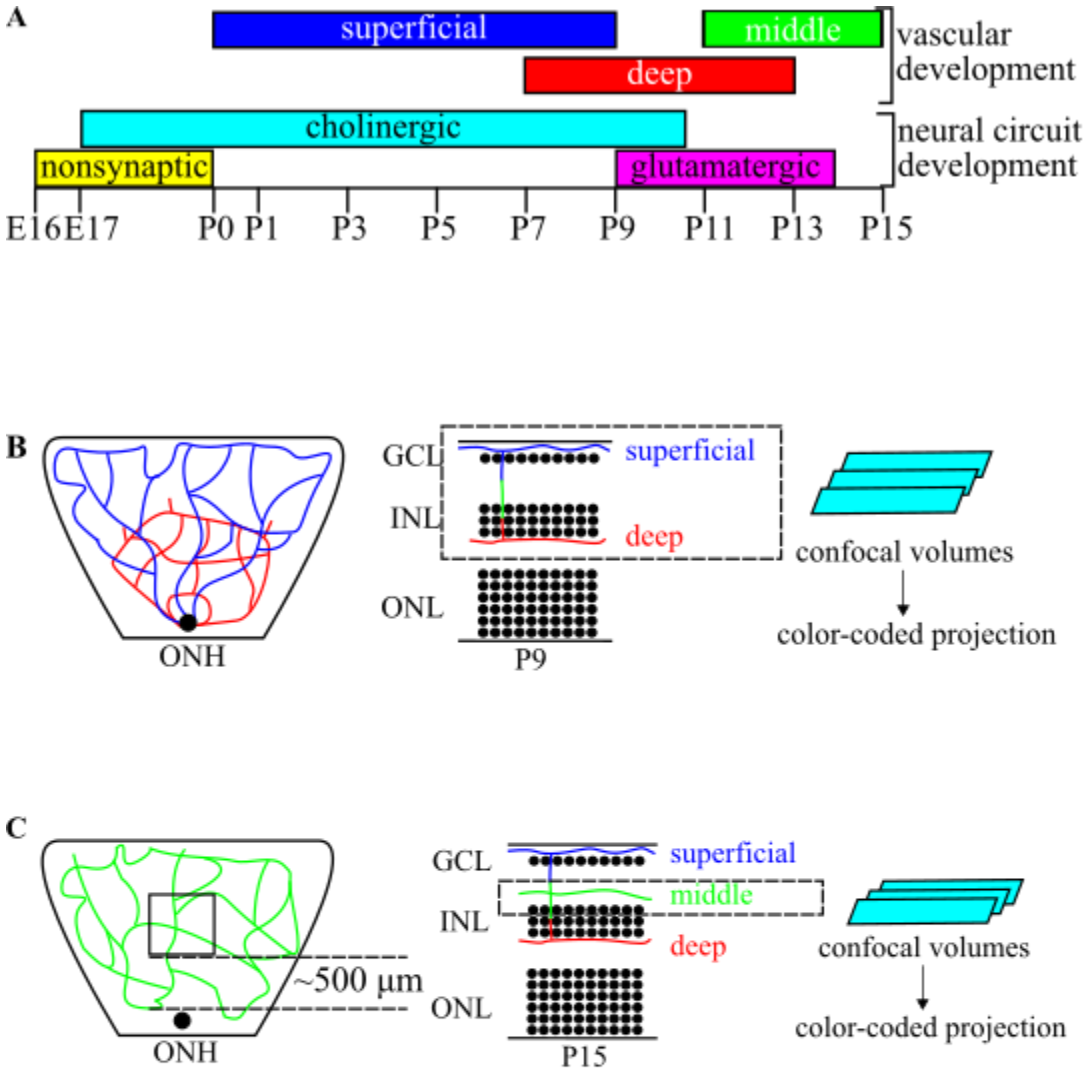

Figure 2.1. Retinal waves and angiogenesis overlap during development. (A) Neural circuit maturation in the retina does through three stages: non-synaptic, cholinergic, and glutamatergic. Vascular development in to the retina also proceeds in three stages: superficial layer first then the deep layer, then the middle layer. (B) Confocal imaging strategy for retinas imaged at P9 after activity modulation from P3 to P9. At P9 the superficial layer covers the entire retinal surface, there is no middle layer, and the deep layer covers ~50% of the retinal area. The superficial layer is located in the ganglion cell layer (GCL) and nerve fiber layer. The deep layer is located just below the inner nuclear layer (ONL). (C) Confocal imaging strategy for the middle layer by sampling 500 uM eccentric from the optic nerve head (ONH). The middle layer is located just above the INL. ONL, outer plexiform layer.

Results

Inhibition of SAC activity prevents deep layer formation

We tested whether SAC activity was required for normal vascularization of the retina. Cholinergic retinal waves partially overlap in development with the formation of the superficial (P0 to P9) and deep (P7-P13) vascular plexuses. Layer-specific quantification of vessel growth can be achieved by confocal imaging. At P9, the the superficial layer completely covers the retinal surface and the deep layer extends from the optic nerve head to cover 30-50% of the retinal area, and can be visualized by color-coded depth projections of confocal volumes (Figure 2.2B). At P15 all 3 capillary layers are extensive at their respective depths in the retina, but the middle layer can be selectively imaged with confocal volumes (Figure 2.2C). Because the middle layer does not develop concentrically like the other layers, we quantified the vessel density in a ~2.5 mm^2 patch halfway between the ONH and retinal edge. We took three approaches to the inhibition of neural activity: 1) pharmacologic inhibition by epibatidine (EPI), tetrodotoxin (TTX), and 2-amino-4-phosphonobutyric acid (APB); 2) targeted-toxin mediated depletion of SACs; and 3) expression of an engineered receptor in SACs capable of inhibiting SAC activity (ChatGi). EPI, but not TTX or APB, reduced deep layer coverage from 45.6% to 2.2% ($p = 3.41x10^{-8}$) and had no effect on superficial layer formation (Figure 2.2). ChAT-SAP but not the untargeted toxin IgG-SAP reduced deep layer coverage from 43.8% to 2.4% ($p = 1.6x10^{-10}$) and had no effect on superficial layer formation (Figure 2.2). No treatment affected the growth of the middle layer, measured at P15 (Figure 2.3). Taken together, this suggests that cholinergic activity from P3 to P9 is required for deep-layer angiogenesis but is dispensable for superficial and middle layer formation (once the deep layer has formed).

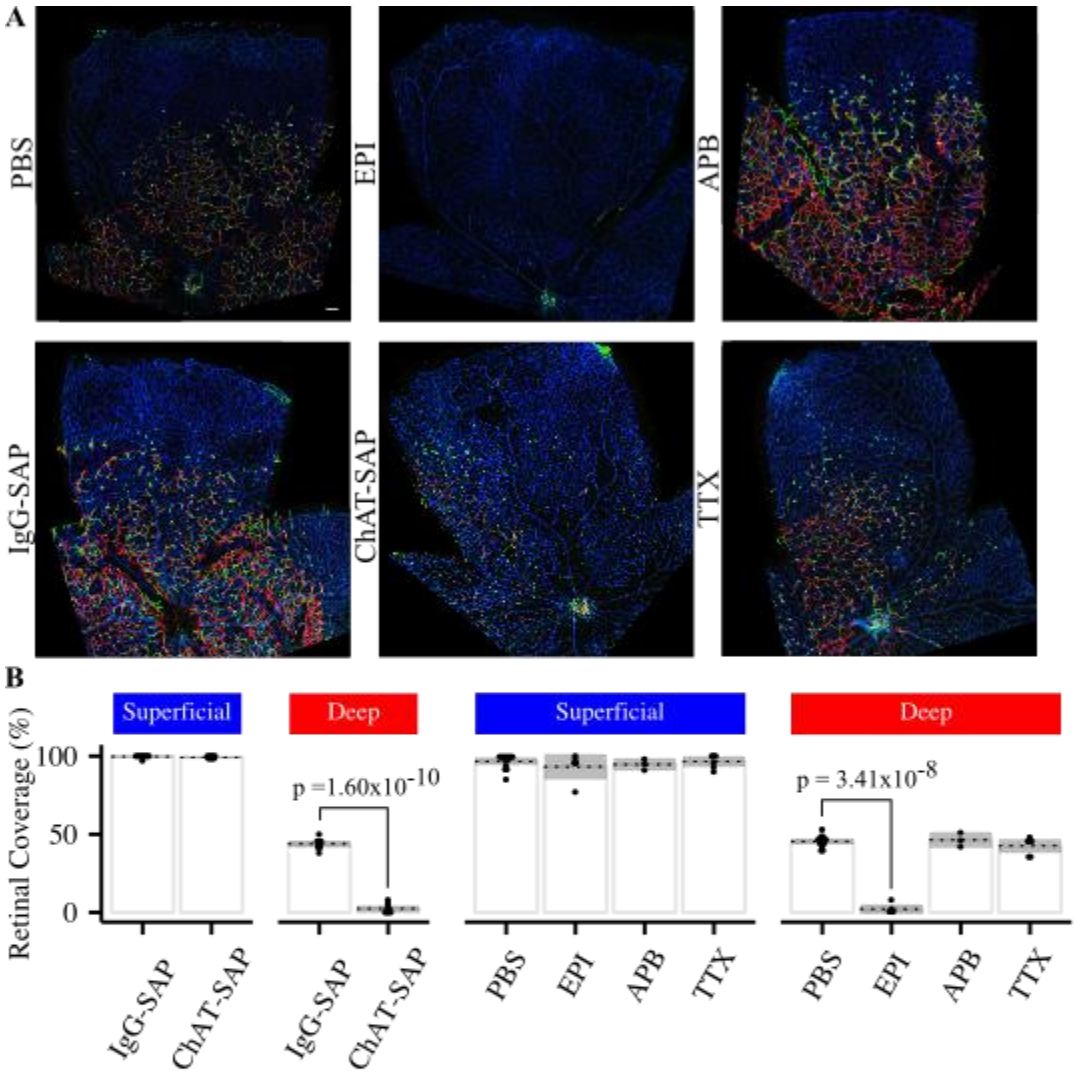

Figure 2.2. Inhibition of starburst amacrine cell (SAC) activity prevents deep vascular plexus formation. (A) Inhibition of SAC activity from P3 to P9 by targeted-toxin mediated depletion of SACs and pharmacological inhibition prevents formation of the deep vascular plexus, but has no effect on the superficial layer. A glutamatergic antagonist and TTX had no effect on vascularization. (B) Quantification of the coverage of the deep and superficial layers at P9 after interventions during the cholinergic period. ChAT-SAP and epibatadine (EPI) were both significant. Statistical tests are Student's two-tailed t-tests, paired when comparing control and treated eyes from the same animal, otherwise assuming unequal variances. All other comparisons were not significant. PBS data is from the set of animals injected with EPI but statistical tests on each treatment were vs fellow eye. Plot shows the mean (hatched line), individual data points (points) and 95% confidence interval (gray box). IgG-SAP, immunoglobulin G conjugated to saporin (untargeted control); ChAT-SAP, anti-choline acetyltransferase conjugated to saporin; PBS, phosphate buffered saline (vehicle control); APB, 2-amino-4-phosphonbutyric acid; TTX, tetrodotoxin.

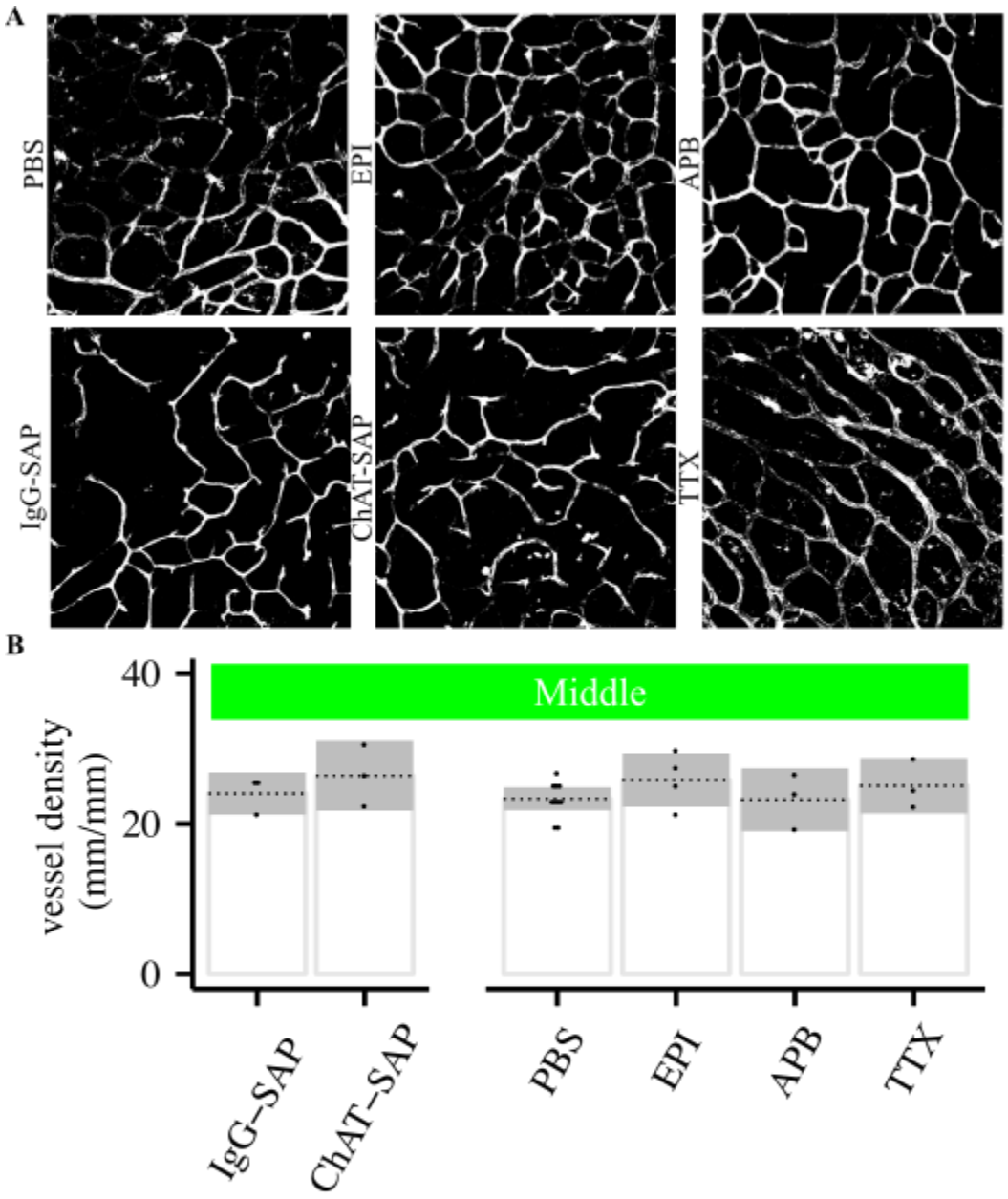

Figure 2.3. Inhibition of starburst amacrine cell (SAC) activity has no effect on middle vascular plexus formation. (A) Inhibition of SAC activity from P11 to P15 by targeted-toxin mediated depletion of SACs and pharmacological inhibition does not prevent formation of the middle vascular plexus. (B) Quantification of the middle layer after interventions during the glutamatergic period. All statistical tests were not significant. Statistical tests are Student's two-tailed t-tests, paired when comparing control and treated eyes from the same animal, otherwise assuming unequal variances. PBS data is from the set of animals injected with EPI but statistical tests on each treatment were vs fellow eye.

Inhibition of SAC activity disrupts the BRB

We assessed the integrity of the BRB by NHS-biotin perfusion and quantification of extravascular NHS-biotin fluorescence. SAC activity was inhibited using the same 3 techniques previously described, either from P3 to P9 or from P11 to P15. EPI, but not TTX or APB, led to increased extravascular NHS-biotin fluorescence from 2.1 arbitrary units (AU) to 17.2 AU ($p = 3.58x10^{-10}$). ChAT-SAP, but not IgG-SAP, led to increased NHS-biotin fluorescence from 1.5 AU to 11.8 AU ($p = 0.005$).

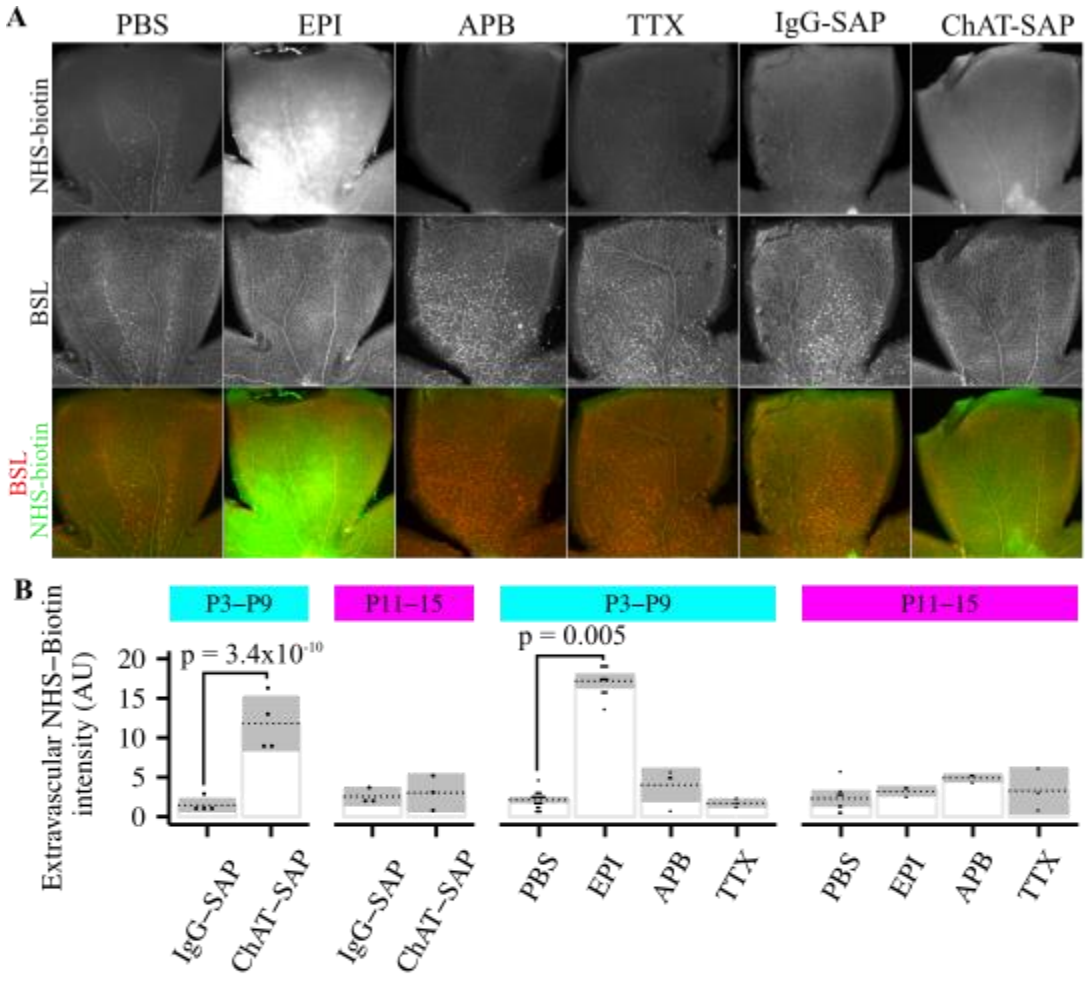

Figure 2.4. Inhibition of starburst amacrine cell (SAC) activity during the cholinergic period leads to increased NHS-biotin leakage. (A) Inhibition of SAC activity from P11 to P15 by targeted-toxin mediated depletion of SACs and pharmacological inhibition does not prevent formation of the middle vascular plexus. (B) Quantification of the middle layer after interventions during the glutamatergic period. All statistical tests were not significant. Statistical tests are Student's two-tailed t-tests, paired when comparing control and treated eyes from the same animal, otherwise assuming unequal variances. PBS data is from the set of animals injected with EPI but statistical tests on each treatment were vs fellow eye.

To distinguish BRB dysfunction from frank hemorrhage we looked for the presence of extravascular red blood cells (RBCs) after EPI injection by Ter119 immunofluorescence staining. We never observed an extravascular RBC in any condition, but we did find an increase in the number of intravascular RBCs from 0.4 RBCs/field to 4.6 RBCs/field ($p = 3.73x10^{-4}$) after transcardial perfusion (Figure 2.5).

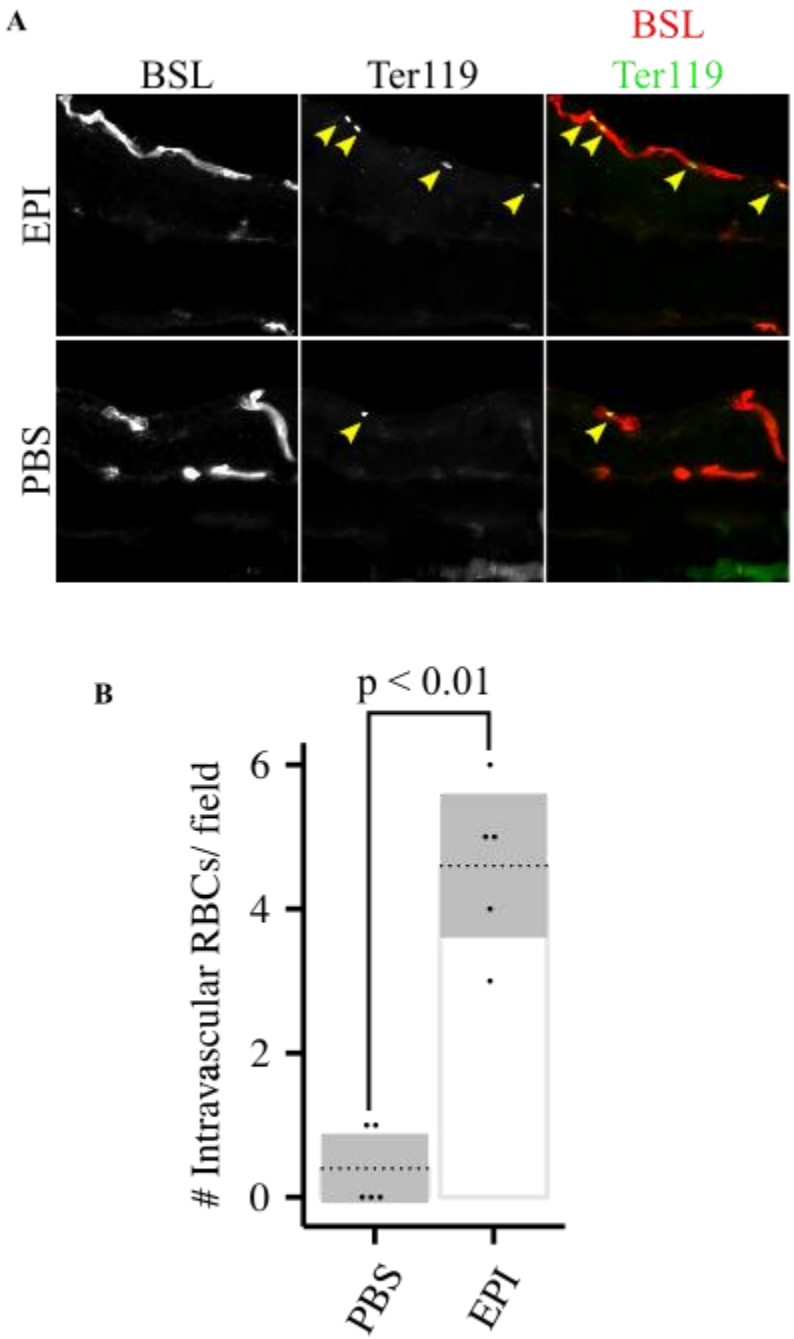

Figure 2.5. SAC inhibition does not lead to hemorrhage, but does produce an increase in intravascular RBCs after perfusion. (A) No extravascular RBCs, visualized by Ter119 staining, were present after transcardial perfusion after EPI or PBS injections from P3 to P9. There were more RBCs remaining intravascularly after perfusion. Arrowheads indicate individual RBCs within formed vessels. (B) Quantification of the number of intravascular RBCs. Statistical test is the Mann-Whitney U.

Cldn5 is known to regulate BRB permeability to small molecules like NHS-biotin, so we examined Cldn5 expression by immunofluorescence after EPI injection. We found that although most retinal vessels still expressed Cldn5, some evidence of altered Cldn5 expression was apparent. We observed two alterations: 1) breaks in continuous Cldn5 expression along a single junctional line, and 2) loss of Cldn5 expression along short vessel segments (Figure 2.6). The number of Cldn5 gaps increased from 1.5 gaps/mm vessel in PBS injected eyes to 5.6 gaps/mm vessel in EPI injected eyes ($p = 0.0019$). The amount of Cldn5- vasculature increased from 0.2 mm vessel/mm^2 retina in PBS injected eyes to 1.9 mm vessel/mm^2 retina ($p = 9.3x10^{-4}$) after EPI injection.

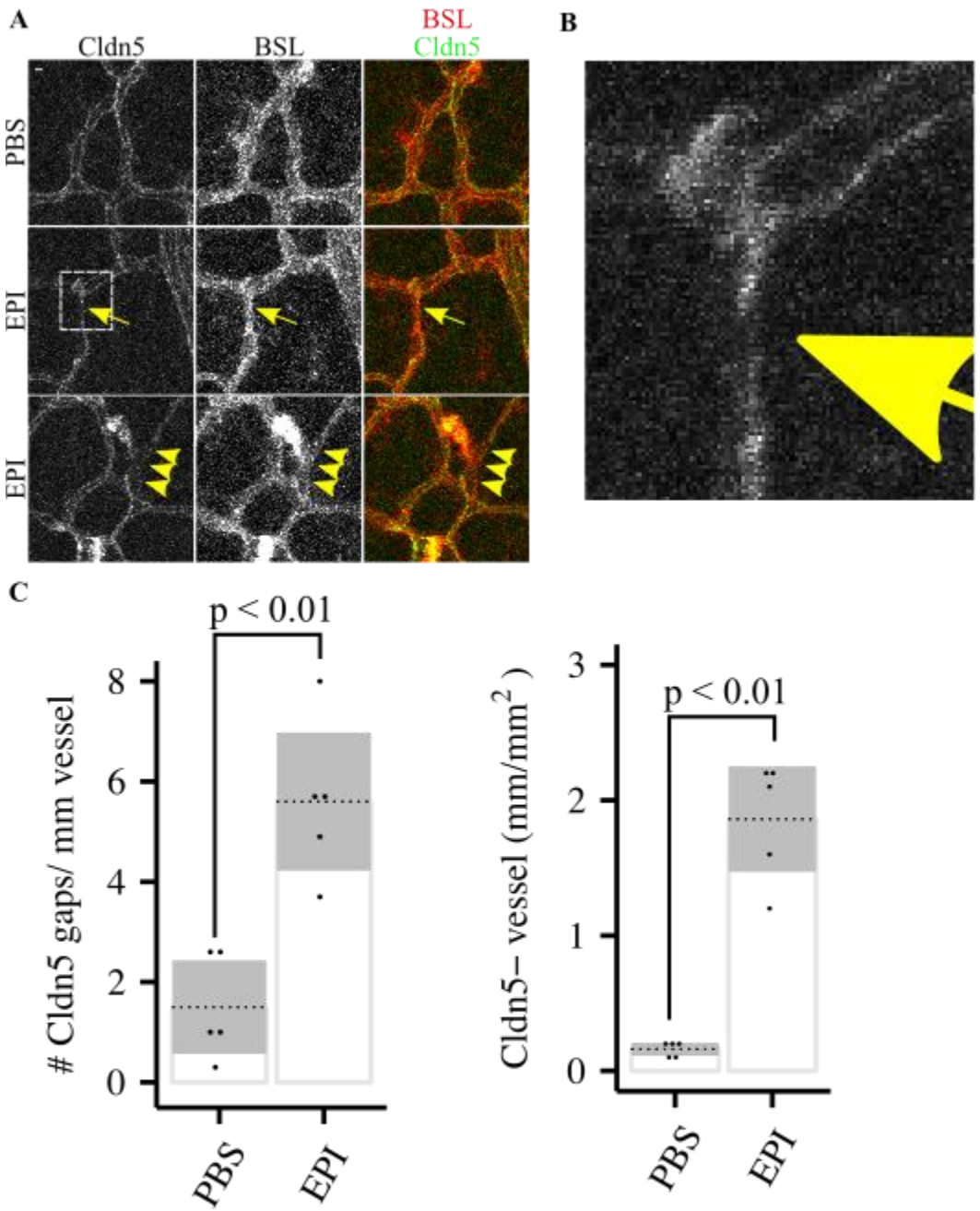

Figure 2.6. Inhibition of starburst amacrine cell (SAC) activity during the cholinergic period perturbs Cldn5 expression. (A) Breaks in continuous junctional strands (middle row, arrow) and loss of Cldn5 across small vascular segments (bottom row, arrowheads) were observed after EPI injection. (B) Zoomed-in view of the junctional strand gap boxed in (A). (C) These Cldn expression patterns were rarely observed in PBS injected eyes, but significantly increased after EPI injection. Statistical tests are the Mann-Whitney U test.

Taken together, this suggests that cholinergic activity from P3 to P9 is required for proper BRB function, patency of the vasculature, and Cldn5 expression.

Cholinergic activity regulates VEGF, Wnt signaling, and metabolism

VEGF is an important regulator of developmental angiogenesis in the retina, and norrin is the retina-specific Wnt ligand required for BRB function. We assessed whether EPI injection decreased the expression of VEGF and norrin by western blot and found a 3.2-fold reduction ($p = 0.039$) in VEGF and a 6.6-fold reduction ($p = 0.023$) in norrin (Figure 2.7).

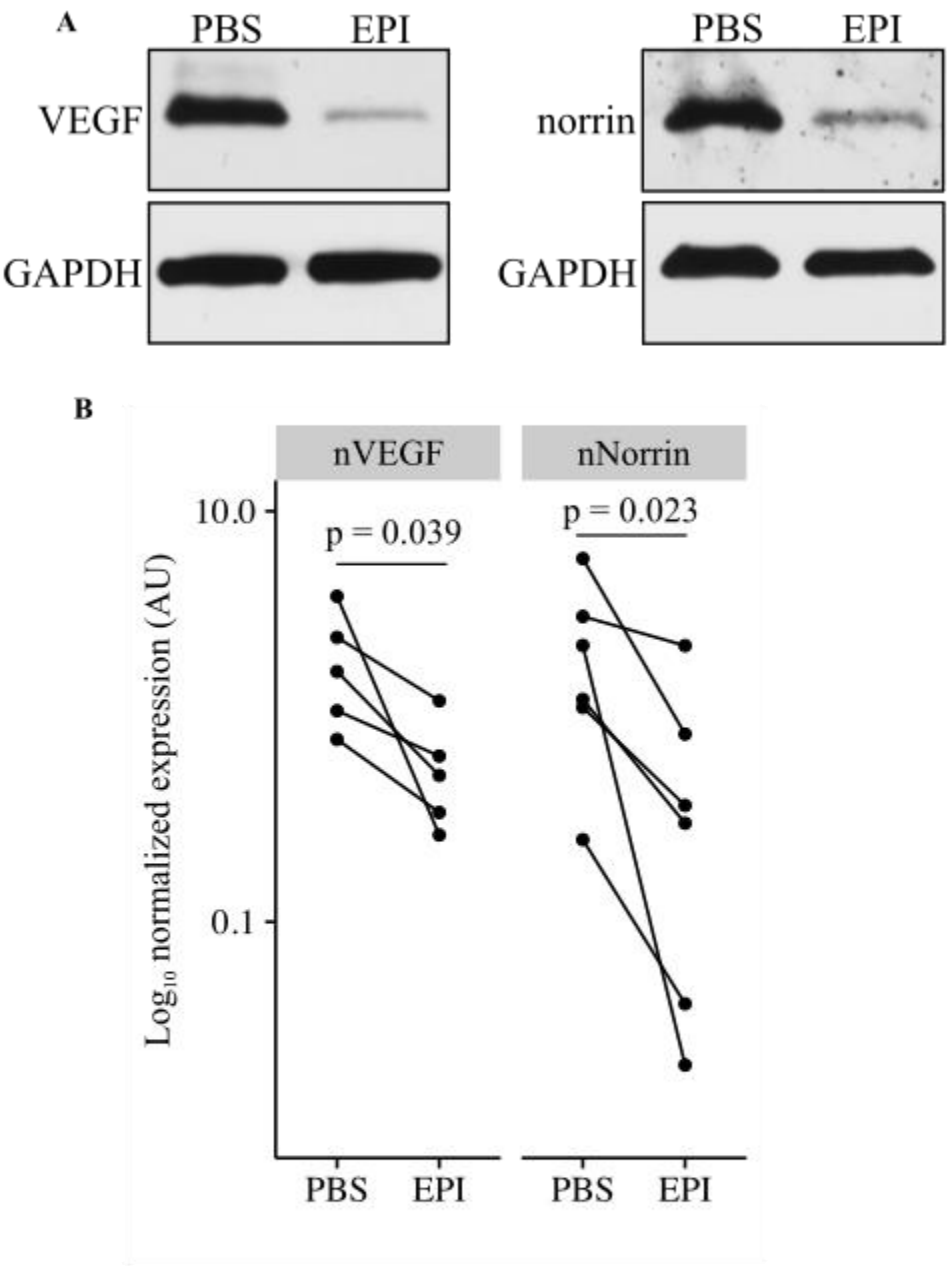

Figure 2.7. Inhibition of starburst amacrine cell (SAC) activity during the cholinergic period decreases VEGF and norrin. (A) Expression of the pro-angiogenic signaling molecule VEGF is decreased (3.2-fold), as is the barrier-inducing Wnt-ligand norrin (6.6-fold) after inhibition of SAC activity from P3 to P9. Connected points are left and right eyes from the same animal. (B) Zoomed-in view of the junctional strand gap boxed in (A). (C) These Cldn expression patterns were rarely observed in PBS injected eyes, but significantly increased after EPI injection. Statistical tests are the Mann-Whitney U test.

To determine whether the decrease in VEGF and norrin expression were causative in the angiogenic and barrier defects we previously observed, we performed rescue experiments. For VEGF rescue, recombinant VEGF protein was co-injected intravitreally with EPI. For Wnt-pathway rescue, we expressed a stabilized form of beta-catenin (BGOF) in endothelial cells under the control of the VE-cadherin CreERT2 promoter (VECre+;BGOF). We also used i.p. injections of lithium chloride (LiCl) to stabilize beta-catenin activity - LiCl has been shown to stimulate beta-catenin signaling in retinal endothelial cells (*102–104*) and restore vascular function under some disease conditions (*105*). VEGF, but not BGOF or LiCl restored some EPI-inhibited deep layer angiogenesis, from 1.3% to 20.7% retinal coverage ($p = 0.039$, Figure 2.8). BGOF and LiCl, but not VEGF, reduced EPI-induced extravascular leakage of NHS-biotin from 14.4 AU (EPI) to 4.9 AU (PBS, $p = 0.0021$) in Cre- animals to 4.2 AU (EPI) to 2.9 AU (PBS, $p = 0.116$) in Cre+ animals (Figure 2.9), and from 12.7 AU (VEH/EPI) to 2.8 AU (LiCl/EPI, $p = 0.00134$).

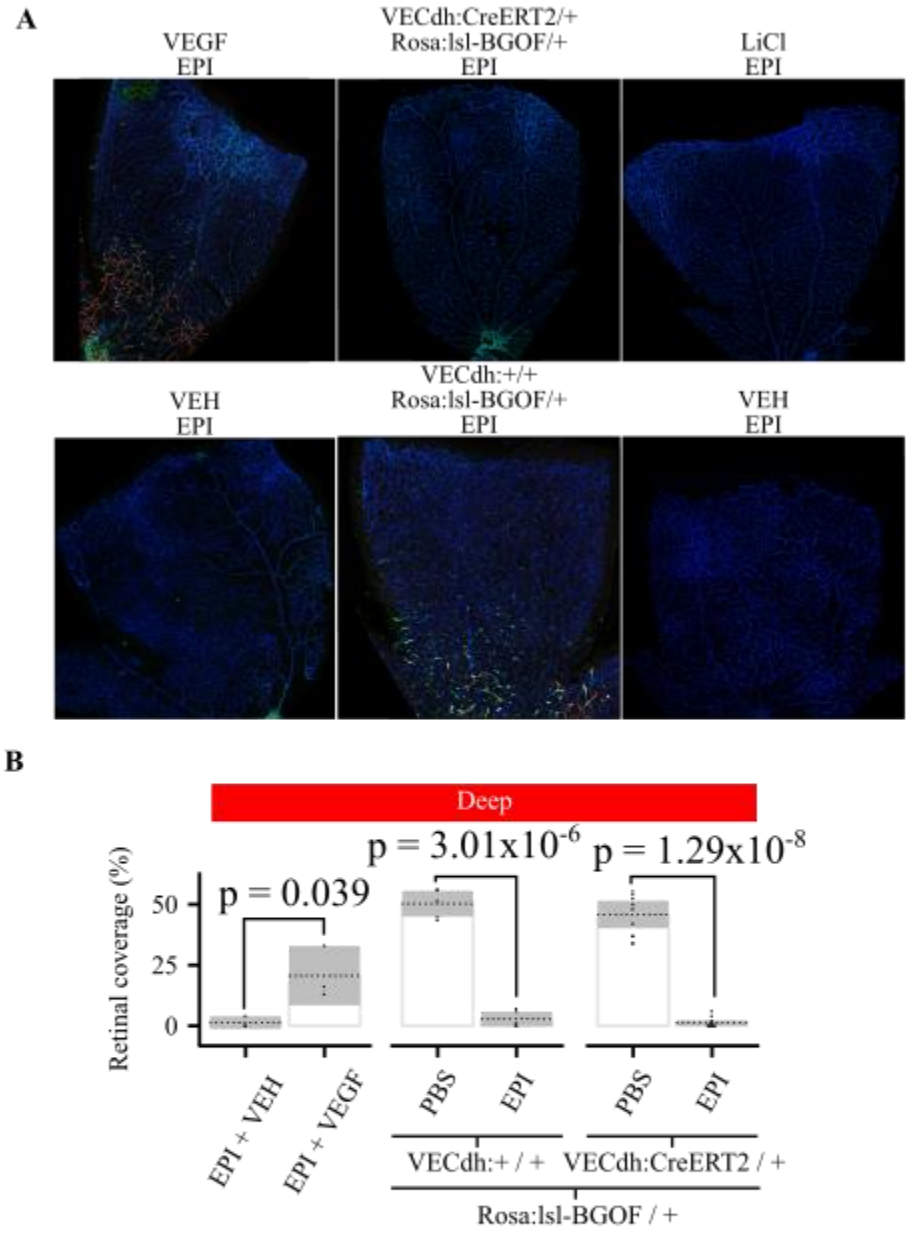

Figure 2.8. Intravitreal VEGF, but not enhancement of beta-catenin signaling in retinal endothelial cells, restores some deep layer angiogenesis after EPI-induced inhibition. (A) VEGF co-injected with EPI from P3 to P9 led to an increase in deep layer vascularization from 1.3% coverage to 20.7% coverage. Expressing a stabilized form of beta catenin (BGOF) had no effect on deep layer coverage, and activation of beta-catenin by systemic administration of lithium chloride (LiCl) had no effect. (B) Quantification of vascular coverage. Statistical tests are Students t-test, 2-tailed, paired when comparing eyes from the same animal, otherwise assuming unequal variances. VECdh, the vascular endothelial cadherin promoter; CreERT2, tamoxifen-inducble cre-recombinase; Rosa, the (Gt(ROSA)26Sor) locus; lsl-BGOF, lox-stop-lox upstream of stabilized beta-catenin.

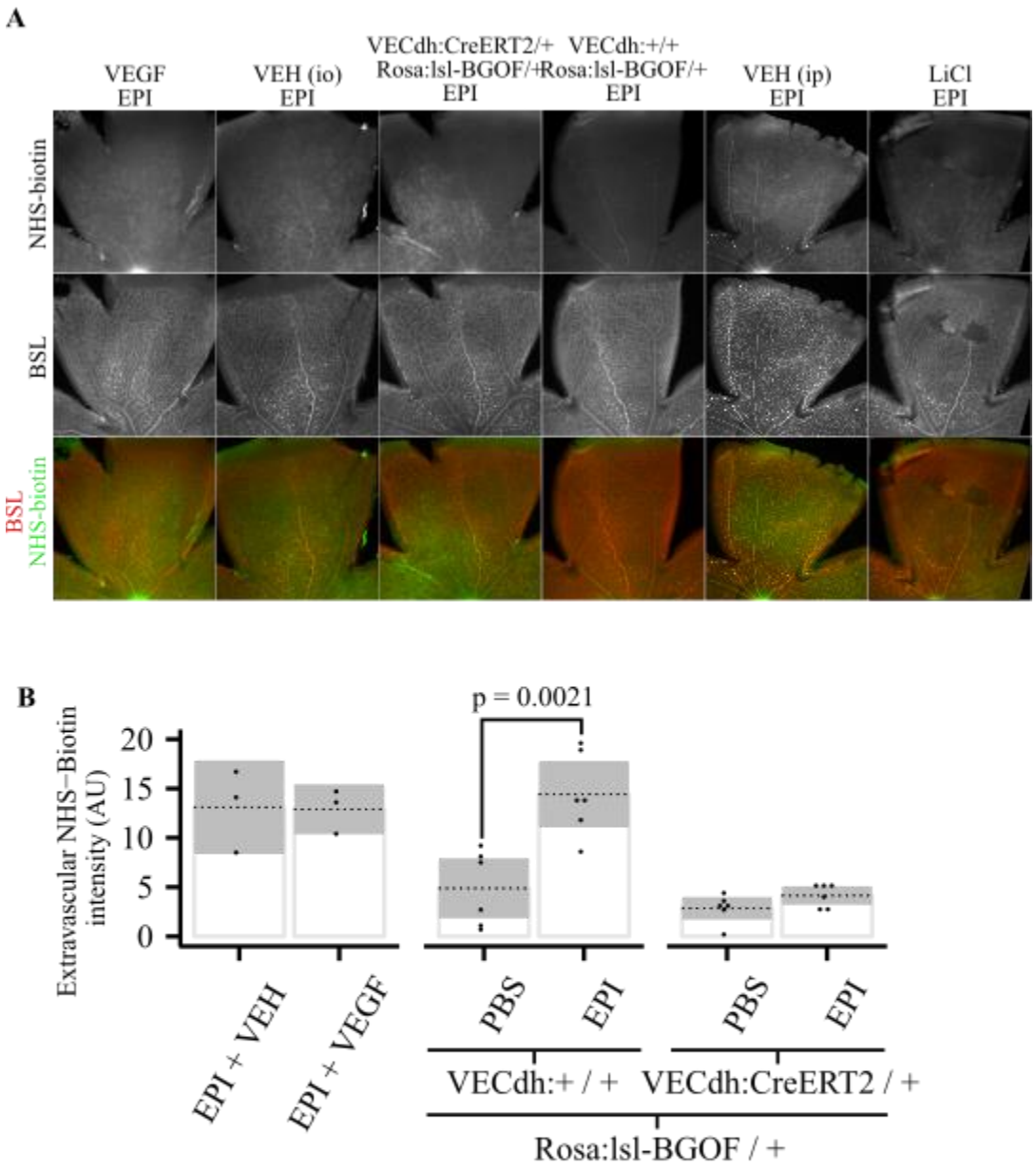

Figure 2.9. Enhancement of beta-catenin signaling in retinal endothelial cells, but not intravitreal VEGF, decreases BRB permeability after EPI injection. (A) BRB permeability was measured by NHS-biotin leakage. BGOF and LiCl led to an decrease in extravascular NHS-biotin. VEGF co-injected with EPI had no effect. (B) Quantification of NHS-biotin leakage. Statistical tests are Students t-test, 2-tailed, paired when comparing eyes from the same animal, otherwise assuming unequal variances. All other comparisons were not significant.

We measured the oxygen consumption rate (OCR) of whole retinal punches isolated from P9 ChatGi mice. Addition of clozapine-N-oxide (CNO) to the incubation medium led to a 31% (0.93 to 0.64 baselined OCR units) decrease in OCR in ChatGi (ChatCre/+;Rosa lsl hM4Di/+) mice compared to ChatCre (ChatCre/+;Rosa +/+) controls (Figure 2.10A). Mitochondrial function in the same preparation was assessed by successive addition of 2 µM oligomycin, 1 µM FCCP, and 2 µM rotenone/antimycin A to the incubation medium and calculated from the raw OCR readings. We found that ATP production was decreased from 78.36 pmol/min to 39.68 pmol/min ($p = 0.024$) in ChatGi compared to ChatCre after addition of CNO, a consequence of the reduction in OCR observed because ATP production is the difference between the last basal period reading and the minimum reading after addition of oligomycin (Figure 2.10B).

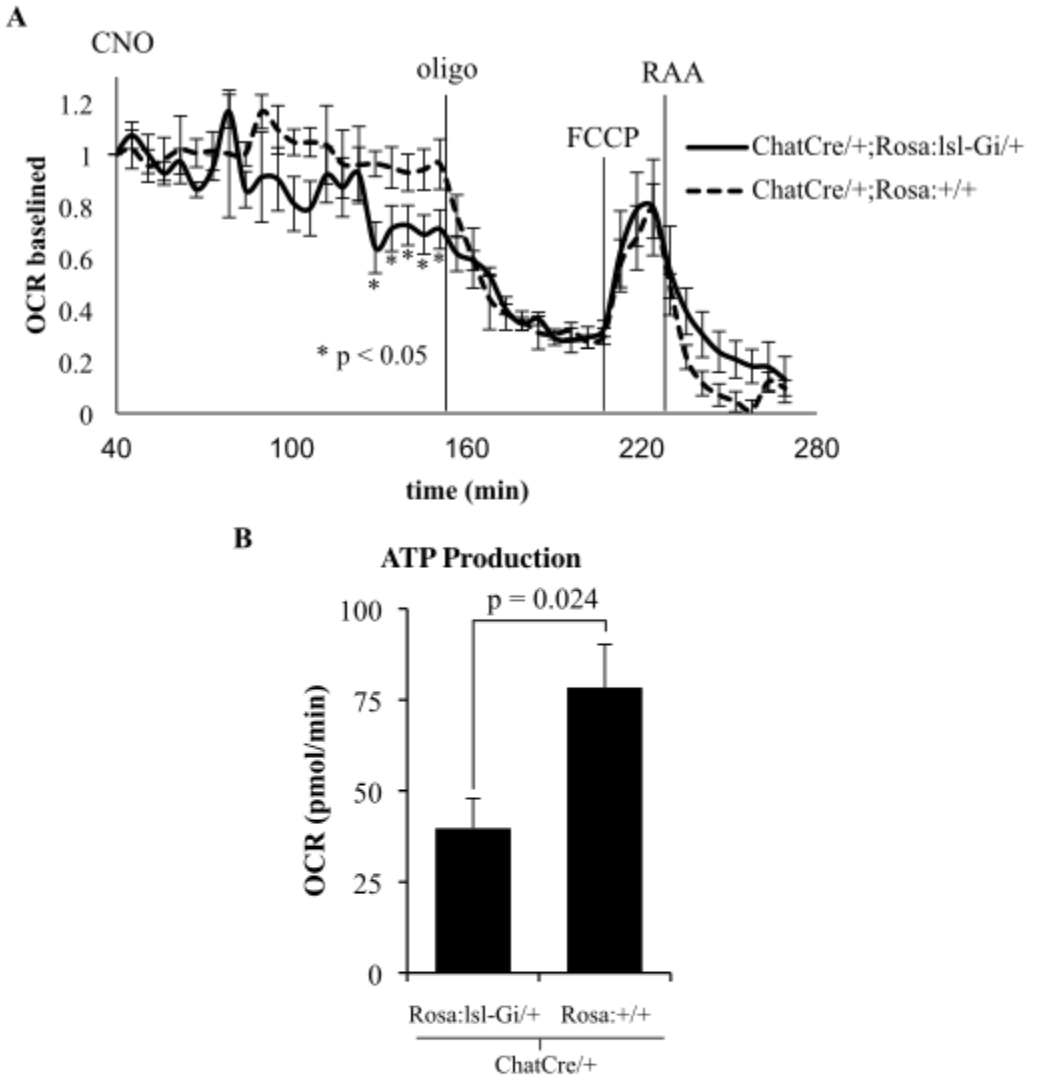

Figure 2.10. Inhibition of SAC activity reduces retinal metabolism. hM4Di was expressed in SACs and use to inhibit SAC activity. (A) Oxygen consumption rate was measured in isolated retinal punches on a Seahorse XFe96 Analyzer. Baseline measurement period not shown, all OCRs were baselined to the last reading in each well prior to CNO injection. Oligomycin (oligo), Carbonyl cyanide-4-(trifluoromethoxy)phenylhydrazone (FCCP), and rotenone/anti-A (RAA) were aplied sequentially to interrogate mitochondrial function. Application of CNO led to a >30% decrease in OCR in retinas expressing the inhibitory DREADD. (B) ATP production, defined as the difference between the last measurement prior to oligo minus the minimum reading during oligo, was decreased in retinas expressing the inhibtory DREADD. Statistical tests are Students t-test, 2-tailed, assuming unequal variances. All other comparisons were not significant. ChatCre, IRES-cre knocked into the ChAT locus upstream of ChAT; Rosa:lsl-Gi, hM4Di inserted in the Rosa locus upstream of a lox-stop-lox sequence; CNO, clozapine-N-oxide.

Taken together, these results show that cholinergic retinal activity modulates angiogenesis and barrier function by regulating the production of VEGF and norrin, respectively, and that inhibition of SAC activity decreases metabolic demand.

Cholinergic blockade improves vascularization and reduces retinal hemorrhage after OIR

We wanted to ask whether cholinergic activity is an important regulator of pathological angiogenesis as well as physiological angiogenesis. The oxygen-induced retinopathy model previously described, is a reproducible way to cause pathological neovascularization in mouse pups. Mice are housed in a hyperoxic (75% O_2) chamber from P7 to P12, during which time pre-establish vessels deteriorate. From P12 to P17 abnormal neovessels grow in, and then from P17 to P25 the abnormal vessels regress and the retina revascularizes. To examine the effect on neovascularization, we injected EPI or PBS intravitreally at P13 and P15 and examined the vasculature at the height of neovascularization on P17. To examine the effect on revascularization, we injected EPI or PBS intravitreally at P21 and P23 and examined the vasculature at the height of neovascularization on P25. We did not examine BRB function by NHS-biotin perfusion because it is impossible to separate hemorrhage from BRB leakage in this model.

We found that EPI compared to PBS decreased the area of vaso-obliteration observed at P17. Additionally, the number of pre-retinal neovascular buds and the average size of buds was reduced. We were able to observe retinal hemorrhages by brightfield imaging, and found that the area of retinal hemorrhage was decreased after EPI injection. EPI did not prevent revascularization from P21 to P25. Despite the fact that vessels grow into the retina during this period, the resulting vascular network is highly abnormal, and the processes that regulate revascularization are likely different from those mediating normal physiologic angiogenesis.

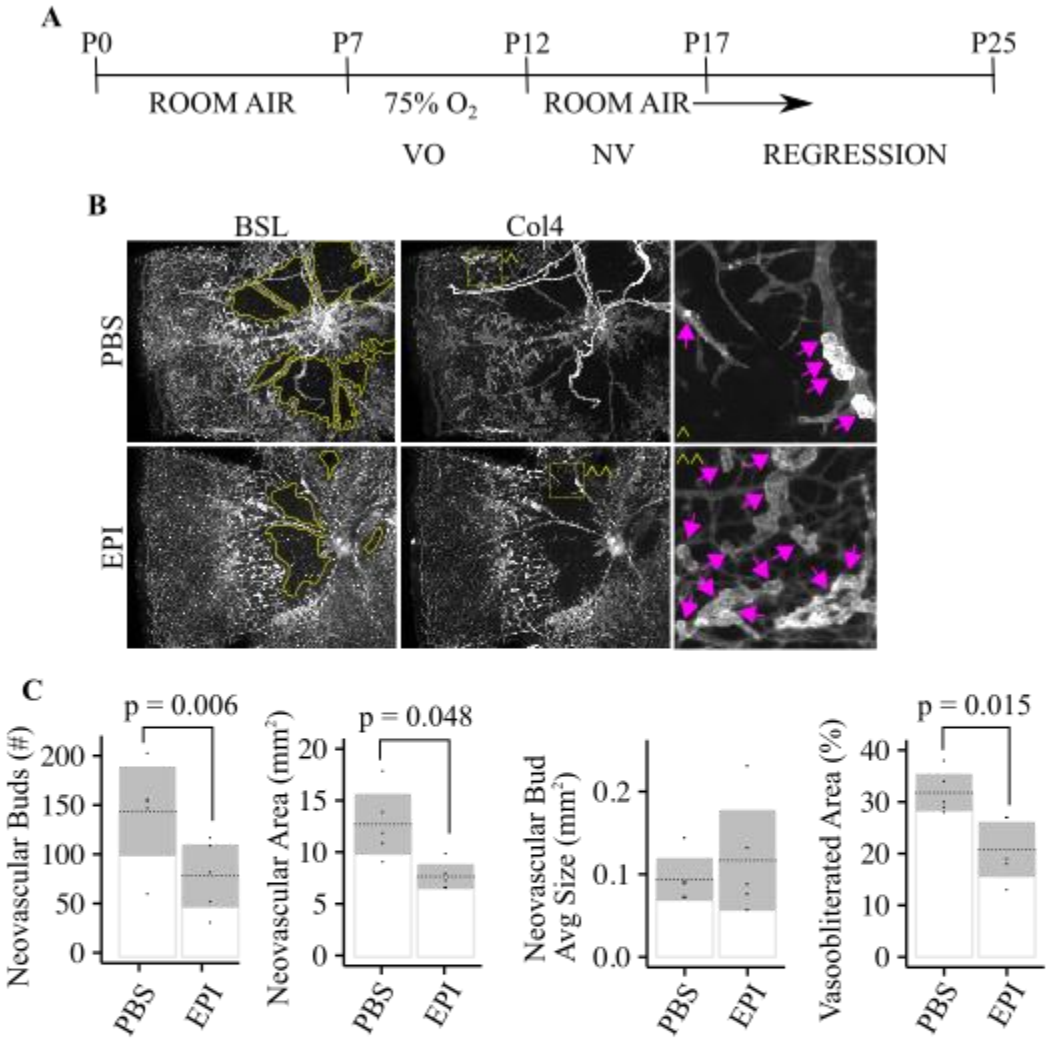

Figure 2.11. Inhibition of SAC activity decreases pathological neovascularization. (A) In OIR P7 animals are placed in a hyperoxic environment, leading to retinal vasoobliteration (VO). Upon return to a normoxic environment 5 days later, a neovascular (NV) and hemorrhagic retinopathy develops, the severity of which is maximal at P17. Neovessels regress by P25. EPI was injected at P13 and P15 to determine the effect on neovascularization at P17. (B) Effects on the vasculature were visualized by BSL staining of vessels and collagen-4 (Col4) staining of the vascular basement membrane. (C) Total remaining vasoobliterated area at P17 was decreased from 32% to 21% ($p = 0.015$) after EPI injection. There was a reduction in the number of neovascular buds from 148 to 82 per retina ($p = 0.006$) and a reduction in total neovascular area across the retina from 12.8 mm^2 to 7.8 mm^2 ($p = 0.048$). The average size of each bud was not different. Statistical tests are Students t-test, 2-tailed, paired. All other comparisons were not significant.

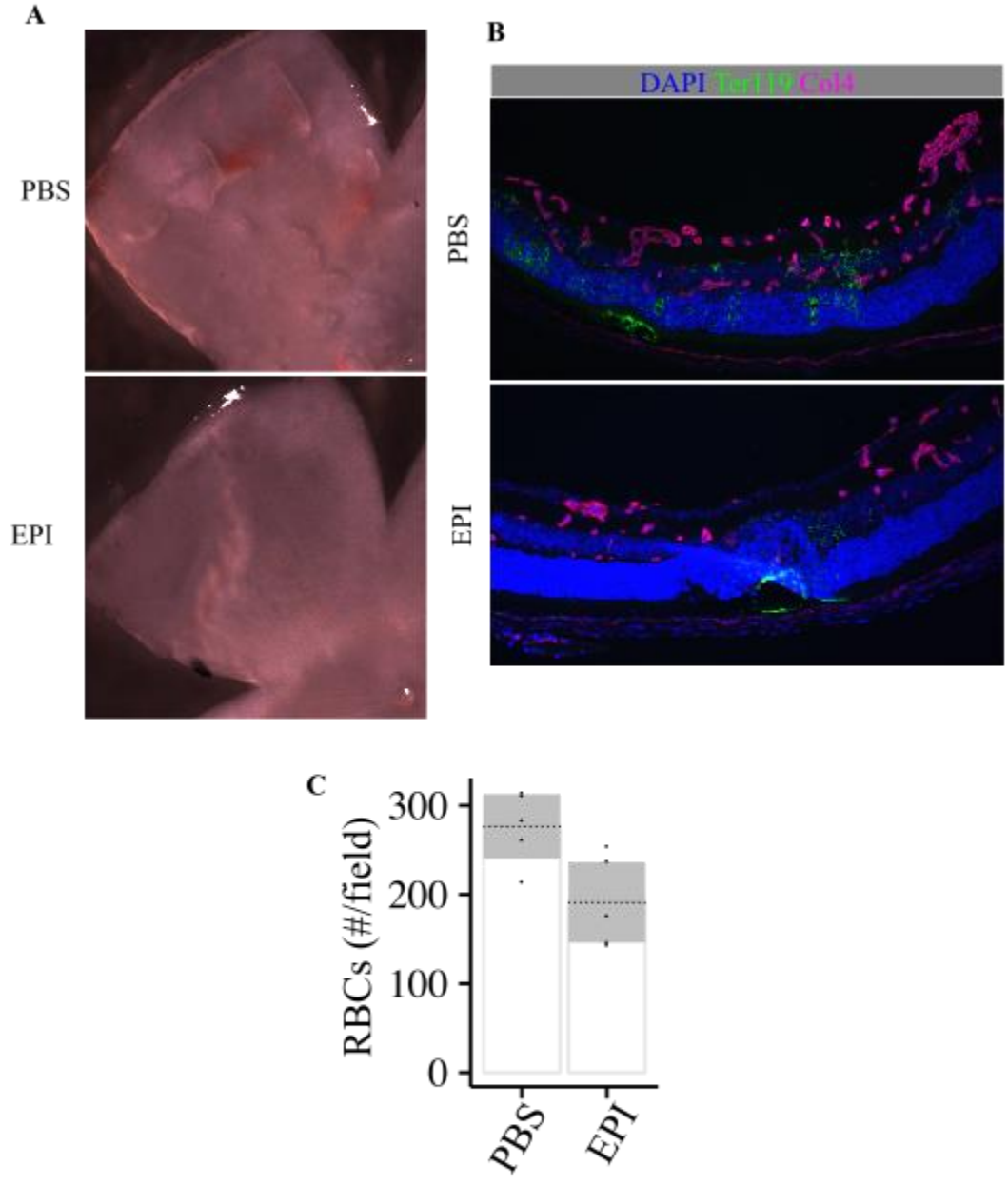

Figure 2.12. Inhibition of SAC activity decreases retinal hemorrhage in OIR. (A) Brightfield images of freshly dissected P17 OIR retinas injected with either PBS or EPI. Hemorrhage is clearly visible in the PBS eye and decreased in the EPI eye. (B) Red blood cells (RBCs) were visualized by Ter-119 immunostaining and counted to quantify hemorrhage. (C) Number of RBCs per field decreased from 277 to 191 ($p = 0.008$). Statistical tests are Students t-test, 2-tailed, paired. All other comparisons were not significant.

Conclusions and Discussion

The studies detailed in this chapter demonstrate a previously unappreciated link between neural circuit-specific activity and region-specific angiogenesis in the CNS. We showed, using several different methods of manipulating retinal activity, that cholinergic neural activity is required for appropriate vascularization of the deep capillary plexus of the retina and for proper formation of the BRB. We showed that the signaling pathways affected by activity blockade go through VEGF and norrin, and that the cholinergic circuit contributes to a substantial proportion of overall retinal metabolic demand during development. Finally, we showed that cholinergic activity may be important in pathological angiogenesis. In OIR, cholinergic blockade reduced abnormal neovascular buds, improved re-vascularization of the retina, and reduced intraretinal hemorrhage.

Our first set of experiments tested the hypothesis that neural activity drives normal angiogenesis in the developing retina. A crucial observation underlying this hypothesis is shown in Figure 1.1A. As far as we know, no one has previously recognized that neural circuit maturation and circuit-specific activity in the retina coincides developmentally with layer-specific angiogenesis. We decided to test the effect of cholinergic activity on the development of the retinal vasculature because there are well-described methods for manipulating the activity of the cells involved in the cholinergic circuit using pharmacology (*106*). We used intravitreal injections of epibatidine (EPI) during development to inhibit cholinergic activity and found that, when administered during the period of cholinergic-dominant activity, EPI completely prevented formation of the deep vascular plexus. When EPI was injected during the period of glutamatergic activity, there was no effect on the developing middle vascular plexus. In contrast, TTX and APB had no effect on vascular development at any time point. The different effects of TTX and EPI warrant discussion, since both affect cells in the cholinergic circuitry, but in our system had very different effects on the retinal vasculature. From P3 to P9 SACs make synapses onto other SACs and onto RGCs. These synapses are

cholinergic - acetylcholine released by SACs stimulates nicotinic cholinergic receptors on both RGCs and other SACs. SACs themselves can fire action potentials at this stage of development but, importantly, these action potentials are not blocked by TTX (*107*, *108*). TTX blocks action potentials in RGCs during development and maturity. EPI, which blocks transmission from SACs to RGCs, does not completely silence activity in RGCs (*107*). So the activity required to drive angiogenesis is not RGC action potentials, it is SAC activity. We also ablated SACs using a target-toxin approach previously described to inhibit developmental cholinergic activity (*109*) and found the same deficits in normal angiogenesis.

Our second set of experiments tested the hypothesis that neural activity supports normal function of the BRB. Using the same approaches to manipulating activity previously described, we measured the function of the BRB by its ability to restrict diffusion of a small hydrophilic molecule, NHS-biotin, into the retinal parenchyma. We found a ~8-fold increase in permeability of the barrier to NHS-biotin after EPI injection. This effect was restricted to EPI injections from P3 to P9; it was not observed at later time points and TTX and APB had no effect at any time point. Although impermeability to small hydrophilic molecules is not the sole function of the BRB, it is a well-described property of CNS endothelial cell function. It is known that Cldn5, a tight junction protein, is part of the intercellular barrier system that prevents diffusion of small molecules between endothelial cells. We found alterations in Cldn5 expression after EPI injection. We observed gaps in continuous Cldn5 expression along a single junction, which are almost never observed in normal retinal vasculature. We also observed segments of vessels that had completely lost expression of Cldn5.

Our third set of experiments tested the hypothesis that neural activity regulates VEGF and norrin expression, and that defects in these signaling pathways account for the effects on angiogenesis and barrier function we observed. The motivation to test VEGF and norrin can best be described separately. VEGF is known to be an important regulator of angiogenesis in

the retina and other organs, and high levels of VEGF alone are sufficient to drive pathological angiogenesis, as the experience of anti-VEGF therapy in the setting of wet AMD and diabetic macular edema demonstrate. Since we had observed that inhibition of cholinergic activity decreases angiogenesis, we wanted to test whether VEGF was decreased in this setting. Norrin is the Wnt ligand in the retina that is secreted by Muller glia and acts on an endothelial cell receptor complex to stabilize beta-catenin and turn on barrier properties cell-autonomously. Norrin knockout causes a phenotype very similar to what we observed after cholinergic blockade - failure of the deep layer to vascularize and increased BRB permeability. There are important differences between norrin knockout and cholinergic blockade, which include the observation that in norrin knockout abnormal clusters of endothelial cells partially invade the retina and norrin KO retinas have intraretinal hemorrhages. After SAC activity blockade, in contrast, we did not observe any intraretinal hemorrhage and also no penetrating intraretinal vessels; all vessels were confined to the superficial layer on the vascular surface. The difference may be explained by the fact that in norrin KO, VEGF is actually increased (*110*) and as previously mentioned, high VEGF alone may be enough to cause leaky hemorrhagic neovessels. Whether upstream regulatory events control the expression of norrin is not known. We assayed VEGF and norrin levels after activity blockade and found them both to be decreased. We sought to determine whether the decrease in VEGF and norrin was a cause of either the decreased angiogenesis or decreased barrier function. To replace VEGF we injected recombinant VEGF intravitreally. To mimic norrin function we both expressed a stabilized form of beta-catenin in endothelial cells and injected lithium chloride systemically, which has also been shown to stabilize beta-catenin in retinal blood vessels. Intravitreal VEGF co-administered with EPI led to a significant increase in deep layer vascularization, but neither BGOF nor LiCl had any effect on vascular growth. Intravitreal VEGF had no effect on EPI-

induced barrier permeability, but the increased permeability was blocked by both methods of restoring beta-catenin function.

Although not much is known about the regulation of norrin, the regulation of VEGF is well-described. Relative tissue hypoxia leads to stabilization of hypoxia-inducible factor 1 alpha (Hif1a), which is normally degraded, and Hif1a is a transcription factor that induces transcription of hypoxia-related genes, including VEGF (*111*). Normally this leads to increased vascularization to relieve the hypoxia-driven production of VEGF. Thus, one important regulator of VEGF is oxygen availability. Neural activity is thought to drive metabolic demand, so we wanted to test the hypothesis that manipulating cholinergic activity has a disparate impact on overall tissue oxygen consumption. We measured the oxygen consumption rates (OCR) of isolated pieces of mouse retina with a lox-stop-lox inhibitory DREADD receptor in the Rosa locus and an IRES-Cre in knocked into the ChAT locus upstream of ChAT and found a ~35% decrease in OCR after inhibition of cholinergic activity, but not after TTX. Overall ATP production was decreased. The ability of the activity of cholinergic circuitry to drive such a substantial proportion of total tissue oxygen consumption was not previously appreciated. Computational modeling has shown that neurons with highly branched dendrites are likely to have a higher metabolic demand than other neurons, and SACs have a uniquely high dendritic coverage in the retina. Most retinal cell types have 1-5x dendritic coverage, meaning any given point in the retina is covered by the dendrites from 1-5 individual cells of a given type, but SACs have been described to have up to 70x coverage. This would position them to control a substantial amount of retinal metabolic demand.

Our fourth set of experiments sought to test the hypothesis that cholinergic activity may play an important role in pathological neovascularization in the retina. We used the OIR model because of its ability to reproducibly induce a neovascular phenotype in the retina. We found that EPI injected during the period of neovascularization substantially decreased the

amount of intraretinal hemorrhage and preretinal neovascular buds. What does this say about a potential cholinergic or neural activity component to neovascularization? There are two possibilities: 1) the activity of cholinergic cells is altered by the disease process and the cholinergic circuitry becomes active at times when it would normally be dormant; or 2) activation of cholinergic receptors comes from a non-SAC acetylcholine source. Since acetylcholine is present in the blood and OIR retinas have a significant amount of hemorrhage, it may be that blood acetylcholine spillover into the retinal parenchyma mediates or modulates pathological angiogenesis. In either case, it suggests that the typical description of the pathology in OIR, which is focused around tissue PO2, hypoxia signaling, and VEGF may not be a complete picture.

There are several important extensions of this work that would contribute to a fuller understanding of these phenomena.

Neural circuits and metabolism

Our work has suggested that the activity neural circuits contributes differentially to tissue function across specific circuits and developmental timescales. Is this phenomenon specific to development in the retina or are different circuits responsible for other tissue functions in other parts of the CNS? What is the reason different neural circuits contribute differently to tissue function? It could be the anatomical organization of the cell types involved, the neurotransmitter systems involved, or some other aspect of neural activity not previously described. Further, does circuit-specific disruption of neural activity during disease contribute to the alterations in metabolism frequently observed during those diseases?

Neural activity and the regulation of norrin production.

We have addressed the reasons for a decrease in VEGF production after neural activity blockade, but an important limitation of this study is that we do not address the decrease in norrin production. Little is known about the pathways that regulate norrin

production in Muller glia. A recent study demonstrated that Muller glia sense acetylcholine spillover from SAC synapses during retinal waves and respond with calcium transients (*33*). Does this neurotransmitter sensing contribute to the production of norrin? Manipulating activity at the glial muscarinic receptor would give insight into this question, and is feasible with current technologies.

Methods

Animals

Wild-type animals were C57/BL6 mice purchased from Envigo. Homozygous ChAT-IRES-Cre knock-in mice (ChatCre) animals were purchased from The Jackson Laboratory (strain 006410). Heterozygous R26-LSL-Gi-DREADD (RGi/+) animals were purchased from The Jackson Laboratory (strain 026219). ChatCre homozygotes were crossed to RGi/+ animals, and littermate R+/+ animals were used as controls. All animal experiments were performed in accordance with national guidelines and UCSD IACUC guidelines. Experimental/surgical procedures were performed to minimize animal stress and the number of animals used.

Inhibition of cholinergic activity

Intravitreal injections were done at P3, P5, and P7 for experiments during the cholinergic period, or at P11 and P13 for experiments during the glutamatergic period. For the OIR model, injections were done at P13 and P15. In each case, the injection procedure was similar. Animals were anesthetized using isoflurane flowing through a rodent facemask. Isoflurane was 1-3%, flow 100 mL/min, and the procedure lasted approximately 20 minutes per animal. After reflex checks, a small cut was made through the eyelid and the lid pulled back to expose the eye. After P13 the eyes were typically open and the eyelids did not need to be cut open. Approximately 0.5 to 1.0 uL of solution was injected using pulled glass micropipettes attached to a picospritzer iii in P3 to P9 pups, 1.5 to 2.0 uL in P11 to P15 pups.

Typically 20-40ms duration pulses at 30 PSI were used, but this was adjusted as needed to inject the appropriate amount. The needle was left in the eye for 30 seconds after injection and withdrawn slowly to minimize leakage. The eyelid was sutured for P3 to P9 animals and covered with antibiotic ointment for animals at every age. One eye was injected with the experimental compound and the other eye was injected with a vehicle control. Drug concentrations and vehicles were epibatidine (Sigma E1145) 1 mM in PBS, APB (Sigma A1910) 1 mM in PBS, TTX (Tocris 1069) 1 mM in citrate buffer, Rabbit anti-ChAT-SAP (Advanced Targeting Systems IT-42) 0.12 mg/mL in PBS. The control for ChAT-SAP was an untargeted Rabbit anti-IgG-SAP (Advanced Targeting Systems IT-35) 0.12 mg/mL in PBS.

CNO injections

Clozapine-n-oxide was purchased from Tocris (4936) dissolved at 20 mM in sterile water, and stored in the dark at -20 degrees. Prior to injection, CNO was diluted in sterile saline and injected to a final concentration of 0.5 mg/kg. Two daily intraperitoneal injections were performed, spaced 12 hours apart.

Retina collection for vascular analysis

Pups were killed and the whole eyes were fixed in 4% PFA in 1x PBS at room temperature for 10 minutes, then transferred to 1x PBS on ice. The retinas were dissected out and fixed in methanol at -20 degrees overnight.

Retina collection for barrier analysis

Pups were deeply anesthetized using a ketamine/xylazine mixture and then sequentially transcardially perfused with ~10-15 mL of 0.25 mg/mL EZ-Link Sulfo-NHS-Biotin in PBS and ~10-15 mL of 4% PFA in PBS. The whole eyes were fixed in 4% PFA in 1x PBS at room temperature for 10 minutes, then transferred to 1x PBS on ice. The retinas were dissected out and post-fixed in 4% PFA for 45 minutes to 1 hour then washed in PBS and stored in PBS plus azide at 4 degrees in the dark.

Immunofluorescence

Whole-mount fixed retinas were washed in PBS then blocked for 30 minutes in 0.2% BSA, 5% serum, and 0.3% Triton X-100, then incubated in primary antibody in blocking buffer overnight at 4 degrees with gentle rocking. Retinas were then washed in 0.3% Triton X-100 three times, and incubated with secondary antibodies in 0.3% Triton X-100 for 2-4 hours at room temperature, protected from light with gentle rocking. They were then washed in 0.3% Triton X-100 twice, 1x PBS twice, and then mounted on slides with Prolong Gold Antifade Reagent. Primary antibodies used were rabbit anti-Cldn5 (Thermo Fisher Scientific 34-1600, 1:500), goat anti-collagen 4 (SouthernBiotech 1340-08, 1:500), and rat anti-Ter119 (abcam ab91113,1:250). Secondary antibodies used were goat anti-rabbit Alexa Fluor 488 (Thermo Fisher Scientific A-11034, 1:1000), goat anti-rat donkey anti-goat Alexa Fluor 488 (Thermo Fisher Scientific A27012, 1:1000), donkey anti-rabbit Alexa Fluor 488 (Thermo Fisher Scientific A-21206, 1:1000), goat anti-rabbit Alexa Fluor 594 (Thermo Fisher Scientific A-11037, 1:1000), and donkey anti-goat Alexa Fluor 594 (Thermo Fisher Scientific A-11058, 1:1000). BSL was biotinylated griffonia simplicifolia lectin I (Vector Laboratories B-1205, 1:250). Streptavidin was streptavidin conjugated to Alexa Fluor 594 (Thermo Fisher Scientific S32357, 1:1000).

Confocal and epifluorescence imaging

Confocal imaging was done on a Zeiss LSM 710. A 20x/0.8 NA air objective was used. Images were acquired at 1 airy unit resolution with 4x undersampling of pixels in X-Y and 2x undersampling in Z. Excitation lasers were 488 nm (for Alexa Fluor 488 and FITC), 561 nm (for Alexa Fluor 594), and 633 nm (for Alexa Fluor 647). Emissions were collected as separate tracks over wavelength bands exclusive with other mutually excited fluorophores. Epifluorescence images were collected on an Axio Imager D2 (Carl Zeiss) with a 5x Fluor, 0.25 NA or 20x Plan-Apochromat, 0.8 NA objective, using a digital camera (Axiocam HRm,

Carl Zeiss). AxioVision software was used to acquire images; Fiji (ImageJ) and Inkscape were used for image processing and analysis.

Vascular image analysis

Confocal volumes were stitched using Zeiss' Zen software using a strictness of 0.9. Because the stacks were often not completely flat, they were then rotated in ImageJ using the TransformJ plugin so the superficial layer vasculature was in the same plane across every stack in the image. The image was then depth-coded in ImageJ by coloring the stacks according to Z-position along a blue-green-red axis. Retinal area was quantified in ImageJ by manually selecting the extent of the flat mount. Coverage of a vascular layer was quantified by manually selecting the area of the retina covered by that layer and then dividing by the whole retinal area. For analyzing the middle layer, a ~425 um x 425 um z-stack was taken ~500 um away from the center of the retina. Vessels were traced by hand, skeletonized in ImageJ using the Skeletonize plugin, and analyzed for length and branch points using the same plugin.

BRB image analysis

Epifluorescence images were acquired by focusing on the superficial layer vasculature. The whole retina was imaged then stitched together using the MosaicJ plugin in ImageJ or the Zen Software package. Intravascular regions were defined by BSL staining, and used to create a mask of the NHS-biotin image. The masked NHS-biotin image represents extravascular NHS-biotin accumulation. The extent of the retina was defined and the average extravascular NHS-biotin intensity per pixel was divided by the background (non-retinal) intensity per pixel to yield the extravascular NHS-biotin in arbitrary units (AU).

Angiogenesis and barrier rescue experiments

Epibatidine was injected to inhibit cholinergic activity from P3 to P9 as previously described. In wild-type animals EPI was injected into both eyes. For VEGF rescue, recombinant human VEGF-165 (R&D Systems, 293-VE-010) dissolved in PBS was co-

injected with EPI in one eye at 38 ug/mL. Total injection volume was the same for both eyes. In transgenic BGOF animals, EPI was injected as previously described with PBS as control. At P7 20 uL of 2 mg/mL tamoxifen (Sigma T5648) dissolved in corn oil was injected intraperitoneally. For lithium chloride (LiCl) rescue, LiCl (Sigma L7026, 30 mg/kg) or saline was injected intraperitoneally once per day at P7, P8, and P9.

Measurement of oxygen consumption rate

OCR was measured on a Seahorse XFe96 Flux Analyzer. 1 mm punches from isolated retinas were placed in the bottom of Seahorse XFe96 spheroid plates. Dissections and incubations were done in DMEM 5030 supplemented to 20 mM glucose, 10 mM HEPES, 2 mM glutamine, and 5 mM pyruvate.

Oxygen-induced retinopathy

At P7 a litter of mice (pups and mom) were introduced in a sealed Biospherix chamber linked to an oxygen line. The O2 is brought up to 75%. Mice were observed daily without opening the chamber. At P12, 5 days later, mice were removed from the chamber and placed back in a normoxic environment.

Western blots

Eyes from mice were removed after CO2 euthanasia and flash frozen with liquid nitrogen and stored in -80°C. After defrosting, the retinas were dissected and homogenized by sonication in 90 uL of cold ddH20 with cOmplete Protease Inhibitor cocktail (CO-RO ROCHE) and 10 uL 10x RIPA Lysis Buffer (20-188 EMD MILLIPORE). Samples were centrifuged at 10,000 x g for 10 minutes at 4°C, and the supernatants collected. Total protein concentration was determined using a BCA assay (Pierce BCA Protein Assay Kit 23225). 30-40g of protein was loaded on a 4-20% Tris-Glycine Gel (Thermo Fisher Scientific XP04202) and transferred to an activated 0.2 um PVDF membrane for immunoblotting. The membranes were saturated with TBS 1x, 0.05% Tween-20, and 5% nonfat dry milk for 1 hour at room

temperature, then incubated overnight at 4°C with mouse anti-norrin (1:300, R&D Systems MAB3014), mouse anti-VEGF C-1(1:300, Santa Cruz Biotechnology sc-7269), or rabbit anti-GAPDH (1:2000, Cell Signaling Technology #2118). All membranes were washed with TBS-Tween between incubations. The membranes were then saturated with peroxidase-conjugated goat anti-mouse or anti-rabbit (1:3000, Abcam, ab6789 and ab6721) secondary antibodies for 3 hours at room temperature, and revealed with SuperSignal West Pico Chemiluminescent Substrate (Thermo Fisher Scientific 34080) and imaged with myECL Imager (Thermo Fisher Scientific). Stripping to ensure equal loading was done with ReBlot Plus Strong Antibody Stripping Solution (EMD Millipore 2504). All quantifications were done with ImageJ densitometry analysis.

Acknowledgements

This chapter is an original document written by Geoffrey Weiner with oversight from Jeffrey Goldberg. The work presented in this chapter was led by Geoffrey Weiner with contributions from members of the laboratories of Jeffrey Goldberg, Richard Daneman, and Eric Nudleman. Sahil Shah was a major contributor to experiment planning, injections, Western blots, and data analysis. Christian Angelopoulos collected, stained, and analyzed tissue. Alena Bartakova put mice through the OIR protocol and helped with injections. Minjin Ju developed immunostaining protocols. Mari Gantner helped with the design of Seahorse experiments. Most experiments were conducted in the laboratories of Jeffrey Goldberg and Richard Daneman. Seahorse experiments were done in the laboratory of Anne Murphy. This work was supported by the Waitt Advanced Biophotonics Core Facility of the Salk Institute with funding from NIH-NCI CCSG: P30 014195, NINDS Neuroscience Core Grant: NS072031 and the Waitt Foundation. Geoffrey Weiner is supported by a fellowship from the San Diego Foundation. Jeffrey Goldberg is supported by the Foundation Fighting Blindness, the Glaucoma Research Foundation, and the NIH. Eric Nudleman is supported by the NIH.

Chapter 3

The Transcriptomic Response of Retinal Microvascular Cells to Optic Nerve Crush

Authors

Weiner GA, Daneman R, Goldberg JL.

Abstract

Blood vessels in the central nervous system (CNS) develop unique features not found elsewhere in the vascular system. These properties contribute to the homeostatic environment of neurons, and are known to be disrupted in human pathology and animal disease models. Neurodegenerative conditions in particular are associated with dysfunction in cells of the neurovascular unit. In the retina, the neurodegenerative disease glaucoma is not known to have associated vascular pathology, but whether it does remains largely unaddressed. Here we report that in mice after optic nerve crush - a model of ganglion cell degeneration - the retinal vasculature is not remodeled and no barrier leakage occurs. However, purified endothelial cells and microglia show alterations in gene expression by RNA-sequencing. Pathway analysis revealed upregulation of immune related pathways 5 days after crush and dysregulated neurotransmitter receptor expression 14 days after crush. We attempted to localize changes in specific proteins by immunostaining and surprisingly found that some differentially expressed genes in our data set were strongly expressed in non-microvascular cells. This raises the question of whether RNA is transferred to microvascular cells during normal or disease processes, and what the functional significance of this is. This work suggests that even neurodegenerative conditions without frank vascular pathology can have gene expression changes in microvascular cells.

Introduction

CNS vasculature response to injury

CNS vasculature reacts to injury in a variety of human diseases and animal disease models. This response has been primarily studied in two contexts: blood-brain barrier (BBB)

breakdown and recruitment of inflammatory cells. The common denominator of these pathologies is changes in the function of CNS endothelial cells.

BBB permeability to circulating molecules

Neurodegenerative diseases have been convincingly shown to include a component of BBB breakdown. The list of diseases that have this phenotype includes Alzheimer's disease, multiple sclerosis, stroke, epilepsy, Parkinson's disease, HIV associated neurodegeneration, and trauma. In the retina, AMD, diabetic retinopathy, retinopathy of prematurity, and ischemia all are associated with BRB breakdown. These conditions are frequently visualized by oedematous swelling on MRI in the brain, or fluorescein leakage in the retina. Both modalities rely on the permeability of the barrier to small hydrophilic molecules, so that is the most well described pathological change.

In addition to classic neurodegenerative diseases having a BBB breakdown component, other conditions are now known to have this association. Aging has been suggested to have associated increases in BBB permeability as have (*159–161*) ischemia-reperfusion (*162*), chronic hypoperfusion (*163*), hypertension (*164*), and hyperglycemia (*165–167*).

What changes happen at the BBB to mediate these effects? There is almost certainly some core element of BBB dysfunction across diseases, as well as changes that are specific to each pathology. In AD models, accumulation of amyloid-beta plaques can cause decreased Zo-1 and occludin expression (*168, 169*) and increase the rate of autophagy (*170*), possibly impairing endothelial cell turnover. Decreased expression of junctional proteins corresponds to the small molecule leakage observable in clinical practice. ApoE, an important protein in amyloid clearance, may also control MMP-9 activity in pericytes, which can pathologically break down the BBB (*171*). In MS, Zo-1 localization is disrupted (*172*), and tight junction

defects are believed to contribute to the pathogenesis of the disease (*173*, *174*). In ALS models, Zo-1, occludin, and Cldn5 are decreased (*175*).

Recruitment of inflammatory cells

Normally, the movement of circulating immune cells into the CNS parenchyma is tightly restricted. CNS vasculature expresses very low levels of leukocyte adhesion molecules and other receptors necessary to bring immune cells in. In disease, leukocyte trafficking becomes dysregulated and white blood cells come into the brain, creating and perpetuating inflammation. Tau fragments increase the level of leukocyte trafficking into the brain (*176*). In EAE, a model of MS, inflammatory cells accumulate near the lesions (*172*). Chemokines and receptors on endothelial cells are upregulated in MS (*177*). HIV infection upregulates CD40, ICAM-1, and VCAM-1 in CNS endothelium and exposure to HIV can change the expression of hundreds of endothelial cell proteins (*178–180*), partly through Stat1.

Optic nerve crush

Optic nerve crush (ONC) is a model of RGC degeneration sometimes used as a model for glaucoma, because it is relatively easy to perform compared to other glaucoma models. The optic nerve is exposed with a small cut in the conjunctiva, the optic nerve exposed, and then crushed, typically with a pair of forceps. The optic nerve is composed of the axons of RGCs that have exited the globe, so ONC creates RGC-specific injury without any intraocular interventions. Many publications on ONC have characterized the usefulness of this model in rats, mice, rabbits, goldfish, and zebrafish. In rodents, the population of RGCs shows a characteristic response to ONC with 20% cell death by 5 days and 80% cell death at two weeks(*181*, *182*). A minority of RGCs escape death, and some will regrow their axons past the crush site(*183*). Rodent ONC is frequently used as a model to study neuronal regeneration(*184–186*).

Although there are other models of ganglion cell dysfunction that may more closely approximate the pathogenesis of glaucoma, ONC is a practically useful tool. Intraocular microbead or polymer injections, cannulation of the anterior chamber with a pressure reservoir, and manipulation of the scleral vessels have all been used to chronically increase intraocular pressure (IOP) and lead to ganglion cell degeneration(*187–190*). However these models are technically demanding, difficult to reproduce, only produce moderate ganglion cell loss, and may have heterogeneous effects on ganglion cells across the retina. The DBA2J mouse line is sometimes used as a glaucoma model because these mice get high IOP and have RGC degeneration(*191*), but the glaucoma is associated with inflammation and for the purposes of studying the BRB it is known that inflammation has an independent effect on endothelial cell function.

Biomarkers for glaucoma

Glaucoma is one of the leading causes of blindness in the developed world. Glaucoma is defined clinically as degeneration of the optic nerve with associated vision loss. Acute glaucoma is rapid RGC degeneration due to ischemia from very high pressures. RGCs also degenerate in chronic glaucoma; chronic glaucoma is sometimes associated with high IOP, but often is associated with normal pressures. The pathogenesis of glaucoma remains a subject of controversy. However, one of the most salient clinical features of glaucoma is that patients can lose up to 40% of their RGCS without noticing vision loss. Therefore many glaucoma patients present late in the disease state, after years of high IOP and ganglion cell loss. RGCs, like other neurons in the CNS, have a very low intrinsic regenerative capacity, so it is impossible to restore vision in these patients. Thus, the need for a biomarker to detect early signs of glaucoma so that intervention can preserve the existing RGCs, becomes apparent. There are several clinical biomarkers and signs used for the evaluation and detection of glaucoma, but they fail to meet the criteria for a very useful, early-stage biomarker.

IOP

IOP is a clinically relevant sign related to glaucoma but it is increasingly recognized that IOP itself is insufficient to explain the spectrum of glaucomatous patients presentations. It is clear that higher than normal IOPs can lead to RGC damage, dysfunction, and death over time. Many glaucoma patients present with normal IOP, and even patients presenting with IOP in the normal range may respond to IOP-lowering therapy, the current standard of care for glaucoma. In some cases, even lowering IOP to extremely low levels does not prevent the progression of glaucoma. These clinical data, combined with an understanding of RGC biology, has suggested that glaucoma is more a disease of RGC susceptibility to injury, than a disease caused by a specific type of insult. This interpretation, combined with emerging genome-wide association studies (GWAS) which have consistently failed to find high correlations between genetic polymorphisms and glaucoma risk, means that there may never be a good clinical sign indicating RGC injury. The underlying insult may come from a variety of sources. As a screening tool, IOP is sometimes able to identify patients at risk for development of glaucoma, but the specificity is low for a diagnosis that will require a patient to commit to lifelong, multiple times daily treatment.

RGC imaging

Although the original insult in glaucoma may be multifactorial, the converge on the common biological output of RGC dysfunction and death. The retina is approachable to many imaging modalities like optical coherence tomography (OCT), scanning-laser ophthalmoscopy (SLO), and fundus photography. These technologies, which are critical in the diagnosis and management of many other retinal disorders, have limited usefulness in glaucoma. One reason is that RGCs have proven refractory to classic imaging. RGCs are intrinsically low contrast, because the retina is organized such that incoming light must pass through the RGCs prior to being absorbed by photoreceptors. RGCs are low-contrast and refractive-matched so that light

passes through them without deforming the image. Imaging and counting RGCs would be a significant advancement in glaucoma detection. However, even being able to image RGCs directly may not yield an easily-appreciable biomarker. RGC density varies significantly across individuals, from eye to eye in a single individual, and across retinal eccentricity in a single eye. Additionally RGC density may decline with age. Further, imaging the death of RGCs is still not optimal because dead RGCs still can't be regenerated. An ideal RGC-based imaging biomarker would be based on some type of functional imaging and able to identify dysfunctional ganglion cells prior to cell death. Several modalities have been proposed, including metabolic imaging (oxygen consumption), but the results have not yet shown the approach to be useful as a clinical biomarker.

Vascular biomarkers

A number of studies have focused on the role of blood vessels in glaucoma. The connection between the vasculature and glaucoma is most easily appreciated by first considering acute angle-closure glaucoma (AACG). In AACG IOP is typically > 21 mmHg, and the diagnosis is made by considering other aspects of the patient presentation. Pressure inside the globe opposes the pressure in the circulatory system - the blood pressure (BP) - to push blood through the central retinal artery and into the inner retinal circulation. Ocular perfusion pressure (OPP) can be defined as arterial BP minus IOP, and has been shown to be related to glaucoma incidence and prevalence (*192*). If the pressure inside the eye is high enough, blood flow into the eye will cease and retinal ischemia will happen. In fact, inducing very high IOP > 80 mmHg is a mainstay in animal models of retinal ischemia. There is evidence in humans that lowering IOP alters the distribution of blood flow in the retina (*192, 193*). In primary open angle glaucoma (POAG), glaucoma without increased IOP, 24-hour IOP and systemic BP measurements showed that OPP in glaucoma patients is highly variable throughout the day, declining sharply overnight (*194–196*). Many studies have shown that OPP

is an independent risk factor for POAG (*197–202*). POAG is associated with other systemic vascular abnormalities that hint at a primary component of vascular dysfunction in the pathogenesis (*203–205*). Although functional measures of the vasculature have been correlated with glaucoma, no molecular characterization of the BRB has been performed, and it is known whether RGC dysfunction more broadly is associated with endothelial cell changes.

Role of the present study

We recognized that changes in retinal endothelial cells may reflect the health of RGCs and provide a leverage point for the discovery of clinical biomarkers. To determine whether retinal vessels change their transcription in response to RGC injury we isolated endothelial cells from the retinas of mice 5 days or 14 days after ONC and examined the transcriptome by RNA-sequencing. We determined differentially expressed genes, and attempted to localize differences in protein expression to endothelial cells after injury.

Results

ONC causes mild vascular remodeling and no BRB leakage

We characterized two gross aspects of the vascular response to ONC. It has not previously been reported that ONC has an effect on the intraretinal vessels, but this was important to know for our subsequent studies. We tested two different hypotheses related to vascular function. The first hypothesis was that ONC would lead to anatomical remodeling of capillaries in the retinal vascular plexuses. We examined the layer-specific density of retinal blood vessels by confocal microscopy 14 days after ONC. There was a slight decrease in capillary density in the superficial vascular plexus from 41.0 mm/mm^2 to 34.9 mm/mm^2 ($p = 0.046$), but differences in other layers were not significant (Figure 3.1A). We also examined the number of branch points per length of vessel, which can be indicative of vascular remodeling. We detected no change in the branching patterns of vessels in any vascular plexus (Figure 3.1B).

The second hypothesis was that ONC would lead to increased BRB permeability. Many injuries to neural tissue result in BRB breakdown, but this has not been previously examined in the retina. Five days or 14 days after ONC we injected sodium fluorescein intraperitoneally in mice, let the fluorescein circulate, then collected the retinas and blood and extracted the soluble fraction to measure the amount of fluorescence in the retina (normalized to serum fluorescein concentration for each animal). We found that there was no change in the amount of fluorescein in the retina at any either point compared to the control retina (Figure 3.1C). Taken together, these results suggest that there is not a dramatic effect of ONC on vascular integrity and BRB function.

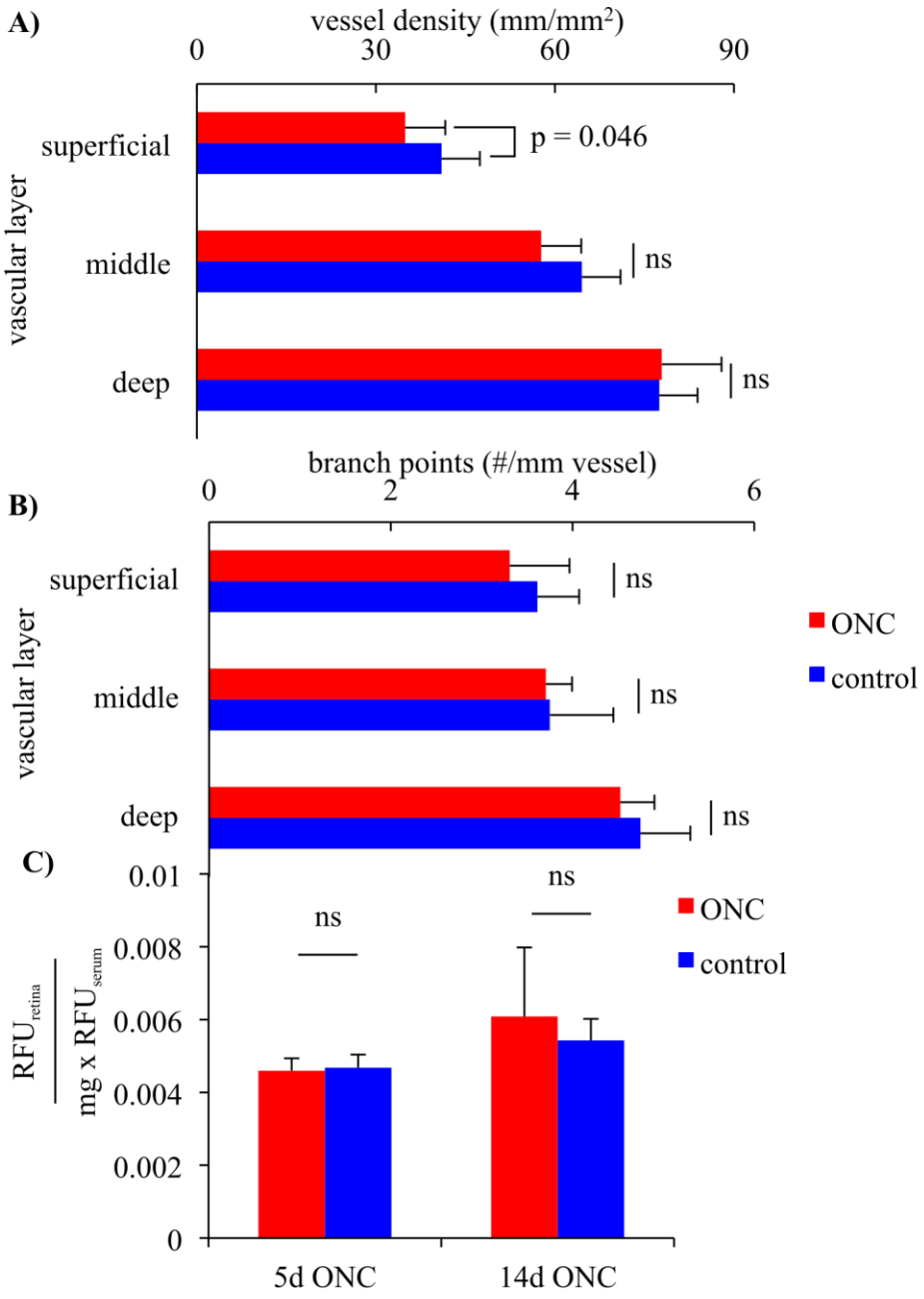

Figure 3.1. Effect of ONC on the vascular network and BRB function. (A) 14 days after ONC there was a slight decrease in capillary density in the superficial vascular plexus. No difference was detected in the superficial or deep plexus. No difference was detected in number of branch points in the vascular network. (B) Fluorescein uptake assay shows that there is not increased uptake after ONC at 5 or 14 days post-ONC. Error bars are + SEM. Statistical tests are paired Student's t-test, two-tailed; ns is not significant.

Isolation of retinal endothelial cells by immunopanning

To look for changes in retinal vessels after ONC we isolated endothelial cells, as these cells form the blood-facing component of the vasculature. We adapted a method for immunopanning endothelial cells from the brain previously described (*206*) for use in the retina. Briefly, anti-mouse CD45 and anti-mouse CD31 antibodies were immobilized on petri dishes. Retinas were enzymatically and mechanically dissociated to create a single-cell suspension, panned over the CD45 plate to remove microglia, then panned over the CD31 plate to select for endothelial cells. Examples of phase contrast images from cells on the panning plates are shown (Figure 3.2A). The eyes from 8 to 12 mice were pooled together to create a single sample.

We measured the purity of the endothelial cell preparations by immunostaining against Cldn5, a tight junction protein expressed only in RECs in the retina. We found that isolated cells came in a combination of clusters and single-cells (Figure 3.2B). Ninety-five percent of cells were Cldn5 positive. We also stained whole retina suspension for Cldn5 and found that less than 5% of the cells were Cldn5 positive, giving an estimate of how enriched

our preparation was for endothelial cells (Figure 3.2C).

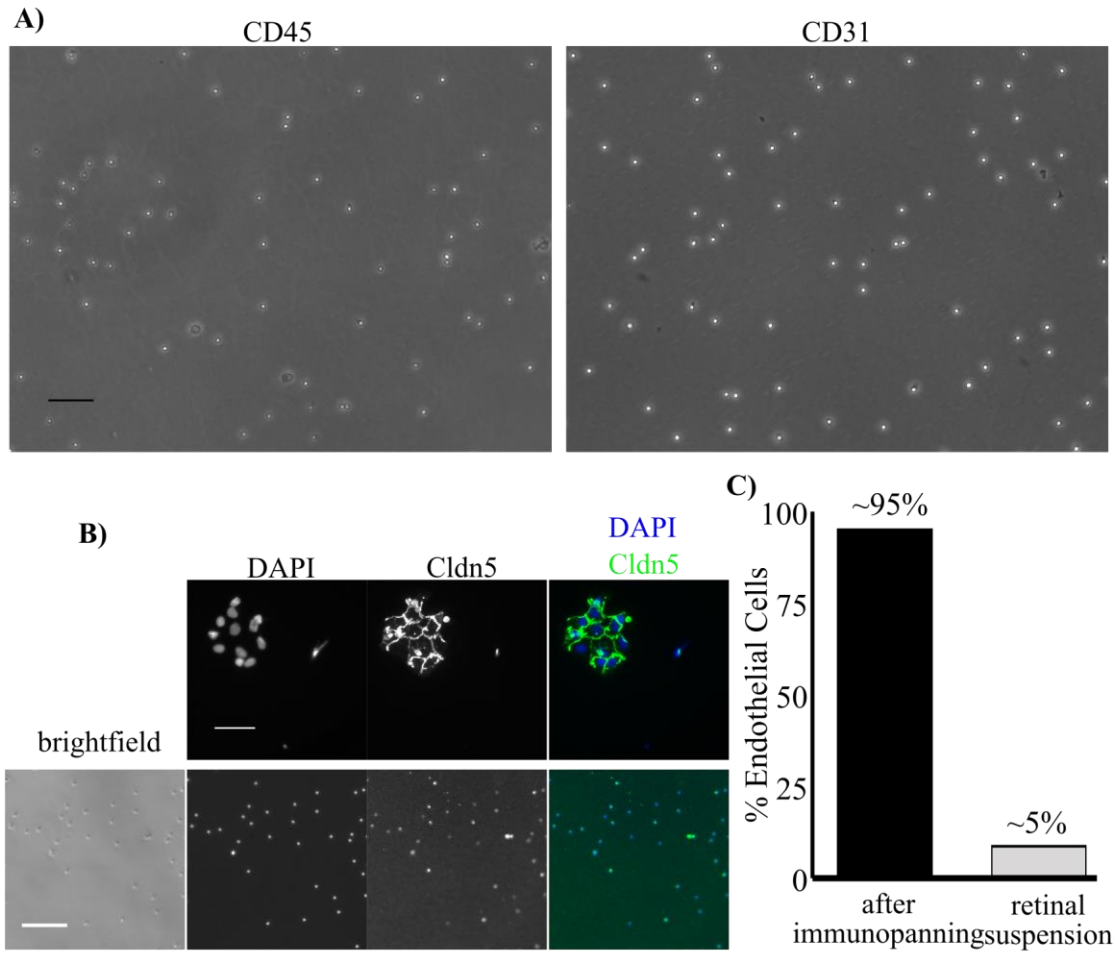

Figure 3.2. Immunopanning endothelial cells post-ONC. (A) Brightfield images show the density and morphology of cells on CD45 negative selection plates and CD31 positive selection plates. (B) mmunofluorescence staining for Cldn5, a tight junction protein, was used to indentify retinal endothelial cells.(C) Immunopanning resulted in preparations enriched to 95% endothelial cells. Retinal suspension prior to immunopanning was <5% endothelial cells. Scale bar in (A) is 100 um, in (B) upper panel is 50 um, lower panel is 100 um.

Purity, differential expression, and pathway analysis of RNA-seq data

We isolated total RNA from immunopanned and performed 2 x 150-bp sequencing after ribosomal RNA depletion. Reads were aligned to the Ensembl (mm9) transcriptome

using Bowtie2 and Tophat2, and differential expression was determined using DESeq2. A summary of the RNA sequencing data is shown in Table 3.1.

Table 3.1: Summary of RNA sequencing results from retinal microvascular cells 5 days (5D) and 14 days (14D) after optic nerve crush.

Condition	# of Samples	Genes >= 1.0 MNC	Sequencing	Total reads	Mapped reads
5D post-ONC	5 ONC/6 control	16940	2x150bp	25 million	~19 million
14D post-ONC	4 ONC/4 control	16927	2x150bp	25 million	~19 million

Since our endothelial cell preparations were only 95% pure endothelial cells, we wanted to discover what other retinal cell types might account for the other 5%. We selected a panel of genes known to be specific for endothelial cells (Pecam1, Cldn5, Tjp1, Ocln), pericytes (Pdgfrb, Cspg4), neurons (Rbfox3, Pou4f1, Thy1), microglia (Cx3cr1, C1qa, Ccl4), and astrocytes/Muller glia (Gfap, Slc1a3, Aldh1l1) to determine what the contaminating cell type might be. We found a significant number of reads aligning to Cx3cr1, C1qa, and Ccl4, but none of the other cell types (Figure 3.3). This suggests that the major contaminant of our endothelial cell preparations was microglia.

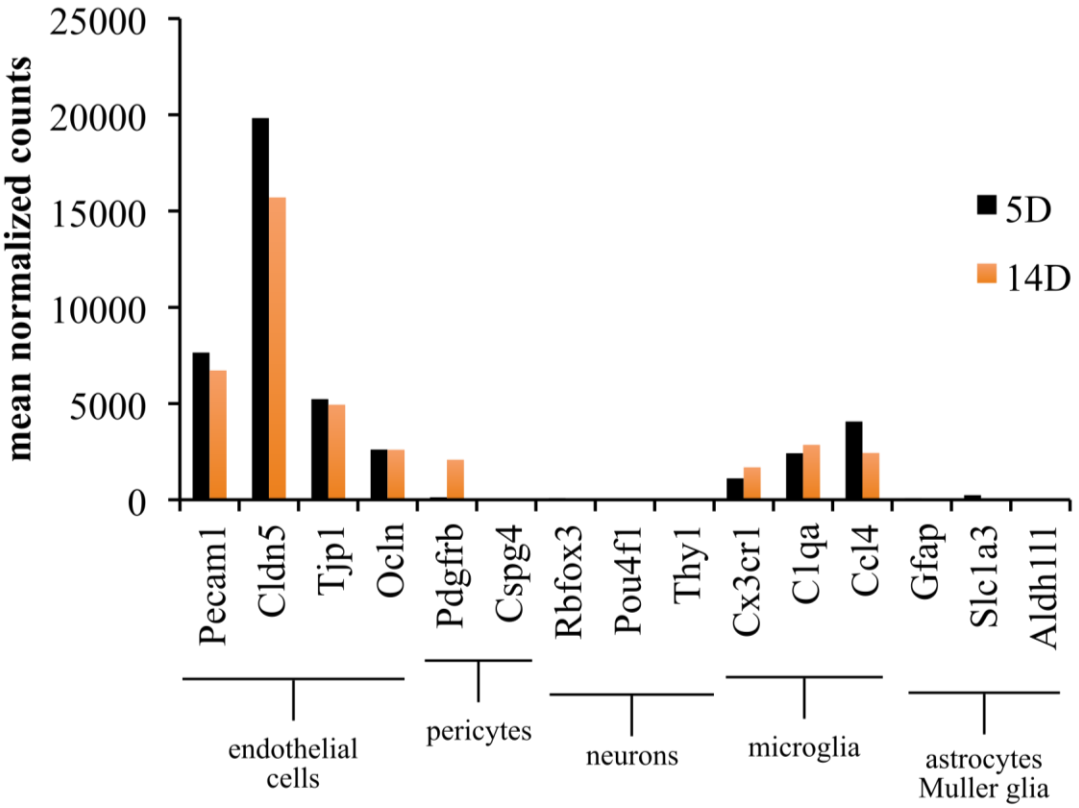

Figure 3.3. Post-transcriptome purity analysis. Representative genes from non-vascular cell types in the retina were examined for expression levels. We found very little evidence of RNA from neurons(Rbfox3, Thy1, Pou4f1), astrocytes/Muller glia (Gfap, Slc1a3, Aldh1l1), and pericytes (Pdgfrb, Cspg4). However, there was a significant amount of RNA from genes typically expressed in microglia (Cx3cr1, C1qa, Ccl4). Mean normalized counts of these genes approached the values of genes known to be specific for endothelial cells (Tjp1, Ocln, Pecam1, Cldn5).

Figure 3.4A shows the PCA plots for the samples at both timepoints. Although the samples did not cluster together well, we were still able to identify differentially expressed genes with confidence (Figure 3.4B, Table 3.2, Table 3.3). Applying a threshold of $p < 0.05$, there were 433 (388 up, 45 down) and 297 (104 up, 192 down) genes differentially expressed at 5 days and 14 days post-ONC, respectively (Table 3.2). Interestingly, 90% of differentially

expressed genes at 5 days were upregulated, compared to 24% at 14 days. Thirty-two genes were differentially expressed at both timepoints.

Table 3.2: Summary of differential gene expression patterns in retinal microvascular cells 5 days (5D) and 14 days (14D) after optic nerve crush.

Differntial Expression Summary

	5D - Total	5D - Up	5D - Down	14D - Total	14D - Up	14D - Down	5D & 14D - Total
# genes (p<0.05)	433	388	45	297	104	193	32
# genes (FDR<0.05)	37	36	1	1	1	0	0

Table 3.3: Most significant differentially expressed genes in retinal microvascular cells 5 days (5D) and 14 days (14D) after optic nerve crush.

Top 20 most significant differentially expressed genes

5D post-ONC					14D post-ONC				
Gene	MN Counts	log2 fold chang	p-val	FDR	Gene	MN Counts	log2 fold chang	p-val	FDR
Ptpn7	22.1	3.48	1.10E-08	0.0002	C3	86.0	1.71	5.05E-07	0.0088
Ccl6	768.5	2.67	4.86E-08	0.0003	Anks1b	74.5	-1.26	1.68E-05	0.1470
Clec7a	467.2	3.02	3.82E-08	0.0003	Lpl	257.9	1.39	6.11E-05	0.3289
Ltbp1	34.1	-3.05	3.61E-07	0.0014	Cox6a2	14.9	1.38	7.54E-05	0.3289
Spp1	5680.9	3.02	8.18E-07	0.0021	Hk3	87.9	1.38	1.22E-04	0.3917
Hcar2	538.9	2.94	9.02E-07	0.0021	Met	21.7	1.31	1.73E-04	0.3917
Lst1	78.6	2.60	8.09E-07	0.0021	Lrfn5	18.7	-1.33	1.80E-04	0.3917
Pbk	26.1	2.98	1.30E-06	0.0026	Fgfr4	16.5	-1.33	1.64E-04	0.3917
Hmmr	31.7	2.94	1.74E-06	0.0031	Gm35612	16.8	-1.28	2.60E-04	0.5045
Cd68	1589.0	2.35	3.98E-06	0.0062	Apoc1	14.5	1.29	4.04E-04	0.7055
Fcgr2b	402.3	2.53	4.28E-06	0.0062	C4b	126.8	1.27	4.77E-04	0.7185
BC147527	10.8	2.80	5.62E-06	0.0075	Il21r	88.4	1.18	4.94E-04	0.7185
Exo1	10.0	2.77	7.03E-06	0.0086	Ncam2	25.6	-1.23	5.44E-04	0.7296
Plbd1	48.5	2.75	8.19E-06	0.0093	Rap1gap2	159.6	-1.21	6.39E-04	0.7939
Ifi30	530.8	2.46	9.46E-06	0.0097	Naip5	88.4	0.98	6.83E-04	0.7939
Mpeg1	133.8	2.13	9.74E-06	0.0097	Camkv	510.7	-1.01	8.13E-04	0.8518
Fcer1g	1886.1	2.35	1.39E-05	0.0116	Calb2	509.2	-1.22	8.30E-04	0.8518
Fcgr3	817.5	2.00	1.38E-05	0.0116	Apoe	11657.6	0.76	3.28E-02	0.9998
Ms4a6c	148.6	2.56	1.34E-05	0.0116	Snap25	9152.9	-0.32	4.08E-02	0.9998
Gal	7.5	2.66	1.59E-05	0.0127	Ttyh1	1858.3	-0.44	1.86E-02	0.9998

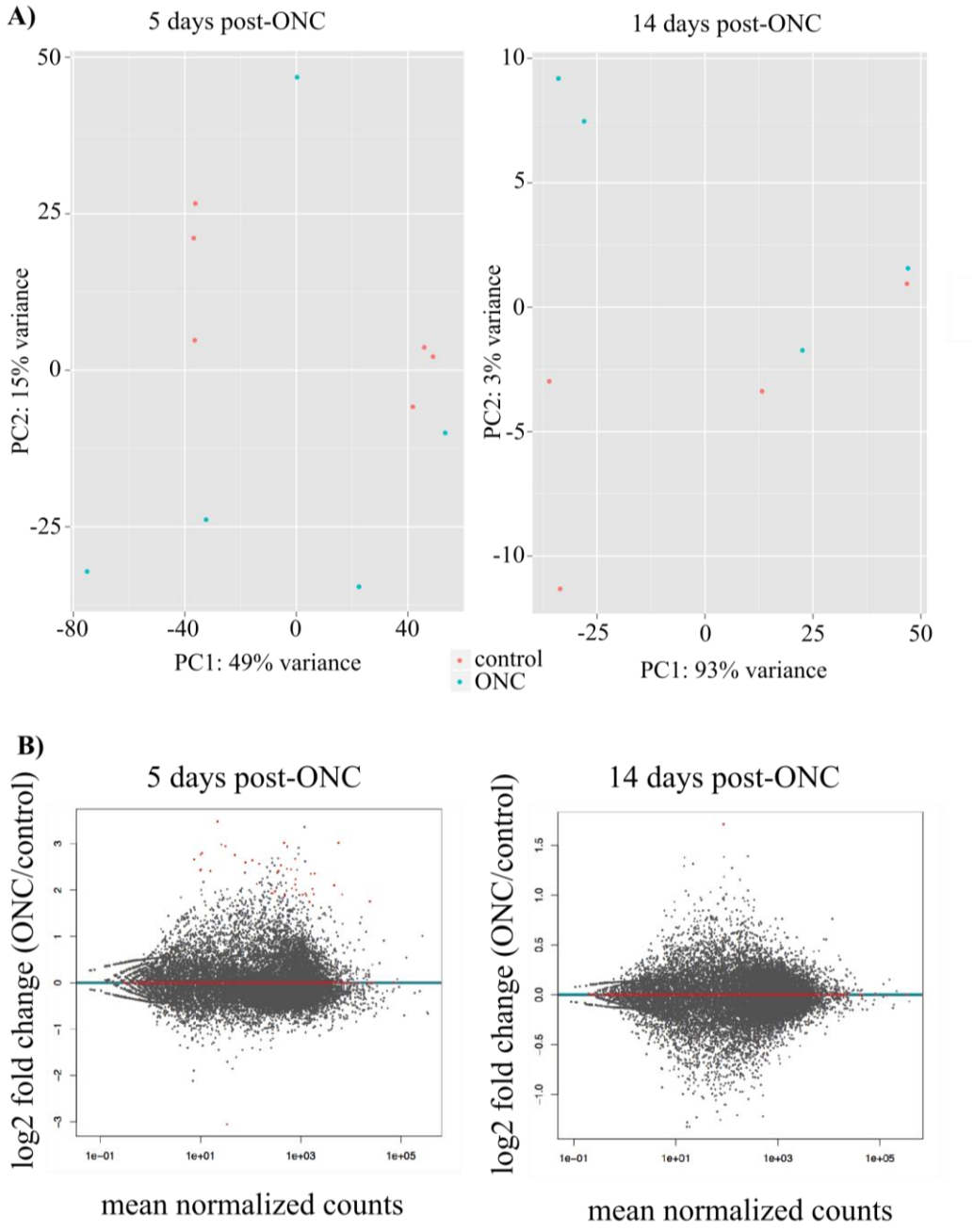

Figure 3.4. Differential gene expression in retinal vascular cells after optic nerve crush. (A) PCA plots show the clustering of samples from 5D and 14D post-ONC. (B) MA plots show that some genes were found to be differentially expressed at each time point. List of top differentially expressed genes is in Table 3.3.

Pathway analysis using the KEGG 2016 pathway database (executed through Enrichr) revealed annotated pathways for the genes differentially expressed at both timepoints. At 5D most of the significant pathways were related to immune function. At 14D only one pathway, the neuroactive ligand-receptor interaction pathway, was found. From the list of genes differentially expressed at both 5 and 14D, the toll-like receptor signaling pathway was significant. Taken together, these results suggest that microvascular cells have transcriptomic changes in response to ONC.

Immunostaining potential vascular biomarkers

We wanted to determine whether the differentially expressed genes also had differences in the amount of protein product present. We use immunofluorescence staining with a panel of antibodies against the product of the differentially expressed genes. We used two different methods of tissue fixation: methanol (precipitation fix), and paraformaldehyde (PFA, cross-linking fix) since these fixation methods can lead to different staining patterns for the same antibody/target combination. We examined retinas in both flat-mounts and cross-sections for qualitative differences in immunostaining. Many of the antibodies we used did not stain anything above background, or stained the tissue diffusely without any obvious differences between treatment groups. Some antibodies stained a subset of retinal cell types without showing clear differential staining. Some antibodies stained retinal cells differentially. We were able to identify the likely staining of different retinal cell types by morphology and location in the retina. We did not observe clear staining in endothelial cells, or differential staining in endothelial cells.

Conclusions and Discussion

The studies detailed in this chapter explore the response of the retinal vasculature to ONC. We showed that minor alterations in vascular patterning were induced in ONC, and that there was no increase in BRB permeability. We examined transcriptional changes in purified

endothelial cells and microglia and showed both that these cells respond to ONC, and that they respond differently at 5 days post-crush than at 14 days post-crush. By immunostaining, we found that many of the differentially expressed genes are highly expressed in cell types other than microglia and endothelial cells.

Our first set of experiments tested the hypothesis that there were gross vascular abnormalities in the retina after ONC. Injury to CNS tissue is frequently associated with two reactive pathologies: angiogenesis and increased barrier permeability. We examined the vascular network using confocal imaging to find evidence of vascular remodeling. To this end, we measured the total vessel density in the 3 vascular plexuses 14 days after ONC, when RGC death is highest. We also analyzed the vascular network by counting the number of branch points (the intersection between two independent vessel segments). Branch points provide some information about the state of the network; during development there are periods of rapid proliferation with high numbers of branch points which then get pruned back. We found that capillary density in the superficial layer, which is the layer that runs through the ganglion cell and nerve fiber layer had slightly reduced vessel density. No other capillary layers had reduced vessel density, and none had an altered number of branch points. Degeneration of vessels in the superficial layer may be related to a lack of trophic support from neurons - 14 days post-crush, only about 20% of RGCs remain. We analyzed the permeability of the BRB to the small molecule fluorescein and found that fluorescein uptake was not increased either 5 or 14 days after ONC. Barrier permeability in the retina after ONC has not been studied previously. It is known that the BRB is leaky at the crush site in the ON for several weeks post-crush (*207–209*). Although in other parts of the CNS barrier disruption is considered a negative phenomenon that adds additional insult to the original injury, in the ON permeability is viewed differently. In the ONs of animals with high intrinsic axonal regenerative capacity like goldfish and frog the ON and the retina are far more leaky than in mammals like rats and

mice, which have minimal axonal regeneration (*210, 211*). Our results suggest that any barrier and vascular defects arising from crush are likely confined to the ON and are not apparent in the retina.

Our second set of experiments was designed to isolate pure endothelial cells from the retina. We used sequential immunopanning of enzymatically and mechanically dissociated retinas to remove contaminating cell types and select for endothelial cells. Endothelial cells have a close association with CD45+ microglia, so we removed them by panning over an anti-CD45 plate, followed by the anti-CD31 selection plate for endothelial cells. We were able to generate a highly enriched preparation of endothelial cells, 95% pure as determined by Cldn5 positivity. Cldn5 is a tight junctional protein only expressed in endothelial cells in the retina. We were unable to positively identify the other 5% of cells by immunostaining.

Our third set of experiments tested the hypothesis that endothelial cells would have a transcriptional response to ONC. We isolated total RNA from immunopanned endothelial cells 5 and 14 days after ONC and found that a number of genes were differentially expressed in the ONC eye group compared to the sham surgery group. At 5 days post-ONC a large number of the genes were related to immune function. It has been previously described that ONC activates the immune system in the retina (*212–214*), leading to neutrophil and leukocyte infiltration, expression of pro-inflammatory receptors, and upregulation of immune-related signaling. Our data show that some of these changes localize to endothelial cells and microglia. By 14 days post-ONC very few differentially expressed genes were related to immune function. The only pathway change detected was the neuroactive ligands pathway, which was supported by differential expression of the gene group PTGER4, GABRA1, ADCYAP1R1, CHRNA4, PTAFR, GRIK2, ADRA2A, P2RX6, GLRA2, P2RY6, GRIN3A, EDNRB, GLRB, C3AR1, S1PR2. Many of these are purinergic or neurotransmitter receptors known to be expressed on RGCs. Indeed we observed staining of some differentially

expressed candidates in RGCs. But why would isolated endothelial cells and microglia show differential expression of proteins localized to RGCs? One explanation could be that RGCs are constantly sharing material (proteins, RNA, etc) with endothelial cells and/or microglia via phagocytosis, and after the crushed RGCs degenerate there are fewer cells around to generate phagocytic material. However, the set of genes contributing to neuroactive ligands was split in direction of differential expression - 6 out of 15 were up and the other 9 were down in ONC compared to control. It has been reported that RGC subtypes are differentially susceptible to injury (*187*, *215*), so perhaps different subtypes contribute differentially to the presence of RNA and protein inside microvascular cells.

Our fourth set of experiments were intended to localize the protein products of differentially expressed genes and discover endothelial-cell specific changes in protein expression. We immunostained 5D and 14D ONC retinas with a panel of antibodies. Most antibodies stained nothing, but some did clearly stain a subset of retinal cells. We were not able to observe clear staining of retinal endothelial cells, as determined by overlap with the signal from BSL staining.

Methods

Animals

Wild-type C57/BL6 mice purchased from Envigo. All animal experiments were performed in accordance with national guidelines and UCSD IACUC guidelines. Experimental/surgical procedures were performed to minimize animal stress and the number of animals used.

Optic nerve crush (ONC) surgery

Optic nerve crush surgery was performed in P28-P35 animals. The left optic nerve (ON) was exposed from the outer canthus, and crushed for 5 seconds with a Dumont # 5 forceps (91150–20, F.S.T.) approximately 1.5 mm behind the globe. Care was taken to avoid

damaging the blood supply to the retina. The right ON was exposed and encircled with the forceps but not crushed. Topical antibiotics and pain medication were administered in accordance with approved protocols.

Retina collection for vascular analysis

At 5 or 14 days after ONC mice were killed and the whole eyes were fixed in 4% PFA in 1x PBS at room temperature for 10 minutes, then transferred to 1x PBS on ice. The retinas were dissected out and fixed in methanol at -20 degrees overnight or post-fixed in 4% PFA for 45 minutes to 1 hour.

Immunofluorescence

Whole-mount fixed retinas were washed in PBS then blocked for 30 minutes in 0.2% BSA, 5% serum, and 0.3% Triton X-100, then incubated in primary antibody in blocking buffer overnight at 4 degrees with gentle rocking. Retinas were then washed in 0.3% Triton X-100 three times, and incubated with secondary antibodies in 0.3% Triton X-100 for 2-4 hours at room temperature, protected from light with gentle rocking. They were then washed in 0.3% Triton X-100 twice, 1x PBS twice, and then mounted on slides with Prolong Gold Antifade Reagent. BSL was biotinylated griffonia simplicifolia lectin I (Vector Laboratories B-1205, 1:250). Streptavidin was streptavidin conjugated to Alexa Fluor 594 (Thermo Fisher Scientific S32357, 1:1000).

Confocal and epifluorescence imaging

Confocal imaging was done on a Zeiss LSM 710. A 20x/0.8 NA air objective was used. Images were acquired at 1 airy unit resolution with 4x undersampling of pixels in X-Y and 2x undersampling in Z. Excitation lasers were 488 nm (for Alexa Fluor 488 and FITC), 561 nm (for Alexa Fluor 594), and 633 nm (for Alexa Fluor 647). Emissions were collected as separate tracks over wavelength bands exclusive with other mutually excited fluorophores. Epifluorescence images were collected on an Axio Imager D2 (Carl Zeiss) with a 5x Fluor,

0.25 NA or 20x Plan-Apochromat, 0.8 NA objective, using a digital camera (Axiocam HRm, Carl Zeiss). AxioVision software was used to acquire images; Fiji (ImageJ) and Inkscape were used for image processing and analysis.

Vascular image analysis

Volumes of the retina were sampled by confocal microscopy. ~425 um x 425 um z-stacks were taken ~500 um away from the center of the retina from each of the 4 sections of a flat-mounted retina. Confocal volumes were stitched using Zeiss' Zen software using a strictness of 0.9. Because the stacks were often not completely flat, they were then rotated in ImageJ using the TransformJ plugin so the superficial layer vasculature was in the same plane across every stack in the image. Portions of the image corresponding to each vascular layer were extracted and analyzed separately. Vessels were traced by hand, skeletonized in ImageJ using the Skeletonize plugin, and analyzed for length and branch points using the same plugin.

Fluorescein uptake assay

Mice were induced to a plane of surgical anesthesia by a mixture of ketamine/xylazine. Sodium fluorescein dissolved at 10% (w/v) in PBS was injected i.p. 2.5 uL per gram mouse. The fluorescein was allowed to circulate for 15 minutes, then the animals was sacrificed the retinas were dissected into tubes and weighed. Blood was also retrieved from cardiac puncture. Retinas were homogenized and the soluble fraction extracted with trichloroacetic acid (TCA). Extracts were centrifuged at 10,000 x g to remove the insoluble fraction. The supernatant was transferred to a fresh tube and neutralized with sodium hydroxide. Serum was separated from the blood, and the same TCA extraction protocol was used to collect serum fluorescein. Fluorescence intensity was read on a Tecan Spark Microplate reader, with excitation at 485 nm and emission at 530 nm. The fluorescein uptake ratio was calculated as $(RFU_{retina}/mg_{protein})/(RFU_{serum}/\mu L_{serum})$.

Immunopanning

Secondary antibodies included affinity purified Goat anti-Rat IgG (H & L), Jackson ImmunoResearch 112-005-167. Primary antibodies included rat anti-mouse CD45 (AbD Serotec MCA1031GA) and rat anti-mouse CD31 (BD Pharmingen 553370). Petri dishes (one 150 x 15 mm and one 100 x 15 mm; Fisher) were incubated with 5-15 ml of Tris buffer solution (pH 9.5) with 10 p.g/ml secondary antibody for 12 hr at 4°C. The dishes were washed three times with DPBS, and the small dish was incubated with 40 uL of rat anti-mouse CD31 antibody and the large dish was incubated with 20 uL of rat anti-mouse CD45 for 2 hr at room temperature in 0.2% BSA to prevent nonspecific binding of cells to plate.

Retinas obtained from ONC mice were dissociated enzymatically to make a suspension of single cells. Briefly, the tissue was incubated at 37°C for 30-45 min in a papain solution (15 U/ml for retina; Worthington) in an DPBS containing L-cysteine and 2 mM EDTA. Then calcium and magnesium were supplemented into the solution to 2 mM each and the tissue was incubated for an additional 15 min. The tissue was then triturated sequentially with a 1 mL pipette in a solution containing ovomucoid (1.5 mg/ml; Roche), DNase (0.004%; Sigma), and bovine serum albumin (BSA; 1 mg/ml; Sigma) to yield a suspension of single cells. Another ovomucoid/BSA solution (10 mg/mL) was layered underneath and the cells were centrifuged through it at 140 x g.

The retinal suspension was resuspended in panning buffer (DPBS with 0.02% BSA and 5 ug/mL insulin) and poured over the 150 mm anti-CD45 panning plate. The plate was incubated for 30 minutes at room temperature with gentle swirling at 15 minutes. The supernatant was then transferred to the two anti-CD31 panning plates, split equally between the two. The plate was incubated for 30 minutes at room temperature with gentle swirling at 15 minutes. The retinal suspension was then discarded and the CD31 panning plates washed 8 times with 10 mL DPBS. Plates were inspected visually for the presence of nonadherent cells

and imaged for cell counting. Endothelial cells were lysed on the plate by removal of the final DPBS wash and addition of 700 uL RLT buffer with beta-mercaptoethanol (Qiagen). Both plates were collected in one 700 uL volume of RLT buffer, spun through a QIAshredder column, and stored at -80 degrees.

mRNA purification, NGS library preparation, RNA-sequencing and bioinformatic analysis

Total RNA was isolated using the Qiagen RNeasy micro kit according to the manufacturer's instructions. Total RNA was then processed for library construction by Cofactor Genomics (http://cofactorgenomics.com, St. Louis, MO) according to the following procedure: Briefly, total RNA was reverse-transcribed using an Oligo(dT) primer, and limited cDNA amplification was performed using the SMARTer® Ultra® Low Input RNA Kit for Sequencing – v4 (Takara Bio USA, Inc., Mountain View, CA). The resulting full-length cDNA was fragmented and tagged, followed by limited PCR enrichment to generate the final cDNA sequencing library (Nextera® XT DNA Library Prep, Illumina, San Diego, CA). Libraries were sequenced as paired-end 150 base pair reads on an Illumina NextSeq500 following the manufacturer's instructions.

Sequenced reads were aligned to the Ensembl reference genome mm10 using tophat v2.0.11 and bowtie2 v2.2.1 with parameters --no-coverage-search -m 2 -a 5 -p 7. Alignment files were sorted using SAMtools v.0.1.19. Count tables were generated using HTSeq-0.6.1. Differential expression was analyzed using DESeq2.

Acknowledgements

This chapter is an original document written by Geoffrey Weiner with oversight from Jeffrey Goldberg. The work presented in this chapter was led by Geoffrey Weiner with contributions from members of the laboratories of Jeffrey Goldberg and Richard Daneman. Richard Daneman provided advice and protocols for immunopanning. Experiments were conducted in the laboratories of Jeffrey Goldberg.This work was supported by the Waitt

Advanced Biophotonics Core Facility of the Salk Institute with funding from NIH-NCI CCSG: P30 014195, NINDS Neuroscience Core Grant: NS072031 and the Waitt Foundation. Geoffrey Weiner is supported by a fellowship from the San Diego Foundation. Jeffrey Goldberg is supported by the Foundation Fighting Blindness, the Glaucoma Research Foundation, and the NIH.

References

Abboud, H., Labreuche, J., Meseguer, E., Lavallee, P.C., Simon, O., Olivot, J.-M., Mazighi, M., Dehoux, M., Benessiano, J., Steg, P.G., Amarenco, P., 2007. Ischemia-modified albumin in acute stroke. Cerebrovasc. Dis. 23, 216–220.

Allcutt, D., Berry, M., Sievers, J., 1984. A qualitative comparison of the reactions of retinal ganglion cell axons to optic nerve crush in neonatal and adult mice. Brain Res. 318, 231–240.

Ames, A., 3rd, Li, Y.Y., Heher, E.C., Kimble, C.R., 1992. Energy metabolism of rabbit retina as related to function: high cost of Na+ transport. J. Neurosci. 12, 840–853.

Anderson, B., Jr, Saltzman, H.A., 1964. RETINAL OXYGEN UTILIZATION MEASURED BY HYPERBARIC BLACKOUT. Arch. Ophthalmol. 72, 792–795.

Anderson, K.D., Pan, L., Yang, X.-M., Hughes, V.C., Walls, J.R., Dominguez, M.G., Simmons, M.V., Burfeind, P., Xue, Y., Wei, Y., Macdonald, L.E., Thurston, G., Daly, C., Lin, H.C., Economides, A.N., Valenzuela, D.M., Murphy, A.J., Yancopoulos, G.D., Gale, N.W., 2011. Angiogenic sprouting into neural tissue requires Gpr124, an orphan G protein-coupled receptor. Proc. Natl. Acad. Sci. U. S. A. 108, 2807–2812.

Angers, S., Moon, R.T., 2009. Proximal events in Wnt signal transduction. Nat. Rev. Mol. Cell Biol. 10, 468–477.

Antonetti, D.A., Wolpert, E.B., DeMaio, L., Harhaj, N.S., Scaduto, R.C., Jr, 2002. Hydrocortisone decreases retinal endothelial cell water and solute flux coincident with increased content and decreased phosphorylation of occludin. J. Neurochem. 80, 667–677.

Attwell, D., Laughlin, S.B., 2001. An energy budget for signaling in the grey matter of the brain. J. Cereb. Blood Flow Metab. 21, 1133–1145.

Baldridge, W.H., 1996. Optical recordings of the effects of cholinergic ligands on neurons in the ganglion cell layer of mammalian retina. J. Neurosci. 16, 5060–5072.

Bansal, A., Singer, J.H., Hwang, B.J., Xu, W., Beaudet, A., Feller, M.B., 2000. Mice lacking specific nicotinic acetylcholine receptor subunits exhibit dramatically altered spontaneous activity patterns and reveal a limited role for retinal waves in forming ON and OFF circuits in the inner retina. J. Neurosci. 20, 7672–7681.

Barber, A.J., Antonetti, D.A., 2003. Mapping the blood vessels with paracellular permeability in the retinas of diabetic rats. Invest. Ophthalmol. Vis. Sci. 44, 5410–5416.

Bazzoni, G., Dejana, E., 2004. Endothelial cell-to-cell junctions: molecular organization and role in vascular homeostasis. Physiol. Rev. 84, 869–901.

Ben-Ari, Y., Spitzer, N.C., 2010. Phenotypic checkpoints regulate neuronal development. Trends Neurosci. 33, 485–492.

Benedito, R., Roca, C., Sörensen, I., Adams, S., Gossler, A., Fruttiger, M., Adams, R.H., 2009. The notch ligands Dll4 and Jagged1 have opposing effects on angiogenesis. Cell 137, 1124–1135.

Bennett, J., Basivireddy, J., Kollar, A., Biron, K.E., Reickmann, P., Jefferies, W.A., McQuaid, S., 2010. Blood–brain barrier disruption and enhanced vascular permeability in the multiple sclerosis model EAE. J. Neuroimmunol. 229, 180–191.

Blankenship, A.G., Feller, M.B., 2010. Mechanisms underlying spontaneous patterned activity in developing neural circuits. Nat. Rev. Neurosci. 11, 18–29.

Blankenship, A.G., Ford, K.J., Johnson, J., Seal, R.P., Edwards, R.H., Copenhagen, D.R., Feller, M.B., 2009. Synaptic and extrasynaptic factors governing glutamatergic retinal waves. Neuron 62, 230–241.

Bonomi, L., Marchini, G., Marraffa, M., Bernardi, P., Morbio, R., Varotto, A., 2000. Vascular risk factors for primary open angle glaucoma: the Egna-Neumarkt Study. Ophthalmology 107, 1287–1293.

Calkins, D.J., Lambert, W.S., Formichella, C.R., McLaughlin, W.M., Sappington, R.M., 2018. The Microbead Occlusion Model of Ocular Hypertension in Mice. Methods Mol. Biol. 1695, 23–39.

Cameron, E.G., Goldberg, J.L., 2016. NEUROREGENERATION. Promoting CNS repair. Science 353, 30–31.

Carlisle, R., Lanphier, E.H., Rahn, H., 1964. HYPERBARIC OXYGEN AND PERSISTENCE OF VISION IN RETINAL ISCHEMIA. J. Appl. Physiol. 19, 914–918.

Chamney, S., McLoone, E., Willoughby, C.E., 2011. A mutation in the Norrie disease gene (NDP) associated with familial exudative vitreoretinopathy. Eye 25, 1658.

Chen, Z.-Y., Battinelli, E.M., Fielder, A., Bundey, S., Sims, K., Breakefield, X.O., Craig, I.W., 1993. A mutation in the Norrie disease gene (NDP) associated with X–linked familial exudative vitreoretinopathy. Nat. Genet. 5, 180–183.

Choi, Y.K., Kim, J.H., Kim, W.J., Lee, H.Y., Park, J.A., Lee, S.-W., Yoon, D.-K., Kim, H.H., Chung, H., Yu, Y.S., Kim, K.-W., 2007. AKAP12 Regulates Human Blood–Retinal Barrier Formation by Downregulation of Hypoxia-Inducible Factor-1α. J. Neurosci. 27, 4472–4481.

Clarke, D.D., Sokoloff, L., Others, 1999. Circulation and energy metabolism of the brain. Basic neurochemistry: molecular, cellular and medical aspects 6, 637–670.

Cohen, L.H., Noell, W.K., 1960. Glucose catabolism of rabbit retina before and after development of visual function. J. Neurochem. 5, 253–276.

Connolly, S.E., Hores, T.A., Smith, L.E., D'Amore, P.A., 1988. Characterization of vascular development in the mouse retina. Microvasc. Res. 36, 275–290.

Cullen, M., Elzarrad, M.K., Seaman, S., Zudaire, E., Stevens, J., Yang, M.Y., Li, X., Chaudhary, A., Xu, L., Hilton, M.B., Logsdon, D., Hsiao, E., Stein, E.V., Cuttitta, F., Haines, D.C., Nagashima, K., Tessarollo, L., St Croix, B., 2011. GPR124, an orphan G protein-coupled

receptor, is required for CNS-specific vascularization and establishment of the blood-brain barrier. Proc. Natl. Acad. Sci. U. S. A. 108, 5759–5764.

Daneman, R., Agalliu, D., Zhou, L., Kuhnert, F., Kuo, C.J., Barres, B.A., 2009. Wnt/β-catenin signaling is required for CNS, but not non-CNS, angiogenesis. Proceedings of the National Academy of Sciences 106, 641–646.

Daneman, R., Prat, A., 2015. The blood-brain barrier. Cold Spring Harb. Perspect. Biol. 7, a020412.

Daneman, R., Zhou, L., Kebede, A.A., Barres, B.A., 2010. Pericytes are required for blood-brain barrier integrity during embryogenesis. Nature 468, 562–566.

Dejana, E., Orsenigo, F., Lampugnani, M.G., 2008. The role of adherens junctions and VE-cadherin in the control of vascular permeability. J. Cell Sci. 121, 2115–2122.

Detry, M., Boschi, A., Ellinghaus, G., De Plaen, J.F., 1996. Simultaneous 24-hour monitoring of intraocular pressure and arterial blood pressure in patients with progressive and non-progressive primary open-angle glaucoma. Eur. J. Ophthalmol. 6, 273–278.

Dohgu, S., Takata, F., Yamauchi, A., Nakagawa, S., Egawa, T., Naito, M., Tsuruo, T., Sawada, Y., Niwa, M., Kataoka, Y., 2005. Brain pericytes contribute to the induction and up-regulation of blood–brain barrier functions through transforming growth factor-β production. Brain Res. 1038, 208–215.

Dorrell, M.I., Friedlander, M., 2006. Mechanisms of endothelial cell guidance and vascular patterning in the developing mouse retina. Prog. Retin. Eye Res. 25, 277–295.

El-Danaf, R.N., Huberman, A.D., 2015. Characteristic patterns of dendritic remodeling in early-stage glaucoma: evidence from genetically identified retinal ganglion cell types. J. Neurosci. 35, 2329–2343.

Elias, B.C., Suzuki, T., Seth, A., Giorgianni, F., Kale, G., Shen, L., Turner, J.R., Naren, A., Desiderio, D.M., Rao, R., 2009. Phosphorylation of Tyr-398 and Tyr-402 in occludin prevents its interaction with ZO-1 and destabilizes its assembly at the tight junctions. J. Biol. Chem. 284, 1559–1569.

Erickson, K.K., Sundstrom, J.M., Antonetti, D.A., 2007. Vascular permeability in ocular disease and the role of tight junctions. Angiogenesis 10, 103–117.

Famiglietti, E.V., Jr., 1983. “Starburst” amacrine cells and cholinergic neurons: mirror-symmetric ON and OFF amacrine cells of rabbit retina. Brain Res. 261, 138–144.

Fanning, A.S., Little, B.P., Rahner, C., Utepbergenov, D., Walther, Z., Anderson, J.M., 2007. The Unique-5 and -6 Motifs of ZO-1 Regulate Tight Junction Strand Localization and Scaffolding Properties. Mol. Biol. Cell 18, 721–731.

Farquhar, M.G., Palade, G.E., 1963. Junctional complexes in various epithelia. J. Cell Biol. 17, 375–412.

Farrall, A.J., Wardlaw, J.M., 2009. Blood--brain barrier: ageing and microvascular disease--systematic review and meta-analysis. Neurobiol. Aging 30, 337–352.

Feldheim, D.A., O'Leary, D.D.M., 2010. Visual map development: bidirectional signaling, bifunctional guidance molecules, and competition. Cold Spring Harb. Perspect. Biol. 2, a001768.

Felinski, E.A., Antonetti, D.A., 2005. Glucocorticoid regulation of endothelial cell tight junction gene expression: novel treatments for diabetic retinopathy. Curr. Eye Res. 30, 949–957.

Feller, M.B., Wellis, D.P., Stellwagen, D., Werblin, F.S., Shatz, C.J., 1996. Requirement for cholinergic synaptic transmission in the propagation of spontaneous retinal waves. Science 272, 1182–1187.

Feng, Y., Venema, V.J., Venema, R.C., Tsai, N., Behzadian, M.A., Caldwell, R.B., 1999. VEGF-induced permeability increase is mediated by caveolae. Invest. Ophthalmol. Vis. Sci. 40, 157–167.

Fenstermacher, J., Gross, P., Sposito, N., Acuff, V., Pettersen, S., Gruber, K., 1988. Structural and functional variations in capillary systems within the brain. Ann. N. Y. Acad. Sci. 529, 21–30.

Firth, S.I., Wang, C.-T., Feller, M.B., 2005. Retinal waves: mechanisms and function in visual system development. Cell Calcium 37, 425–432.

Forman, D.S., Brown, K.J., Livengood, D.R., 1983. Fast axonal transport in permeabilized lobster giant axons is inhibited by vanadate. J. Neurosci. 3, 1279–1288.

Frank, M., Wolburg, H., 1996. Cellular reactions at the lesion site after crushing of the rat optic nerve. Glia 16, 227–240.

Fried, S.I., Münch, T.A., Werblin, F.S., 2002. Mechanisms and circuitry underlying directional selectivity in the retina. Nature 420, 411–414.

Fruttiger, M., 2007. Development of the retinal vasculature. Angiogenesis 10, 77–88.

Gariano, R.F., Gardner, T.W., 2005. Retinal angiogenesis in development and disease. Nature 438, 960–966.

Gerhardt, H., Golding, M., Fruttiger, M., Ruhrberg, C., Lundkvist, A., Abramsson, A., Jeltsch, M., Mitchell, C., Alitalo, K., Shima, D., Betsholtz, C., 2003. VEGF guides angiogenic sprouting utilizing endothelial tip cell filopodia. J. Cell Biol. 161, 1163–1177.

Godinho, L., Mumm, J.S., Williams, P.R., Schroeter, E.H., Koerber, A., Park, S.W., Leach, S.D., Wong, R.O.L., 2005. Targeting of amacrine cell neurites to appropriate synaptic laminae in the developing zebrafish retina. Development 132, 5069–5079.

Goldberg, J.L., Espinosa, J.S., Xu, Y., Davidson, N., Kovacs, G.T.A., Barres, B.A., 2002. Retinal ganglion cells do not extend axons by default: promotion by neurotrophic signaling and electrical activity. Neuron 33, 689–702.

Graham, S.L., Drance, S.M., 1999. Nocturnal hypotension: role in glaucoma progression. Surv. Ophthalmol. 43 Suppl 1, S10–6.

Graymore, C., 1959. Metabolism of the developing retina. I. Aerobic and anaerobic glycolysis in the developing rat retina. Br. J. Ophthalmol. 43, 34–39.

Greiner, J.V., Weidman, T.A., 1981. Histogenesis of the ferret retina. Exp. Eye Res. 33, 315–332.

Grubb, M.S., Rossi, F.M., Changeux, J.P., Thompson, I.D., 2003. Abnormal functional organization in the dorsal lateral geniculate nucleus of mice lacking the beta 2 subunit of the nicotinic acetylcholine receptor. Neuron 40, 1161–1172.

Gunhan, E., Choudary, P.V., Landerholm, T.E., Chalupa, L.M., 2002. Depletion of cholinergic amacrine cells by a novel immunotoxin does not perturb the formation of segregated on and off cone bipolar cell projections. J. Neurosci. 22, 2265–2273.

Gyllensten, L.J., Hellström, B.O.E., 1954. Experimental Approach to the Pathogenesis of Retrolental Fibroplasia: I. Changes of the Eye Induced by Exposure of Newborn Mice to Concentrated Oxygen. Acta Pædiatrica 43, 131–148.

Hawkins, B.T., Lundeen, T.F., Norwood, K.M., Brooks, H.L., Egleton, R.D., 2007. Increased blood–brain barrier permeability and altered tight junctions in experimental diabetes in the rat: contribution of hyperglycaemia and matrix metalloproteinases. Diabetologia 50, 202–211.

Hayashi, S.-I., Sato, N., Yamamoto, A., Ikegame, Y., Nakashima, S., Ogihara, T., Morishita, R., 2009. Alzheimer disease-associated peptide, amyloid beta40, inhibits vascular regeneration with induction of endothelial autophagy. Arterioscler. Thromb. Vasc. Biol. 29, 1909–1915.

Hayden, S.A., Mills, J.W., Masland, R.M., 1980. Acetylcholine synthesis by displaced amacrine cells. Science 210, 435–437.

Hellström, M., Gerhardt, H., Kalén, M., Li, X., Eriksson, U., Wolburg, H., Betsholtz, C., 2001. Lack of pericytes leads to endothelial hyperplasia and abnormal vascular morphogenesis. J. Cell Biol. 153, 543–553.

Hellström, M., Phng, L.-K., Hofmann, J.J., Wallgard, E., Coultas, L., Lindblom, P., Alva, J., Nilsson, A.-K., Karlsson, L., Gaiano, N., Yoon, K., Rossant, J., Iruela-Arispe, M.L., Kalén, M., Gerhardt, H., Betsholtz, C., 2007. Dll4 signalling through Notch1 regulates formation of tip cells during angiogenesis. Nature 445, 776–780.

Hofman, P., Blaauwgeers, H.G.T., Tolentino, M.J., Adamis, A.P., Nunes Cardozo, B.J., Vrensen, G.F.J.M., Schlingemann, R.O., 2000. VEGF-A induced hyperpermeability of blood-retinal barrier endothelium in vivo is predominantly associated with pinocytotic vesicular transport and not with formation of fenestrations. Curr. Eye Res. 21, 637–645.

Holman, D.W., Klein, R.S., Ransohoff, R.M., 2011/2. The blood–brain barrier, chemokines and multiple sclerosis. Biochimica et Biophysica Acta (BBA) - Molecular Basis of Disease 1812, 220–230.

Hoover, F., Goldman, D., 1992. Temporally correlated expression of nAChR genes during development of the mammalian retina. Exp. Eye Res. 54, 561–571.

Hori, S., Ohtsuki, S., Hosoya, K.-I., Nakashima, E., Terasaki, T., 2004. A pericyte-derived angiopoietin-1 multimeric complex induces occludin gene expression in brain capillary endothelial cells through Tie-2 activation in vitro. J. Neurochem. 89, 503–513.

Howard, J., Blakeslee, B., Laughlin, S.B., 1987. The intracellular pupil mechanism and photoreceptor signal: noise ratios in the fly Lucilia cuprina. Proc. R. Soc. Lond. B Biol. Sci. 231, 415–435.

Hsu, S.C., Molday, R.S., 1991. Glycolytic enzymes and a GLUT-1 glucose transporter in the outer segments of rod and cone photoreceptor cells. J. Biol. Chem. 266, 21745–21752.

Huang, H.-M., Huang, C.-C., Wang, F.-S., Hung, P.-L., Chang, Y.-C., 2015. Activating the Wnt/β-Catenin Pathway Did Not Protect Immature Retina from Hypoxic-Ischemic InjuryWnt Signaling With HI Injury in Immature Retina. Invest. Ophthalmol. Vis. Sci. 56, 4300–4308.

Huberman, A.D., Feller, M.B., Chapman, B., 2008. Mechanisms underlying development of visual maps and receptive fields. Annu. Rev. Neurosci. 31, 479–509.

Hulsman, C.A.A., Vingerling, J.R., Hofman, A., Witteman, J.C.M., de Jong, P.T.V.M., 2007. Blood pressure, arterial stiffness, and open-angle glaucoma: the Rotterdam study. Arch. Ophthalmol. 125, 805–812.

Hutchins, J.B., Bernanke, J.M., Jefferson, V.E., 1995. Acetylcholinesterase in the developing ferret retina. Exp. Eye Res. 60, 113–125.

Janzer, R.C., Raff, M.C., 1987. Astrocytes induce blood–brain barrier properties in endothelial cells. Nature 325, 253–257.

Jiao, X., Ventruto, V., Trese, M.T., Shastry, B.S., Hejtmancik, J.F., 2004. Autosomal recessive familial exudative vitreoretinopathy is associated with mutations in LRP5. Am. J. Hum. Genet. 75, 878–884.

Joyal, J.-S., Sun, Y., Gantner, M.L., Shao, Z., Evans, L.P., Saba, N., Fredrick, T., Burnim, S., Kim, J.S., Patel, G., Juan, A.M., Hurst, C.G., Hatton, C.J., Cui, Z., Pierce, K.A., Bherer, P., Aguilar, E., Powner, M.B., Vevis, K., Boisvert, M., Fu, Z., Levy, E., Fruttiger, M., Packard, A., Rezende, F.A., Maranda, B., Sapieha, P., Chen, J., Friedlander, M., Clish, C.B., Smith, L.E.H., 2016. Retinal lipid and glucose metabolism dictates angiogenesis through the lipid sensor Ffar1. Nat. Med. 22, 439–445.

Junge, H.J., Yang, S., Burton, J.B., Paes, K., Shu, X., French, D.M., Costa, M., Rice, D.S., Ye, W., 2009. TSPAN12 regulates retinal vascular development by promoting Norrin- but not Wnt-induced FZD4/beta-catenin signaling. Cell 139, 299–311.

Kaelin, W.G., Jr, 2011. Cancer and altered metabolism: potential importance of hypoxia-inducible factor and 2-oxoglutarate-dependent dioxygenases. Cold Spring Harb. Symp. Quant. Biol. 76, 335–345.

Kageyama, G.H., Wong-Riley, M.T., 1984. The histochemical localization of cytochrome oxidase in the retina and lateral geniculate nucleus of the ferret, cat, and monkey, with particular reference to retinal mosaics and ON/OFF-center visual channels. J. Neurosci. 4, 2445–2459.

Karaküçük, S., Mirza, G.E., 2000. Ophthalmological effects of high altitude. Ophthalmic Res. 32, 30–40.

Kiernan, J.A., 1985. Axonal and vascular changes following injury to the rat's optic nerve. J. Anat. 141, 139–154.

Kiernan, J.A., Contestabile, A., 1980. Vascular permeability associated with axonal regeneration in the optic system of the goldfish. Acta Neuropathol. 51, 39–45.

Kirk, J., Plumb, J., Mirakhur, M., McQuaid, S., 2003. Tight junctional abnormality in multiple sclerosis white matter affects all calibres of vessel and is associated with blood–brain barrier leakage and active demyelination. J. Pathol. 201, 319–327.

Kuhnert, F., Mancuso, M.R., Shamloo, A., Wang, H.-T., Choksi, V., Florek, M., Su, H., Fruttiger, M., Young, W.L., Heilshorn, S.C., Kuo, C.J., 2010. Essential regulation of CNS angiogenesis by the orphan G protein-coupled receptor GPR124. Science 330, 985–989.

Kumagai, A.K., Glasgow, B.J., Pardridge, W.M., 1994. GLUT1 glucose transporter expression in the diabetic and nondiabetic human eye. Invest. Ophthalmol. Vis. Sci. 35, 2887–2894.

Kunzevitzky, N.J., Almeida, M.V., Duan, Y., Li, S., Xiang, M., Goldberg, J.L., 2011. Foxn4 is required for retinal ganglion cell distal axon patterning. Mol. Cell. Neurosci. 46, 731–741.

Kurihara, T., Westenskow, P.D., Friedlander, M., 2014. Hypoxia-inducible factor (HIF)/vascular endothelial growth factor (VEGF) signaling in the retina. Adv. Exp. Med. Biol. 801, 275–281.

Kurimoto, T., Yin, Y., Habboub, G., Gilbert, H.-Y., Li, Y., Nakao, S., Hafezi-Moghadam, A., Benowitz, L.I., 2013. Neutrophils express oncomodulin and promote optic nerve regeneration. J. Neurosci. 33, 14816–14824.

Leske, M.C., Heijl, A., Hyman, L., Bengtsson, B., Dong, L., Yang, Z., EMGT Group, 2007. Predictors of long-term progression in the early manifest glaucoma trial. Ophthalmology 114, 1965–1972.

Leske, M.C., Wu, S.-Y., Hennis, A., Honkanen, R., Nemesure, B., BESs Study Group, 2008. Risk factors for incident open-angle glaucoma: the Barbados Eye Studies. Ophthalmology 115, 85–93.

Lesk, M.R., Hafez, A.S., Descovich, D., 2006. Relationship between central corneal thickness and changes of optic nerve head topography and blood flow after intraocular pressure reduction in open-angle glaucoma and ocular hypertension. Arch. Ophthalmol. 124, 1568–1572.

Liebner, S., Corada, M., Bangsow, T., Babbage, J., Taddei, A., Czupalla, C.J., Reis, M., Felici, A., Wolburg, H., Fruttiger, M., Taketo, M.M., von Melchner, H., Plate, K.H., Gerhardt, H., Dejana, E., 2008. Wnt/β-catenin signaling controls development of the blood–brain barrier. J. Cell Biol. 183, 409–417

.

Lindahl, P., Johansson, B.R., Levéen, P., Betsholtz, C., 1997. Pericyte loss and microaneurysm formation in PDGF-B-deficient mice. Science 277, 242–245.

Liu, C., Nathans, J., 2008. An essential role for frizzled 5 in mammalian ocular development. Development 135, 3567–3576.

Liu, H., Thurig, S., Mohamed, O., Dufort, D., Wallace, V.A., 2006. Mapping canonical Wnt signaling in the developing and adult retina. Invest. Ophthalmol. Vis. Sci. 47, 5088–5097.

Liu, L.-Y., Zheng, H., Xiao, H.-L., She, Z.-J., Zhao, S.-M., Chen, Z.-L., Zhou, G.-M., 2008. Comparison of blood–nerve barrier disruption and matrix metalloprotease-9 expression in injured central and peripheral nerves in mice. Neurosci. Lett. 434, 155–159.

Li, W., Kohara, H., Uchida, Y., James, J.M., Soneji, K., Cronshaw, D.G., Zou, Y.-R., Nagasawa, T., Mukouyama, Y.-S., 2013. Peripheral nerve-derived CXCL12 and VEGF-A regulate the patterning of arterial vessel branching in developing limb skin. Dev. Cell 24, 359–371.

Lobov, I.B., Rao, S., Carroll, T.J., Vallance, J.E., Ito, M., Ondr, J.K., Kurup, S., Glass, D.A., Patel, M.S., Shu, W., Morrisey, E.E., McMahon, A.P., Karsenty, G., Lang, R.A., 2005. WNT7b mediates macrophage-induced programmed cell death in patterning of the vasculature. Nature 437, 417–421.

Lobov, I.B., Renard, R.A., Papadopoulos, N., Gale, N.W., Thurston, G., Yancopoulos, G.D., Wiegand, S.J., 2007. Delta-like ligand 4 (Dll4) is induced by VEGF as a negative regulator of angiogenic sprouting. Proc. Natl. Acad. Sci. U. S. A. 104, 3219–3224.

MacNeil, M.A., Heussy, J.K., Dacheux, R.F., Raviola, E., Masland, R.H., 1999. The shapes and numbers of amacrine cells: matching of photofilled with Golgi-stained cells in the rabbit retina and comparison with other mammalian species. J. Comp. Neurol. 413, 305–326.

Mantych, G.J., Hageman, G.S., Devaskar, S.U., 1993. Characterization of glucose transporter isoforms in the adult and developing human eye. Endocrinology 133, 600–607.

Marco, S., Skaper, S.D., 2006. Amyloid beta-peptide1-42 alters tight junction protein distribution and expression in brain microvessel endothelial cells. Neurosci. Lett. 401, 219–224.

Masland, R.H., Ames, A., 3rd, 1976. Responses to acetylcholine of ganglion cells in an isolated mammalian retina. J. Neurophysiol. 39, 1220–1235.

Masland, R.H., Mills, J.W., Cassidy, C., 1984. The functions of acetylcholine in the rabbit retina. Proc. R. Soc. Lond. B Biol. Sci. 223, 121–139.

Medrano, C.J., Fox, D.A., 1995. Oxygen consumption in the rat outer and inner retina: light- and pharmacologically-induced inhibition. Exp. Eye Res. 61, 273–284.

Mehta, V., Sernagor, E., 2006. Early neural activity and dendritic growth in turtle retinal ganglion cells. Eur. J. Neurosci. 24, 773–786.

Meister, M., Wong, R.O., Baylor, D.A., Shatz, C.J., 1991. Synchronous bursts of action potentials in ganglion cells of the developing mammalian retina. Science 252, 939–943.

Mezu-Ndubuisi, O.J., Teng, P.-Y., Wanek, J., Blair, N.P., Chau, F.Y., Reddy, N.M., Raj, J.U., Reddy, S.P., Shahidi, M., 2013. In vivo retinal vascular oxygen tension imaging and fluorescein angiography in the mouse model of oxygen-induced retinopathy. Invest. Ophthalmol. Vis. Sci. 54, 6968–6972.

Montagne, A., Barnes, S.R., Sweeney, M.D., Halliday, M.R., Sagare, A.P., Zhao, Z., Toga, A.W., Jacobs, R.E., Liu, C.Y., Amezcua, L., Harrington, M.G., Chui, H.C., Law, M., Zlokovic, B.V., 2015. Blood-brain barrier breakdown in the aging human hippocampus. Neuron 85, 296–302.

Mooney, R., Penn, A.A., Gallego, R., Shatz, C.J., 1996. Thalamic relay of spontaneous retinal activity prior to vision. Neuron 17, 863–874.

Mooradian, A.D., Haas, M.J., Batejko, O., Hovsepyan, M., Feman, S.S., 2005. Statins ameliorate endothelial barrier permeability changes in the cerebral tissue of streptozotocin-induced diabetic rats. Diabetes 54, 2977–2982.

Moore, D.L., Blackmore, M.G., Hu, Y., Kaestner, K.H., Bixby, J.L., Lemmon, V.P., Goldberg, J.L., 2009. KLF family members regulate intrinsic axon regeneration ability. Science 326, 298–301.

Morrison, J.C., Johnson, E.C., Cepurna, W.O., 2018. Hypertonic Saline Injection Model of Experimental Glaucoma in Rats. Methods Mol. Biol. 1695, 11–21.

Mumm, J.S., Williams, P.R., Godinho, L., Koerber, A., Pittman, A.J., Roeser, T., Chien, C.-B., Baier, H., Wong, R.O.L., 2006. In vivo imaging reveals dendritic targeting of laminated afferents by zebrafish retinal ganglion cells. Neuron 52, 609–621.

Nakakura, S., Nomura, Y., Ataka, S., Shiraki, K., 2007. Relation Between Office Intraocular Pressure and 24-hour Intraocular Pressure in Patients With Primary Open-angle Glaucoma Treated With a Combination of Topical Antiglaucoma Eye Drops. J. Glaucoma 16, 201–204.

Nicaise, C., Mitrecic, D., Demetter, P., De Decker, R., Authelet, M., Boom, A., Pochet, R., 2009. Impaired blood-brain and blood-spinal cord barriers in mutant SOD1-linked ALS rat. Brain Res. 1301, 152–162.

Okabe, K., Kobayashi, S., Yamada, T., Kurihara, T., Tai-Nagara, I., Miyamoto, T., Mukouyama, Y.-S., Sato, T.N., Suda, T., Ema, M., Kubota, Y., 2014. Neurons limit angiogenesis by titrating VEGF in retina. Cell 159, 584–596.

Okawa, H., Sampath, A.P., Laughlin, S.B., Fain, G.L., 2008. ATP consumption by mammalian rod photoreceptors in darkness and in light. Curr. Biol. 18, 1917–1921.

Ou, Y., Jo, R.E., Ullian, E.M., Wong, R.O.L., Della Santina, L., 2016. Selective Vulnerability of Specific Retinal Ganglion Cell Types and Synapses after Transient Ocular Hypertension. J. Neurosci. 36, 9240–9252.

Pache, M., Flammer, J., 2006. A sick eye in a sick body? Systemic findings in patients with primary open-angle glaucoma. Surv. Ophthalmol. 51, 179–212.

Penn, A.A., Riquelme, P.A., Feller, M.B., Shatz, C.J., 1998. Competition in retinogeniculate patterning driven by spontaneous activity. Science 279, 2108–2112.

Phillips, B.E., Cancel, L., Tarbell, J.M., Antonetti, D.A., 2008. Occludin independently regulates permeability under hydrostatic pressure and cell division in retinal pigment epithelial cells. Invest. Ophthalmol. Vis. Sci. 49, 2568–2576.

Plumb, J., McQuaid, S., Mirakhur, M., Kirk, J., 2002. Abnormal endothelial tight junctions in active lesions and normal-appearing white matter in multiple sclerosis. Brain Pathol. 12, 154–169.

Pournaras, C.J., Rungger-Brändle, E., Riva, C.E., Hardarson, S.H., Stefansson, E., 2008. Regulation of retinal blood flow in health and disease. Prog. Retin. Eye Res. 27, 284–330.

Quigley, H.A., West, S.K., Rodriguez, J., Munoz, B., Klein, R., Snyder, R., 2001. The prevalence of glaucoma in a population-based study of Hispanic subjects: Proyecto VER. Arch. Ophthalmol. 119, 1819–1826.

Ramirez, S.H., Fan, S., Dykstra, H., Reichenbach, N., Del Valle, L., Potula, R., Phipps, R.P., Maggirwar, S.B., Persidsky, Y., 2010. Dyad of CD40/CD40 Ligand Fosters Neuroinflammation at the Blood–Brain Barrier and Is Regulated via JNK Signaling: Implications for HIV-1 Encephalitis. J. Neurosci. 30, 9454–9464.

Rattner, A., Wang, Y., Zhou, Y., Williams, J., Nathans, J., 2014. The role of the hypoxia response in shaping retinal vascular development in the absence of Norrin/Frizzled4 signaling. Invest. Ophthalmol. Vis. Sci. 55, 8614–8625.

Ricardo-Dukelow, M., Kadiu, I., Rozek, W., Schlautman, J., Persidsky, Y., Ciborowski, P., Kanmogne, G.D., Gendelman, H.E., 2007. HIV-1 infected monocyte-derived macrophages affect the human brain microvascular endothelial cell proteome: new insights into blood-brain barrier dysfunction for HIV-1-associated dementia. J. Neuroimmunol. 185, 37–46.

Ritter, M.R., Aguilar, E., Banin, E., Scheppke, L., Uusitalo-Jarvinen, H., Friedlander, M., 2005. Three-dimensional in vivo imaging of the mouse intraocular vasculature during development and disease. Invest. Ophthalmol. Vis. Sci. 46, 3021–3026.

Robitaille, J., MacDonald, M.L.E., Kaykas, A., Sheldahl, L.C., Zeisler, J., Dubé, M.-P., Zhang, L.-H., Singaraja, R.R., Guernsey, D.L., Zheng, B., Siebert, L.F., Hoskin-Mott, A., Trese, M.T., Pimstone, S.N., Shastry, B.S., Moon, R.T., Hayden, M.R., Goldberg, Y.P., Samuels, M.E., 2002. Mutant frizzled-4 disrupts retinal angiogenesis in familial exudative vitreoretinopathy. Nat. Genet. 32, 326–330.

Rosa, J.M., Bos, R., Sack, G.S., Fortuny, C., Agarwal, A., Bergles, D.E., Flannery, J.G., Feller, M.B., 2015. Neuron-glia signaling in developing retina mediated by neurotransmitter spillover. Elife 4.

Ruhrberg, C., Gerhardt, H., Golding, M., Watson, R., Ioannidou, S., Fujisawa, H., Betsholtz, C., Shima, D.T., 2002. Spatially restricted patterning cues provided by heparin-binding VEGF-A control blood vessel branching morphogenesis. Genes Dev. 16, 2684–2698.

Runkle, E.A., Antonetti, D.A., 2011. The blood-retinal barrier: structure and functional significance. Methods Mol. Biol. 686, 133–148.

Sappington, R.M., Carlson, B.J., Crish, S.D., Calkins, D.J., 2010. The microbead occlusion model: a paradigm for induced ocular hypertension in rats and mice. Invest. Ophthalmol. Vis. Sci. 51, 207–216.

Schmidt, M., Giessl, A., Laufs, T., Hankeln, T., Wolfrum, U., Burmester, T., 2003. How does the eye breathe? Evidence for neuroglobin-mediated oxygen supply in the mammalian retina. J. Biol. Chem. 278, 1932–1935.

Sernagor, E., Young, C., Eglen, S.J., 2003. Developmental modulation of retinal wave dynamics: shedding light on the GABA saga. J. Neurosci. 23, 7621–7629.

Shastry, B.S., Hejtmancik, J.F., Trese, M.T., 1997. Identification of novel missense mutations in the Norrie disease gene associated with one X-linked and four sporadic cases of familial exudative vitreoretinopathy. Hum. Mutat. 9, 396–401.

Skou, J.C., 1989. The influence of some cations on an adenosine triphosphatase from peripheral nerves. 1957. Biochim. Biophys. Acta 1000, 439–446.

Staehelin, L.A., 1974. Structure and function of intercellular junctions. Int. Rev. Cytol. 39, 191–283.

Stafford, B.K., Sher, A., Litke, A.M., Feldheim, D.A., 2009. Spatial-temporal patterns of retinal waves underlying activity-dependent refinement of retinofugal projections. Neuron 64, 200–212.

Stahl, A., Connor, K.M., Sapieha, P., Chen, J., Dennison, R.J., Krah, N.M., Seaward, M.R., Willett, K.L., Aderman, C.M., Guerin, K.I., Hua, J., Löfqvist, C., Hellström, A., Smith, L.E.H., 2010. The mouse retina as an angiogenesis model. Invest. Ophthalmol. Vis. Sci. 51, 2813–2826.

Stalmans, I., Ng, Y.-S., Rohan, R., Fruttiger, M., Bouché, A., Yuce, A., Fujisawa, H., Hermans, B., Shani, M., Jansen, S., Hicklin, D., Anderson, D.J., Gardiner, T., Hammes, H.-P., Moons, L.,

Dewerchin, M., Collen, D., Carmeliet, P., D'Amore, P.A., 2002. Arteriolar and venular patterning in retinas of mice selectively expressing VEGF isoforms. J. Clin. Invest. 109, 327–336.

Starr, J.M., Wardlaw, J., Ferguson, K., MacLullich, A., Deary, I.J., Marshall, I., 2003. Increased blood-brain barrier permeability in type II diabetes demonstrated by gadolinium magnetic resonance imaging. J. Neurol. Neurosurg. Psychiatry 74, 70–76.

Stellwagen, D., Shatz, C.J., Feller, M.B., 1999. Dynamics of retinal waves are controlled by cyclic AMP. Neuron 24, 673–685.

Stenman, J.M., Rajagopal, J., Carroll, T.J., Ishibashi, M., McMahon, J., McMahon, A.P., 2008. Canonical Wnt signaling regulates organ-specific assembly and differentiation of CNS vasculature. Science 322, 1247–1250.

Stensløkken, K.-O., Milton, S.L., Lutz, P.L., Sundin, L., Renshaw, G.M.C., Stecyk, J.A.W., Nilsson, G.E., 2008. Effect of anoxia on the electroretinogram of three anoxia-tolerant vertebrates. Comp. Biochem. Physiol. A Mol. Integr. Physiol. 150, 395–403.

Stewart, P.A., Wiley, M.J., 1981. Developing nervous tissue induces formation of blood-brain barrier characteristics in invading endothelial cells: a study using quail--chick transplantation chimeras. Dev. Biol. 84, 183–192.

Stone, J., Itin, A., Alon, T., Pe'er, J., Gnessin, H., Chan-Ling, T., Keshet, E., 1995. Development of retinal vasculature is mediated by hypoxia-induced vascular endothelial growth factor (VEGF) expression by neuroglia. J. Neurosci. 15, 4738–4747.

Sun, C., Speer, C.M., Wang, G.-Y., Chapman, B., Chalupa, L.M., 2008a. Epibatidine application in vitro blocks retinal waves without silencing all retinal ganglion cell action potentials in developing retina of the mouse and ferret. J. Neurophysiol. 100, 3253–3263.

Sun, C., Warland, D.K., Ballesteros, J.M., van der List, D., Chalupa, L.M., 2008b. Retinal waves in mice lacking the β2 subunit of the nicotinic acetylcholine receptor. Proceedings of the National Academy of Sciences 105, 13638–13643.

Sundstrom, J.M., Tash, B.R., Murakami, T., Flanagan, J.M., Bewley, M.C., Stanley, B.A., Gonsar, K.B., Antonetti, D.A., 2009. Identification and analysis of occludin phosphosites: a combined mass spectrometry and bioinformatics approach. J. Proteome Res. 8, 808–817.

Suzuki, T., Elias, B.C., Seth, A., Shen, L., Turner, J.R., Giorgianni, F., Desiderio, D., Guntaka, R., Rao, R., 2009. PKC eta regulates occludin phosphorylation and epithelial tight junction integrity. Proc. Natl. Acad. Sci. U. S. A. 106, 61–66.

Syed, M.M., Lee, S., He, S., Zhou, Z.J., 2004. Spontaneous waves in the ventricular zone of developing mammalian retina. J. Neurophysiol. 91, 1999–2009.

Tai, L.M., Holloway, K.A., Male, D.K., Loughlin, A.J., Romero, I.A., 2010. Amyloid-beta-induced occludin down-regulation and increased permeability in human brain endothelial cells is mediated by MAPK activation. J. Cell. Mol. Med. 14, 1101–1112.

Tam, S.J., Richmond, D.L., Kaminker, J.S., Modrusan, Z., Martin-McNulty, B., Cao, T.C., Weimer, R.M., Carano, R.A.D., van Bruggen, N., Watts, R.J., 2012. Death receptors DR6 and TROY regulate brain vascular development. Dev. Cell 22, 403–417.

Tang, Z., Zhang, S., Lee, C., Kumar, A., Arjunan, P., Li, Y., Zhang, F., Li, X., 2011. An optic nerve crush injury murine model to study retinal ganglion cell survival. J. Vis. Exp.

Tarkkanen, A., Reunanen, A., Kivelä, T., 2008. Frequency of systemic vascular diseases in patients with primary open-angle glaucoma and exfoliation glaucoma. Acta Ophthalmol. 86, 598–602.

Tauchi, M., Masland, R.H., 1984. The shape and arrangement of the cholinergic neurons in the rabbit retina. Proc. R. Soc. Lond. B Biol. Sci. 223, 101–119.

Templeton, J.P., Freeman, N.E., Nickerson, J.M., Jablonski, M.M., Rex, T.S., Williams, R.W., Geisert, E.E., 2013. Innate immune network in the retina activated by optic nerve crush. Invest. Ophthalmol. Vis. Sci. 54, 2599–2606.

Tennant, M., Beazley, L.D., 1992. A breakdown of the blood-brain barrier is associated with optic nerve regeneration in the frog. Vis. Neurosci. 9, 149–155.

Tielsch, J.M., Katz, J., Sommer, A., Quigley, H.A., Javitt, J.C., 1995. Hypertension, perfusion pressure, and primary open-angle glaucoma. A population-based assessment. Arch. Ophthalmol. 113, 216–221.

Toomes, C., Bottomley, H.M., Jackson, R.M., Towns, K.V., Scott, S., Mackey, D.A., Craig, J.E., Jiang, L., Yang, Z., Trembath, R., Woodruff, G., Gregory-Evans, C.Y., Gregory-Evans, K., Parker, M.J., Black, G.C.M., Downey, L.M., Zhang, K., Inglehearn, C.F., 2004. Mutations in LRP5 or FZD4 underlie the common familial exudative vitreoretinopathy locus on chromosome 11q. Am. J. Hum. Genet. 74, 721–730.

Torborg, C.L., Feller, M.B., 2005. Spontaneous patterned retinal activity and the refinement of retinal projections. Prog. Neurobiol. 76, 213–235.

Törnquist, P., Alm, A., 1979. Retinal and choroidal contribution to retinal metabolism in vivo. A study in pigs. Acta Physiol. Scand. 106, 351–357.

Törnquist, P., Alm, A., Bill, A., 1990. Permeability of ocular vessels and transport across the blood-retinal-barrier. Eye 4 (Pt 2), 303–309.

Tout, S., Chan-Ling, T., Holländer, H., Stone, J., 1993. The role of Müller cells in the formation of the blood-retinal barrier. Neuroscience 55, 291–301.

Trible, J.R., Sergott, R.C., Spaeth, G.L., Wilson, R.P., Katz, L.J., Moster, M.R., Schmidt, C.M., 1994. Trabeculectomy is associated with retrobulbar hemodynamic changes. A color Doppler analysis. Ophthalmology 101, 340–351.

Ueno, M., Akiguchi, I., Yagi, H., Naiki, H., Fujibayashi, Y., Kimura, J., Takeda, T., 1993. Age-related changes in barrier function in mouse brain I. Accelerated age-related increase of brain

transfer of serum albumin in accelerated senescence prone SAM-P/8 mice with deficits in learning and memory. Arch. Gerontol. Geriatr. 16, 233–248.

Ueno, M., Sakamoto, H., Tomimoto, H., Akiguchi, I., Onodera, M., Huang, C.-L., Kanenishi, K., 2004. Blood-brain barrier is impaired in the hippocampus of young adult spontaneously hypertensive rats. Acta Neuropathol. 107, 532–538.

Ueno, M., Tomimoto, H., Akiguchi, I., Wakita, H., Sakamoto, H., 2002. Blood--brain barrier disruption in white matter lesions in a rat model of chronic cerebral hypoperfusion. J. Cereb. Blood Flow Metab. 22, 97–104.

Vaney, D.I., 1984. "Coronate" amacrine cells in the rabbit retina have the "starburst" dendritic morphology. Proc. R. Soc. Lond. B Biol. Sci. 220, 501–508.

van Meer, G., Simons, K., 1986. The function of tight junctions in maintaining differences in lipid composition between the apical and the basolateral cell surface domains of MDCK cells. EMBO J. 5, 1455–1464.

Wang, J., Dong, Y., 2016. Characterization of intraocular pressure pattern and changes of retinal ganglion cells in DBA2J glaucoma mice. Int. J. Ophthalmol. 9, 211–217.

Wang, L., Törnquist, P., Bill, A., 1997. Glucose metabolism of the inner retina in pigs in darkness and light. Acta Physiol. Scand. 160, 71–74.

Wang, Y., Rattner, A., Zhou, Y., Williams, J., Smallwood, P.M., Nathans, J., 2012. Norrin/Frizzled4 signaling in retinal vascular development and blood brain barrier plasticity. Cell 151, 1332–1344.

Wang, Z., Liu, C.-H., Sun, Y., Gong, Y., Favazza, T.L., Morss, P.C., Saba, N.J., Fredrick, T.W., He, X., Akula, J.D., Chen, J., 2016. Pharmacologic Activation of Wnt Signaling by Lithium Normalizes Retinal Vasculature in a Murine Model of Familial Exudative Vitreoretinopathy. Am. J. Pathol. 186, 2588–2600.

Warburg, O., 1956. On the origin of cancer cells. Science 123, 309–314.

Warden, S.M., Andreoli, C.M., Mukai, S., 2007. The Wnt signaling pathway in familial exudative vitreoretinopathy and Norrie disease. Semin. Ophthalmol. 22, 211–217.

Warland, D.K., Huberman, A.D., Chalupa, L.M., 2006. Dynamics of spontaneous activity in the fetal macaque retina during development of retinogeniculate pathways. J. Neurosci. 26, 5190–5197.

Watanabe, T., Matsushima, S., Okazaki, M., Nagamatsu, S., Hirosawa, K., Uchimura, H., Nakahara, K., 1996. Localization and ontogeny of GLUT3 expression in the rat retina. Brain Res. Dev. Brain Res. 94, 60–66.

Wiedman, M., Tabin, G.C., 1999. High-altitude retinopathy and altitude illness. Ophthalmology 106, 1924–6; discussion 1927.

Wierzbowska, J., Wierzbowski, R., Stankiewicz, A., Siesky, B., Harris, A., 2012. Cardiac autonomic dysfunction in patients with normal tension glaucoma: 24-h heart rate and blood pressure variability analysis. Br. J. Ophthalmol. 96, 624–628.

Winkler, B.S., 1981. Glycolytic and oxidative metabolism in relation to retinal function. J. Gen. Physiol. 77, 667–692.

Winkler, B.S., Arnold, M.J., Brassell, M.A., Puro, D.G., 2000. Energy metabolism in human retinal Muller cells. Invest. Ophthalmol. Vis. Sci. 41, 3183–3190.

Winkler, B.S., Christen, Y., Doly, M., Droy-Lefaix, M.T., 1995. A quantitative assessment of glucose metabolism in the isolated rat retina. Les Seminaires ophthalmologiques d'IPSEN, Vision et adaptation 6, 78–96.

Winkler, B.S., Pourcho, R.G., Starnes, C., Slocum, J., Slocum, N., 2003. Metabolic mapping in mammalian retina: a biochemical and 3H-2-deoxyglucose autoradiographic study. Exp. Eye Res. 77, 327–337.

Winkler, E.A., Sagare, A.P., Zlokovic, B.V., 2014. The pericyte: a forgotten cell type with important implications for Alzheimer's disease? Brain Pathol. 24, 371–386.

Wolburg, H., Neuhaus, J., Kniesel, U., Krauss, B., Schmid, E.M., Ocalan, M., Farrell, C., Risau, W., 1994. Modulation of tight junction structure in blood-brain barrier endothelial cells. Effects of tissue culture, second messengers and cocultured astrocytes. J. Cell Sci. 107 (Pt 5), 1347–1357.

Wong-Riley, M.T., 1989. Cytochrome oxidase: an endogenous metabolic marker for neuronal activity. Trends Neurosci. 12, 94–101.

Wong-Riley, M.T.T., Huang, Z., Liebl, W., Nie, F., Xu, H., Zhang, C., 1998. Neurochemical organization of the macaque retina: effect of TTX on levels and gene expression of cytochrome oxidase and nitric oxide synthase and on the immunoreactivity of Na+K+ATPase and NMDA receptor subunit I. Vision Res. 38, 1455–1477.

Wong, R.O., 1995. Cholinergic regulation of [Ca2+] i during cell division and differentiation in the mammalian retina. Journal of Neuroscience 15, 2696–2706.

Wong, R.O., Meister, M., Shatz, C.J., 1993. Transient period of correlated bursting activity during development of the mammalian retina. Neuron 11, 923–938.

Wong, R.O., Oakley, D.M., 1996. Changing patterns of spontaneous bursting activity of on and off retinal ganglion cells during development. Neuron 16, 1087–1095.

Wong, W.T., Myhr, K.L., Miller, E.D., Wong, R.O., 2000. Developmental changes in the neurotransmitter regulation of correlated spontaneous retinal activity. J. Neurosci. 20, 351–360.

Wong, W.T., Sanes, J.R., Wong, R.O., 1998. Developmentally regulated spontaneous activity in the embryonic chick retina. J. Neurosci. 18, 8839–8852.

Wong, W.T., Wong, R.O., 2001. Changing specificity of neurotransmitter regulation of rapid dendritic remodeling during synaptogenesis. Nat. Neurosci. 4, 351–352.

Xu, H., Tian, N., 2004. Pathway-specific maturation, visual deprivation, and development of retinal pathway. Neuroscientist 10, 337–346.

Xu, Q., Wang, Y., Dabdoub, A., Smallwood, P.M., Williams, J., Woods, C., Kelley, M.W., Jiang, L., Tasman, W., Zhang, K., Nathans, J., 2004. Vascular development in the retina and inner ear: control by Norrin and Frizzled-4, a high-affinity ligand-receptor pair. Cell 116, 883–895.

Yang, B., Akhter, S., Chaudhuri, A., Kanmogne, G.D., 2009. HIV-1 gp120 induces cytokine expression, leukocyte adhesion, and transmigration across the blood-brain barrier: modulatory effects of STAT1 signaling. Microvasc. Res. 77, 212–219.

Ye, X., Wang, Y., Cahill, H., Yu, M., Badea, T.C., Smallwood, P.M., Peachey, N.S., Nathans, J., 2009. Norrin, frizzled-4, and Lrp5 signaling in endothelial cells controls a genetic program for retinal vascularization. Cell 139, 285–298.

Ye, X., Wang, Y., Nathans, J., 2010. The Norrin/Frizzled4 signaling pathway in retinal vascular development and disease. Trends Mol. Med. 16, 417–425.

Zeilbeck, L.F., Müller, B., Knobloch, V., Tamm, E.R., Ohlmann, A., 2014. Differential angiogenic properties of lithium chloride in vitro and in vivo. PLoS One 9, e95546.

Zheng, J.-J., Lee, S., Zhou, Z.J., 2004. A developmental switch in the excitability and function of the starburst network in the mammalian retina. Neuron 44, 851–864.

Zheng, J., Lee, S., Zhou, Z.J., 2006. A transient network of intrinsically bursting starburst cells underlies the generation of retinal waves. Nat. Neurosci. 9, 363–371.

Zheng, Z., Yuan, R., Song, M., Huo, Y., Liu, W., Cai, X., Zou, H., Chen, C., Ye, J., 2012. The toll-like receptor 4-mediated signaling pathway is activated following optic nerve injury in mice. Brain Res. 1489, 90–97.

Zhou, L., Sohet, F., Daneman, R., 2014. Purification of endothelial cells from rodent brain by immunopanning. Cold Spring Harb. Protoc. 2014, 65–77.

Zhou, Y., Wang, Y., Tischfield, M., Williams, J., Smallwood, P.M., Rattner, A., Taketo, M.M., Nathans, J., 2014. Canonical WNT signaling components in vascular development and barrier formation. J. Clin. Invest. 124, 3825–3846.

Zhou, Z.J., 1998. Direct participation of starburst amacrine cells in spontaneous rhythmic activities in the developing mammalian retina. J. Neurosci. 18, 4155–4165.

Zilka, N., Stozicka, Z., Kovac, A., Pilipcinec, E., Bugos, O., Novak, M., 2009. Human misfolded truncated tau protein promotes activation of microglia and leukocyte infiltration in the transgenic rat model of tauopathy. J. Neuroimmunol. 209, 16–25.

Zlokovic, B.V., 2008. The blood-brain barrier in health and chronic neurodegenerative disorders. Neuron 57, 178–201.

Zlokovic, B.V., 2011. Neurovascular pathways to neurodegeneration in Alzheimer's disease and other disorders. Nat. Rev. Neurosci. 12, 723–738.